Cobalt of the Tyrone Igneous Complex: geochemistry of mafic hosted sulphides and remobilisation.

Matthew Mawson [1,2]

[1] Department of Geology, Museum Building, *Trinity College Dublin, College Green, Dublin 2, Ireland. (mawsonm@tcd.ie)*
[2] *LKAB, Luossavaara-Kiirunavaara AB, LKAB, Kiruna, Sweden. (matthew.mawson@lkab.com)*

Submitted 28th April, 2023

I declare that this thesis has not been submitted as an exercise for a degree at this or any other university and it is entirely my own work.

I agree to deposit this thesis in the University's open access institutional repository or allow the Library to do so on my behalf, subject to Irish Copyright Legislation and Trinity College Library conditions of use and acknowledgement.

This dissertation's main sections contain 11,989 words.

Signed: 

What's past is prologue. William Shakespeare

ABSTRACT

Primary sulphide mineralisation in mafic rocks and secondary remobilised sulphides contain significant cobalt and relate to early Palaeozoic ocean closure and arc-continent collision in the Irish Caledonian terrane. This study presents new laser ablation data, portable Xray diffraction (pXRF) geochemistry, and the recent mineral exploration of Shackleton Resources Ltd whole rock analyses, to study sulphide mineralisation within the Tyrone Igneous Complex (TIC); and the study investigates geochemical similarities and temporal association between sulphide showings. A sulphide mobility event of the TIC can be dated to 455.8 ± 3 (mega annum) Ma age (Rice 2016), or 325 Ma (Parnell 2000), while LA ICP-MS sulphide mapping (Stratford 2019) records element zonation, possibly uniting the origins of sulphides and cobalt. The TIC mineralisation history is complex, the tectonics of terrane accretion and metamorphism may have increased sulphide mobility into adjacent rocks via extensional structures. On the TIC, sulphide showings of different types may be related. Individual sampled cobalt values are locally high at 0.12% Co, indicating an undiscovered economic concentration of the metal, while sulfosalt elements show a close association of bismuth-silver, gold, and copper. Volcanogenic massive sulphide (VMS) type mineralisation is well understood in the adjacent terrane of Newfoundland and Nova Scotia. But no VMS economic metal deposits are found in the Laurentian half of Ireland and Britain. In addition, increasing awareness of resource responsibility, provenance, and critical elements, a domestic supply of cobalt is aligned to the WHO sustainable development goals (https://www.who.int/europe/about-us/our-work/sustainable-development-goals). Therefore, understanding sulphide mineralisation of the TIC may identify a source of metals, metal mobilisation, and metal traps in syn-mineralisation structures. Furthermore, it is hoped the structural concept of northwest striking, large basement fractures and the migration of sulphide hosted metals into cover units may help to explain the lack of discovered VMS or VMS-orogenic mineralisation, economic or otherwise.

Contents

1.INTRODUCTION

The Tyrone Igneous Complex (TIC) has a long history of investigation, but sporadic exposure and limited drilling has yet to find significant bedrock mineralisation. The TIC has an area of circa 350 km^2, situated in counties Tyrone and Londonderry of Northern Ireland. Quaternary drift and blanket peat cover can reach substantial depths and good quality outcrop is limited to a few quarries and cuttings. The landscape is rural. Land use is cattle and dairy farming, with sheep grazing on high ground. Extraction for building materials exploit the fluvial-glacial quaternary deposits. The TIC is the 'most' exposed ophiolite-arc rock package of the Caledonian trend, defined as a north-east south-west (NE-SW) trending strike, in Ireland and Britain. This Trinity College Dublin (TCD) masters project is funded by iCRAG and the Science Foundation Ireland. Shackleton Resources supported the thesis in providing geochemistry data, equipment, and permission to conduct academic research on the Slieve Gallion mineral prospecting licence.

Recently described in terms of their tectonic settings and preservation history, supra-subduction zone (SSZ) ophiolites negate the preservation problem of most oceanic crust i.e., destruction due to subduction. SSZ settings provide opportunities in obduction and conditions for ophiolite preservation. These tectonic conditions are in close temporal and spatial proximity to ocean-continent subduction zones. In addition, volcanogenic massive sulphide (VMS) and porphyry style mineralisation occur in Ireland which indicate, in Phanerozoic settings, an arc-front position. The Bonin islands (Japan) of the Bonin Ridge are a modern-day analogy where sheeted dykes are topped by depleted tholeiites and boninites; and interpillow areas of boninites are filled with sulphides and jaspers as exhalative deposits. The Bonin ridge provides a modern-day analogy of a SSZ ophiolite, arc, and fore-arc with associated mineralisation. Therefore, along strike correlatives to the TIC - Ordovician SSZ ophiolites of Ballantrae (Ayrshire, Scotland) and Deerpark (County Mayo, Ireland) may contain sulphide mineralisation.

This study reports the results of geochemical analysis of pyrite crystals from the mafic ophiolite rocks of County (Co.) Tyrone, County Mayo, and Ayrshire in south-east Scotland. Mapping of fresh quarry outcrops found several interesting sulphide showings and structural features. At Orritor (Co. Tyrone), a shear zone is hosted in gabbro and serpentinite. Ultramafic pods are seen in the sub crop of the quarry floor which contain sulphides, rich in cobalt. Deformed pegmatite intrusions in the shear zone are important and provide a source of zircons (whose analysis could not be included in this thesis). Using cobalt as the main element of interest, this study gives important insight into its high values, source areas, possible remobilisation, and exploration targeting.

Ophiolite locations across the Caledonian trend were sampled targeting sulphide mineralisation. At ophiolite locations mineralised samples were found with the aid of a pXRF unit. Significant sulphide showings occur in outcrop and float material e.g., the Golden Hollow copper-gold-bismuth-silica boulder. Anomalous cobalt concentrations are seen at Corvanaghan Quarry and Orritor Quarry, County Tyrone. Furthermore, as Corvanaghan Quarry is five km to the west of Orritor, vein hosted cobalt may or may not be mobilised from the mafic rocks of Orritor. These questions form the hypothesis (H_1) of the study. H_1: Sulphide showings are related based on a-priori knowledge of sulphide hosted gold deposits in the area. Conversely, the null hypothesis (H_o) is: The sulphide showings are not related.

Further questions which arise are: are the vein hosted cobalt sulphides primary magmatic, or does hydrothermal remobilisation from a primary source, in the sulphide phase, route along extensional pathways to precipitate the quartz-sulphide veins?

Geological studies on the Caledonian trend date to the birth of geology as a science: academic papers are numerous and influential authors abundant. Over four decades, mineral exploration has built up a large geochemical information and knowledge base. In addition, co-ordinated ground geochemical and airborne geophysical survey programmes provide tools for mineral exploration – both national in scale and free to access. This study unites trace element geochemistry, vein textures, sulphide occurrences, and previous dating research. Through petrological analysis of three polished thin sections and laser-ablation inductively-coupled-plasma mass-spectrometry (LA ICP-MS) analysis, whole rock trace element geochemistry, and pXRF geochemistry, some interpretation may be made. Thus, elements related to sulphide mineralisation, interpreted mineralisation history, and sulphide remobilisation events are described.

To summarise, new data from this study's thin section petrology, LA ICP-MS analysis, sulphide geochemistry and mapping may describe cobalt deportment. The null hypothesis – to show the sulphide showings are not related - provides clear measure of success for this study.

2. Geology

2.1 Regional Geology

Britain and Ireland's northern geological terranes are tectonically amalgamated terranes of a Wilson cycle. Wilson cycle tectonics of ocean expansion, contraction, subduction, arc development, and ocean closure can be traced on both sides of the Atlantic Ocean in the Appalachians, Newfoundland, Ireland, Britain, Norway, Greenland, and Svalbard (Van Staal et al 1998), Figure 1. Tuzo's 'early Atlantic', the Iapetus Ocean separated the continents of Laurentia and Gondwana as a closed, or inland ocean (Van Stall et al 1998). The Iapetus closure ended with soft continental collision and orogeny (Bird et al 2013). The Caledonian orogeny consists Neo-Proterozoic - early Phanerozoic formations, although earlier cycles are recorded from the Meso-Proterozoic to Neo-Proterozoic of Rodinia, represented by the Moine Super group (Bird et al 2013). Stratigraphy is complex. Generally, basement rocks in the north of Ireland are Laurentian, Grenville high-grade metamorphic rocks of 963 (mega annum) Ma (Daley 2005), covered by supracrustal metasediments of 510-490 Ma (Dewey 2005), Ordovician arc volcanic units of 475-469 Ma (Hollis et al 2012), Devonian red beds at 410 Ma (Mitchell 2004), and Carboniferous carbonaceous sequences. The distribution of the peri-Laurentian and peri-Gondwana rocks is imperfect, demonstrated by Ganderian rocks in southern Newfoundland and Laurentian material thrusted over the Baltic shield, such as the Tromso Nappe (Steltenpohl et al 2011).

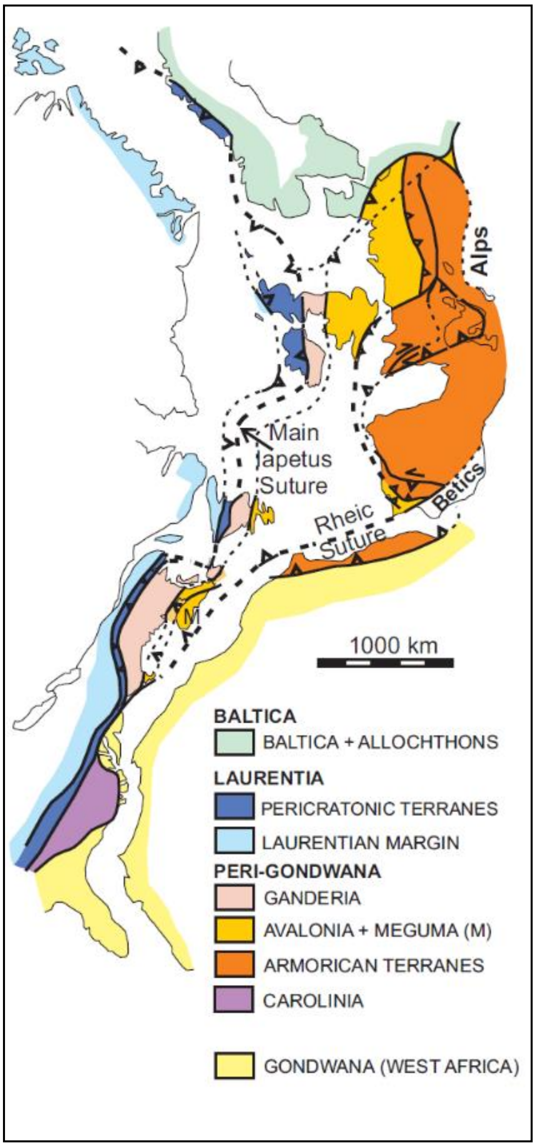

Figure 1 Extent of Iapetus on closure, Van Staal 1998

The pelites and psammites of Northern Ireland belong to the upper units of the Dalradian Supergroup: a 25 kilometre (km) thick sequence of NE-SW strike from western Ireland to Shetland. Known as the Grampian Terrane, metasedimentary units were deposited in the Neo-Proterozoic and metamorphosed to greenschist lower amphibolite facies (Barrow 1893) by early Ordovician (Hollis et al 2013), as the peri-Gondwana micro-craton Avalonia collided with Laurentia and Baltica. The Great Glen fault, a major crustal fault zone and structurally classed as a first order structure, is the Grampian's Scottish northern boundary. The Grampian's southern boundary is the Highland boundary fault, or in Ireland the Fair Head-Clew Bay Line (FHCBL). The Grampian terrane is the regional terrane of highest metamorphic and represents orogenic peak temperatures and pressures.

The Grampian's neighbour, the Midland Valley Terrane (MVT) is an accreted terrane of arc and rift volcano-sedimentary units, foreland basins, and contains tantalising examples of mineralisation related to arc-orogen and rift settings. In Northern Ireland, the MVT is under cover by Grampian terrane thrusting from the north, an accretionary prism complex from the south and many mid to late Palaeozoic basins. Accreted during Arenig (480 Ma), the MVT's northern border - the FHCBL - is partially obscured by the Omagh Thrust. The Omagh Thrust is seen in exposure as mylonite (Mawson unpublished). The Southern Upland Fault (SUF) represents the MVT's southern border. Both boundaries are covered by Variscan thrusting (Omagh Thrust) and late Palaeozoic basins.

South of the MVT, the Southern Uplands Longford-Down Terrane (SULDT) is a thick sequence of mid-Ordovician to Silurian turbidites deposited in a foreland basin setting (Anderson 2004). Greywackes and black shales strike with the Caledonian trend, although internal thrust packages and folds are seen (Mitchell 2004). Individual tracts of the SULDT young to the north due to thrusting, while overall the terrane younging direction is directed south (Mitchell 2004). Rock units of the lower Moffat Shale group and the upper Gala group are continuous over large distances of Ireland, Northern Ireland, and Scotland. The SULDT internal terrane structure of the Orlock Bridge fault is a major dislocation feature (Anderson & Oliver 1986). Bounded to the north by the Southern Upland fault, and the south by thick Carboniferous cover sequences, the SULDT is interpreted as a well-preserved accretionary prism complex (McConnell et al 2016).

The Grampian, Midland valley, and Southern Upland terranes, Figure 2(a), correlate with those of Atlantic Canada. The Dalradian are a high-grade equivalent of the Fleur de Lys Supergroup (Humber zone, Newfoundland (NFL), Figure 2(b)) (Cooper et al 2011). Furthermore, the Notre Dame Subzone of Newfoundland, part of the Dunnage Zone, and the Annieopsquotch ophiolite belt are correlated to the TIC (Hollis et al 2012, Williams 1995), Figure 2(c).

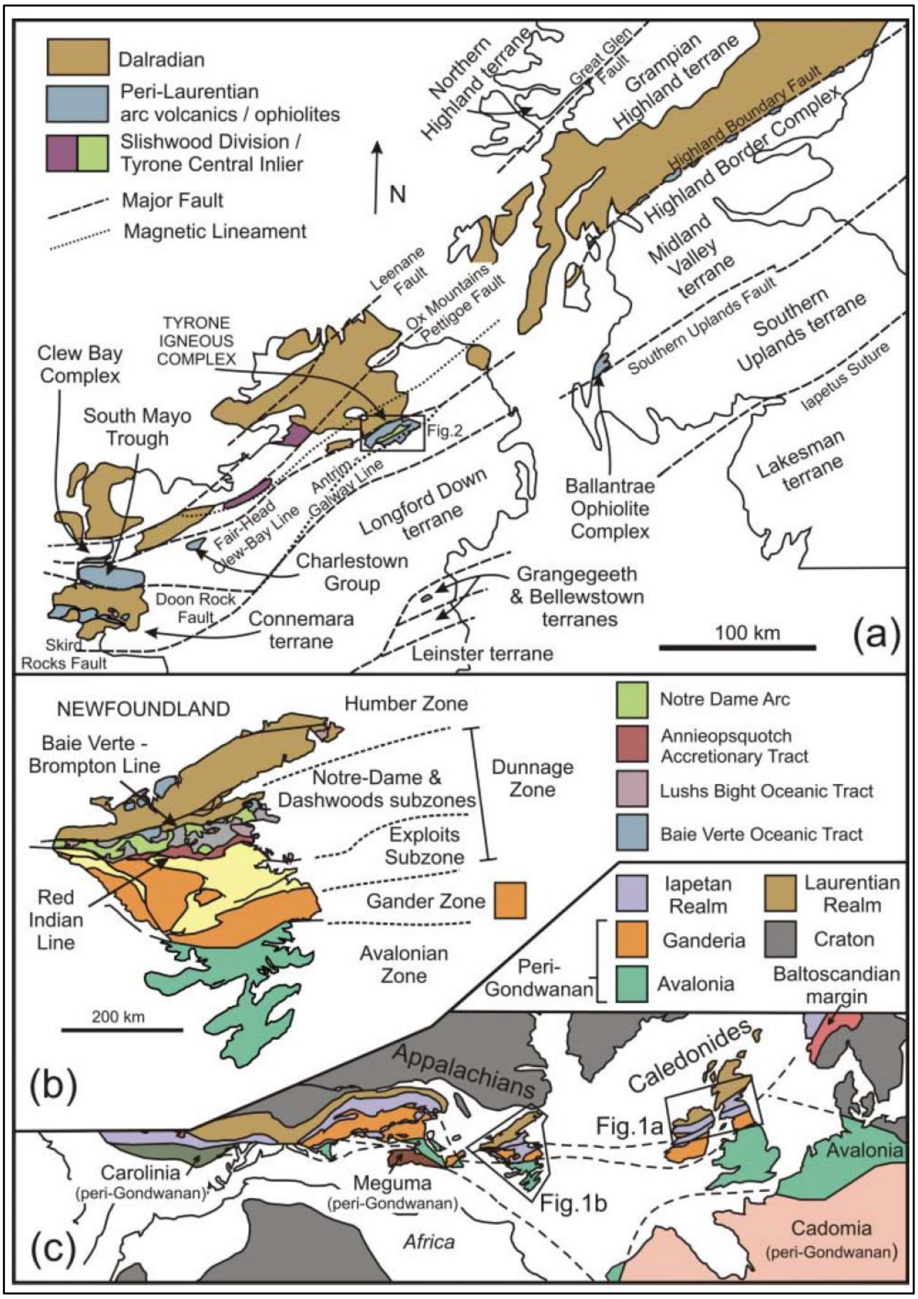

Figure 2(a) Terranes and terrane boundaries of the north of Ireland and Britain. Figure 2(b) Terranes of NFL. Figure 2(c) Terrane correlations from Ireland to NFL and the Appalachians, from Cooper et al 2011

NFL's Notre Dame subzone, a subgroup of the Dunnage Zone, NFL (Van Staal, 1998), provides a key analogy to the Caledonian orogen in the north of Ireland. The upper TIC arc rhyolites, tuffs, and alkali-basalts were dated by Isotope Dilution Thermal Ionization Mass Spectrometry (ID-TIMS) at 473 Ma ±0.8 Ma (Cooper et al 2008). Cooper draws a straight line from the age of the Ballantrae Complex, Scotland to the TIC and Notre Dame subzone. The Meguma terrane correlates to Avalonia. But, to paraphrase Van Staal, continuity along strike is not guaranteed: compression and transpression can be confirmed, with the destruction of detail.

The Palaeozoic tectonic history is interpreted from the terranes and terrane boundaries. Terrane boundaries can be traced along large distances by strike-slip offset, such as the Great Glen Fault (Holmes 1946), geophysical images (Tellus aeromagnetic survey, TMI reduction images: https://dcenr.maps.arcgis.com/) and juxtaposing lithologies of contrasting metamorphic grades

(Clift et al 2004). Significant movement is attributed to the Irish and Scottish terrane boundaries in the last stages of Iapetus closure (Dewey 2005). Movement is dated using boundary shear kinematics of the FHCBL at 448 Ma, dextral slip, then 400 Ma, sinistral slip (Chew et al 2012). Later oblique collision is equal to the Appalachian's Penobscot orogeny (Van Staal et al 1998). Large differences in metamorphic grade occur on both sides of the Highland Boundary Fault and FHCBL, e.g., the high-grade Dalradian Supergroup and low-grade MVT. Correlation of the FHCBL with Atlantic Canada's Baie Verte-Brompton line continues the juxtaposition of metamorphic grades. In summary, these terranes and boundaries are some of the most studied in the world. Since Barrow (1893) over 120 years of investigation has delivered empirical, geochemical, and well constrained geochronological evidence. The geological evidence records the distinct tectonic phases of: Neo-Proterozoic passive-margin sedimentation, followed by early Ordovician island arc development, leading to intense arc-continent collision of the Grampian orogeny (Dewey 2005), Silurian ocean closure, and finally widespread Caledonian orogenesis (Murphy 2009).

North of Ireland basement rocks are interpreted to be Proterozoic Laurentian basement (Cooper et al 2011) of either Lewisian gneiss orthogneisses 3,100 Ma to 1,900 Ma (Love 2010), or significantly younger Grenville rocks of 980 Ma (Kirkland 2013). Grenville basement is exposed in North County Mayo as the Annagh Gneiss where the core of a fold shows high-grade eclogite, and granulite facies metamorphism (Daly 1996). Also, blue schist facies metamorphism is recognised. The maximum age of the Annagh gneiss, an orthogneiss, is dated to 1,753 Ma (Daly 1996) and subsequently enjoyed Grenville deformation events. These deformation events correlate to the Canadian Grenville orogen and Svenco-Norwegian orogen (Daly 1996). Cooling temperatures of titanite date the closure at 963 Ma (Daly 2005). Part of an earlier Wilson cycle, the Grenville-Svenco-Norwegian orogen is a Meso-Proterozoic orogen of Rodinia, similar in extent and affecting the same continental margins of Laurentia and Baltica.

Neo-Proterozoic rifting and ocean crust formation probably began 615-570 Ma (Cawood et al 2001). In the Early Ordovician, Iapetus Ocean closure began in the west and faced east to the Tourquist Sea, Rheic Ocean and Palaeo-Tethys. South-east Laurentia added to its margin several arc terranes (Van Staal et al 1998) and the Silurian turbidite wedge. Fed by slab breakoff and migmatite generation, Devonian to Carboniferous granitoid plutons weld and anchor varying components of the Caledonian terrane. During the Caledonian orogeny the regional, tectonic stress field changed from straight subduction to oblique and transpressional. Therefore, Laurentia, Baltica, and Avalonia meet in a 'soft' continent-continent collision (Bird et al 2012) which sows the seeds for the next Wilson orogenic cycle: Cretaceous and Tertiary rifting to form the Atlantic Ocean.

Neoproterozoic extensional basins are formed along the Laurentian passive margin. Dalradian successions preserve a record of Laurentia's (southern) passive margin sedimentation, and the very lowest units may be as old as 942 Ma (McAteer et al 2010). South dipping subduction at 515 Ma (Waldron & Van Staal 2001) represents a switch to ocean closure along the continental margin up to 2,000 km (Cooper et al 2013). Melting in the subduction zone creates primitive then evolved arc volcanic rocks on island arcs behind the zone of subduction. In addition, high level crustal intrusive rocks are emplaced in the resultant arcs (Cooper et al 2011). By early Ordovician subduction stresses are locally maximum and the SSZ ophiolite is thrusted over a micro-continent – creating persevered crustal slices represented by the TIC.

An early subset of the Caledonian orogen, the Grampian orogen is constrained between 485 Ma and 443 Ma (Dewey 2005) and marked by classic Barrovian zonation of amphibolite facies metamorphic assemblages over large areas of Scotland (Barrow 1893) and Ireland. In County

Mayo, Barrow Zone metamorphic assemblages of staurolite-kyanite-garnet give classic zonation of widespread regional metamorphic conditions. Due to the high metamorphic grades associated with the units of Grampian age, one tectonic interpretation is a hard collision of arc and back-arc followed by terrane docking, and strike-slip (Forster 2013, Murphy 2009). The Grampian equals Atlantic Canada's Taconic orogeny and Scandinavia's Finnmark event (Dewey 2005, Kirkland 2007). More precise geochronological dating allows separation between events and resolution of timings. Age dating of metamorphic fabric forming minerals from the Dalradian pelites (micas, hornblende, and garnets) give metamorphic ages ranging from 475 to 455 Ma, depending on the geographic location of samples (Soper 1999, Flowerdew et al 2000). Scottish Dalradian Sm-Nd garnet ages of 473-465 Ma, west of Ireland ages of 470-459 Ma (Flowerdew et al 2000), and 460 Ma by Sm-Nd garnet age (Friedrich 1999) constrain peak metamorphism. A date of a Connemara syn-tectonic intrusion yields 470 Ma (Soper 1999) which is thought to be the only syn-tectonic deformation intrusion in Ireland and is important in the context of this study's findings.

The Grampian orogeny, defined as short lived, but lasting over 10 Ma (Dewey 2005), reached sillimanite grade conditions (Clift at al 2004). Syn or post peak ophiolite obduction and subsequent orogenic collapse ended the Grampian phase (Dewey 2005). The first deformation event (D_1), closely related to collision with thrusting, is recognised locally as slides. D_2 continued collision forming the Dalradian nappe pile. From the D_2 event, structures (S_2) date to 460 Ma (Chew et al 2003). The D_3 event represents peak metamorphic conditions. S_3 structures date at 448 Ma with dextral shearing and a near vertical orientation of the units. Another S_3 structure is dated at 465 Ma and is related to trusting of the Dalradian southwards possibly over the Tyrone Central Inlier (TCI) (Chew et al 2008).

Along the length of eastern Laurentia, rifting produced microcontinents such as the Dashwoods, the Slishwood Division (Waldron & Van Staal 2001), and the TCI (Cooper et al 2011). Separated from the Laurentian continent back-arc spreading, a line of microcontinents may have been formed prior to early Ordovician accretion (Hollis et al 2012). With continuing subduction and travel of the microcontinents into the subduction zone, lock-up of the subduction zone appears to take place (Dewey 2005, Chew et al 2010). The microcontinents prevent downward travel of the subducted plate. Lock-up of the subduction zone increases the regional tectonic stress field resulting in obduction. SSZ ophiolites are thrusted onto or under the Laurentia margin (Van Staal et al 1998) and a subduction reversal **(**Yardley & Senior 1982, Tanner 1990**)** continues ocean closure - seen in the Notre Dame continental magmatic arc. However, orogenic collapse at 470 – 450 Ma results in extension and exhumation (Flowerdew et al 2000, Clift et al 2004). Orogenic collapse along former thrust faults thinned the crust and enabled fluids and serpentinites to the near surface. The process of exhumation was advanced 7.6 Ma after peak metamorphism. High pressure rocks, Clew Bay blueschists (Gray & Yardley 1979), are exposed during reversal and orogenic collapse (Clift et al 2004) and high-grade detritus in adjacent terrane's sedimentary basins means uplift and deep erosion in the Grampian terrane by 450 Ma.

SSZ ophiolites can occur in orogens as ribbons defining the subduction zone, such as the Annieopsqotch ophiolite belt of Atlantic Canada. Other Caledonian ophiolites are found at: Ballantrae, Scotland (Bluck 1985), Shetland, Clew Bay, Ireland, and NFL (Van Staal, Dewey, Niocaill and McKerrow 1998). In NFL, the Baie Verte ophiolite age is dated to 490 Ma (Van Staal et al 2007), and the Thetford Mines Ophiolite (TMO) to formation age of 479 Ma (U-Pb) with a 477 Ma date for the amphibolite facies metamorphic sole. The TMO is interpreted to overthrust Laurentia by 100s km during the Taconic and its position as a SSZ marks a reoccurring and repeatable tectonic process in early arc-continent collision zones (Tremblay 2011). NFL's ophiolites correlate to north of Ireland and Scotland. Scotland's ophiolites are of similar ages to NFL's TMO. Ballantrae dates include a 478 ±8 Ma potassium – argon (K-Ar) hornblende age (Bluck 1980), and 483 Ma (Bluck 1980). The Shetland ophiolite is dated at 479-465 Ma K-Ar hornblende age (Spray 1988), 498 Ma (Finn 1991), and 492 Ma (Spray and Dunning 1991). The Highland Boundary Ophiolite (HBO) dates between 479.6 ±1.1 Ma (Cooper 2011) and 490 Ma (Chew et al 2010). Chew's HBO date of 490 ±4 Ma is from a ^{40}Ar-^{39}Ar hornblende sample. A date of 488 ±1 Ma (^{40}Ar-^{39}Ar muscovite) is from rock sample fabric and reflects an obduction age. In Ireland, the Deerpark formation dates from 514 Ma (Chew) with obduction or accretion at 510-500 Ma (Spray & Dunning 1991) to 482 Ma (^{40}Ar-^{39}Ar of muscovite, Chew et al 2010). Collectively across NFL, north of Ireland, and Scotland, these data establish a continuous arc of subduction and ophiolite formation across the peri-Laurentian region during the early Ordovician. Therefore, the TIC and Annieopsquotch ophiolite belt represent ophiolites formed in SSZ settings, obducted onto their associated arcs.

Arc development is widespread along the Laurentian south-eastern margin. Irish arc complexes are recognised as Lough Nafooey arc, Tourmakeady Group, Charlestown Group, Grangegeeth arc, Bohaun volcanic formation, Games Loop, Mains Hill, and the Tyrone Igneous Complex (TIC). These formations represent separate arc systems whose original positions, paths and components are erased and simplified (Van Staal et al 1998). Buried arcs may exist. The South Mayo trough, a foreland basin, and the Lough Nafooey volcanic units are ocean-arc related (Draut 2004). Lough Nafooey arc volcanic accretion dates to 480 Ma (Hollis 2013). Subduction dip directions are interpreted as Pacific style (ocean directed dip, Van Staal et al 2010) and several arcs of Laurentia share laterally similar tectonism (Van Staal et al 1998). In summary, Dewey articulated a tectonic model which is comprehensive: early Ordovician ocean directed subduction, arc accretion, blocking of the subduction process, obduction, then a subduction polarity changes to continent directed subduction (Dewey J 2005).

2.2 Local geology

The TIC's lithologies are early Palaeozoic basic and intermediate lavas, tuffs, meta-sediments, meta-basites, and fine to coarse grained mafic intrusive rocks (Hollis 2013). Felsic intrusions penetrate all lithologies and bond supra-crustal and meso-crustal units. The intermediate lavas and tuffs are largely unmetamorphosed. Apart from rare examples, contacts to lithologies are thought to be tectonic, as they remain largely unexposed. Magma mixing of dolerite-gabbro, and dolerite-dolerite is common within the mafic intrusive rocks, and tonalite mixes with all other lithologies. TIC geochemistry is typical to ophiolites of SSZ settings and includes rare earth element (REE) enrichment, negative niobium (Nb) anomalies, and high field strength elements (HFSE) depletion (Cooper 2011). Europium (Eu) negative signatures are found in primitive to evolved basalts (Hollis 2012) interpreted as island arc basalts (IAB). Ocean arc accretion is an important contributor to continental crustal growth (Draut 2002, 2007) and by the early Ordovician the TIC is interpreted to of accreted against south-eastern Laurentia (Hutton, Soper, Dewey, Shackleton, Draut, Van Staal, Cooper, Hollis).

The TIC is subdivided into Tyrone Plutonic Group (TPG), Tyrone Central Inlier (TCI), and the Tyrone Volcanic Group (TVG). The TPG is obducted against and in tectonic contact with the TCI. The TCI mineral assemblages of quartz-biotite-muscovite and a metabasite mineral assemblage quartz-biotite-amphibole are documented by Hollis, Dewey, and Hartley. TCI meta-sediments and meta-basites represent the Neo-Proterozoic basin sediments of Dalradian affinity metamorphosed to lower amphibolite facies during Grampian deformation prior to 468 Ma (Chew et al 2008) and interpreted to be the root units of a micro-continent inlier to the TIC, (Chew et al 2008).

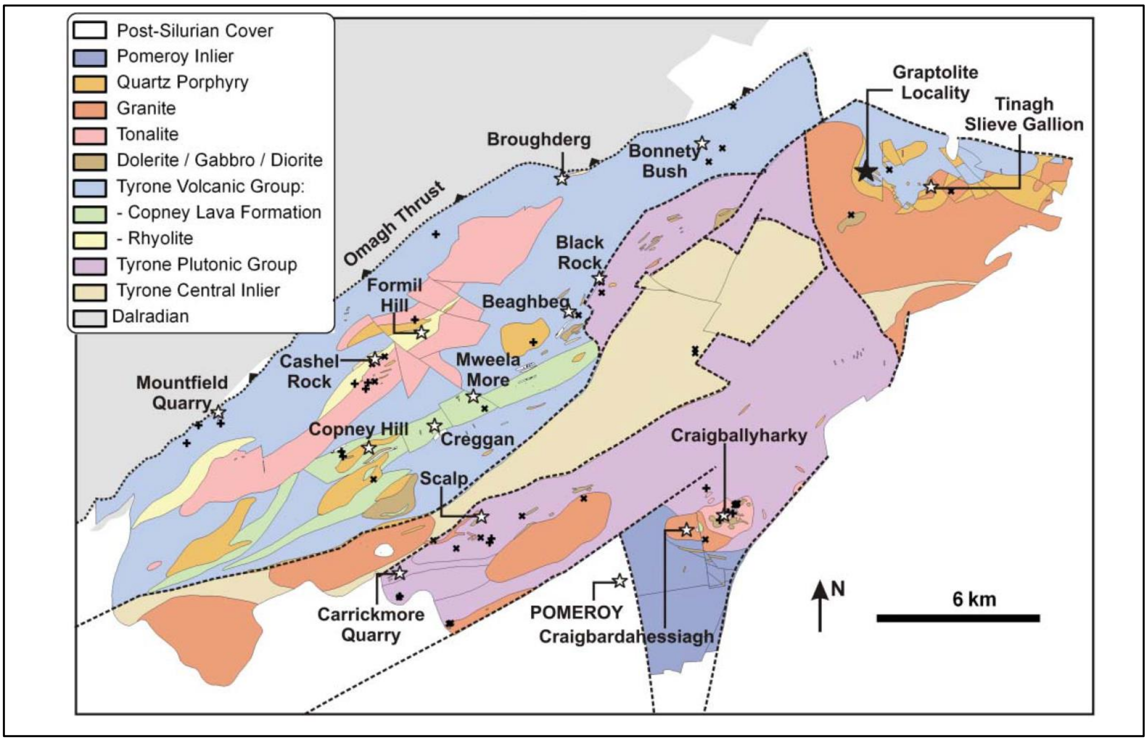

Figure 3 TIC simplified geology map after Cooper et al 2011. Tyrone plutonic Group is the equal of the TPG

The TCI rocks are metamorphosed para-gneiss and metabasites of terrigenous and volcanic derived material. The youngest zircon dated is 999 Ma (Chew et al 2008) and correlates to a Rodina origin. The TCI boundaries are thought to be in tectonic contact with the surrounding mafic units of the TPG. In outcrop, abundant quartz 'sweats' align to the dominant deformation (S_1/ S_2) strike of NE- SW - matching the regional deformation trend the Caledonian trend.

TCI peak metamorphic conditions were reached at temperatures of 670 degrees Celsius (°C) and pressures of 6.8 kilobars (kbar) (Chew et al 2008). Thus, the TCI units have a broad foliation texture, but lower amphibolite grade metamorphism has destroyed original bedding (S_0). The metamorphic assemblages prograde to biotite-plagioclaise-silliminite-quartz-muscovite-garnet. The leucosomes of the para-gneiss are zircon U-Pb dated to 467 Ma, and 468 Ma (Chew et al 2008), while TCI pegmatites date at 466 Ma and 468 Ma (Chew et al 2008). The TCI para-gneiss ages are comparable to other microcontinents of eastern Laurentia like the Slishwood, Ox mountains, and Dashwoods. Separation of the TCI from Laurentia is dated at 540-535 Ma (Cawood et al 2001). At Corvanaghan quarry within undeformed pegmatitic bodies large muscovite sheets (3 to 6 cm) and acicular tourmaline occur interpreted to be post-orogenic.

The Craigballyharky tonalite contains ophiolite roof pendants, arc material, and Proterozoic zircons (Cooper et al 2011). Magma mixing relationships give relative ages of the gabbro, dolerite, and the tonalite pluton being the youngest (Hutton 1985). Tonalite hosted zircon U-Pb dating at Craigballyharky yield 471 Ma and are interpreted to be Laurentian continental material. At Craigballyharky, magma mixing macro-textures suggest tonalite intrusion while the ophiolite was still hot and under significant temperatures and pressure (Hutton 1985). Indeed, boulders across the TPG display mixing between dolerite, gabbro, and tonalite magmas, such as Blaeberry rock which shows gabbro-dolerite, gabbro-tonalite mixing and syn-deformation structures (Hollis 2013). Inter-relations of both the TPG and the TVG indicate obduction and accretion occurred together at 483 Ma (Hollis 2013), while Cooper dates these events to 479 Ma, but it is possible the high temperatures and pressures are achieved at Hutton's date of 471 Ma. The 471 Ma date is taken as the minimum age of obduction as all three components (basement, arc, and ophiolite) are in tectonic contact. Several other granitoid bodies intruding the TPG align NE-SW to the Caledonian trend.

The TPG consists isotropic gabbro, sheeted dolerite dykes, tholeiitic basaltic pillow lava, tonalite, large serpentinite bodies, and ultramafic rocks. Gabbro formation dates range from 493 M (Draut 2009) to 483 Ma of olivine pegmatic gabbro (Hollis 2013), and layered gabbro at 479 Ma (Cooper 2011). The gabbro fabrics record intense and multi-phased fold events, up to 5 generations, and locally form schist layers. Poorly defined litho-geochemistry and characterisation of the basic rocks (due to limited exposure) means mapped lithologies are mainly undifferentiated, and room for improvement exists. The gabbro's primary mineralogy is of hornblende-epidote-actinolite-chlorite minerals with a groundmass of quartz-amphibole-actinolite-chlorite-epidote with lesser zircon-titanite-sericite-biotite-carbonate (Hollis 2013). Layered gabbros are present at (Hollis et al 2012) and magnetite layered gabbros, Figure 4 (Tellus total magnetic intensity (TMI) images). Supra-subduction zone ophiolite geochemistry typically has large ion lithophile element (LILE) (K, Rb, Cs, Th) and light REE (LREE) enrichment, with HFSE depletion (Ti, Nb, Ta, Hf) relative to Mid-Ocean Ridge Basalt (MORB). Therefore, trace element geochemistry interprets the Tyrone mafic suites as a SSZ ophiolite (Dewy & Shackleton 1984, Hutton 1985, Draut 2009). The TPG is close to surface where several outcrops contain sulphide mineralisation, e.g., Orritor. In the Orritor area, anomalous geochemistry is detected in stream sediment surveys and soil surveys (Tellus soil survey and Rio Tinto Zinc (RTZ) soil survey).

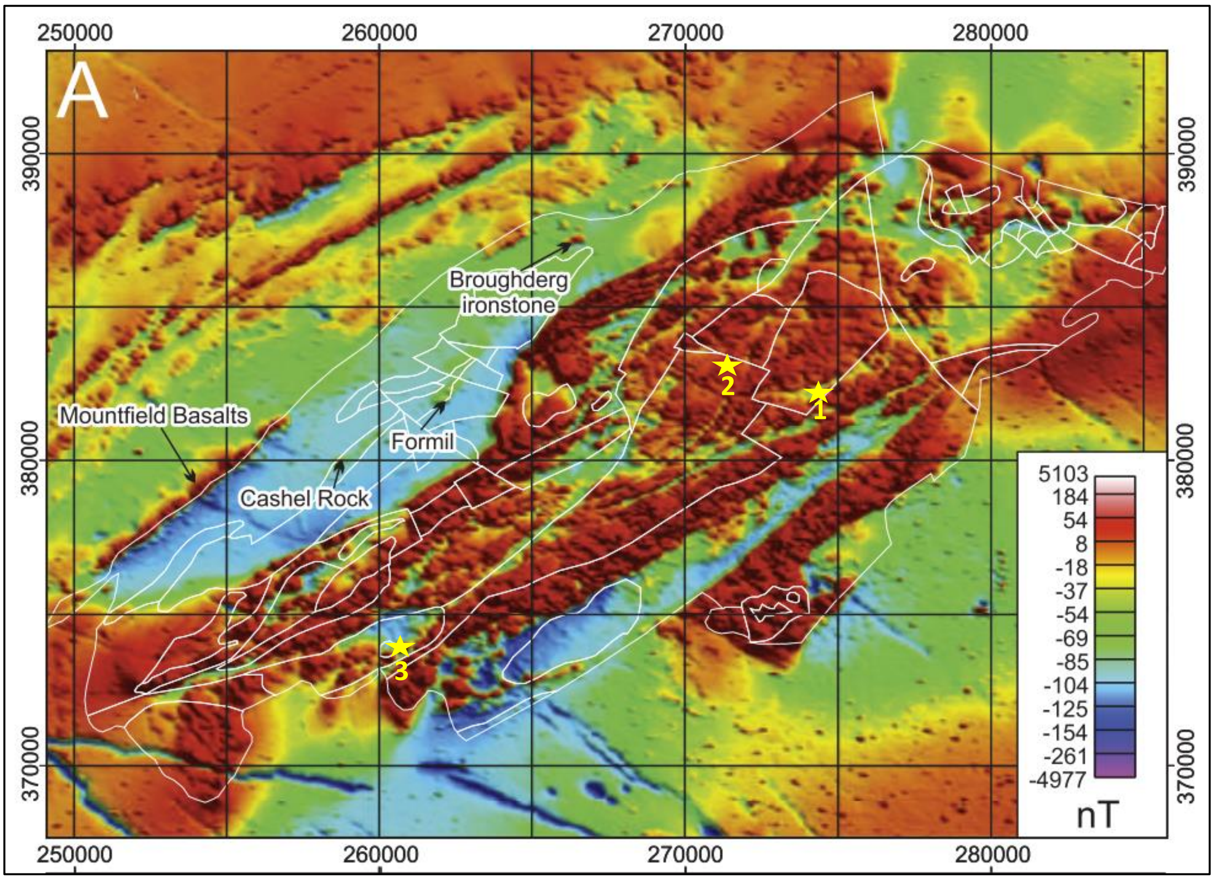

Figure 4 Tellus TMI RTP image with GSNI line map of the 1:250,000 TIC. NW-SE TMI highs are possible magnetite banding. Highlighted are the locations of Orritor Quarry, TPG (1), Corvanaghan Quarry TCI (2), and Carrickmore Quarry TPG (3). Hollis et al 2016

Extrusive volcanic rocks evolve up-sequence. The TVG begins with primitive (enriched in titanium and iron) mid-ocean ridge basalts (eMORB) and date to 475 Ma (Cooper 2011) and 469 Ma (Hollis 2013). Later, rift lavas are low Ti tholeiites, interpreted as mid-ocean ridge basalt (MORB), eMORB, and back arc basin basalts (BABB) (Piercy 2011). At the Sleive Gallion section of the TVG, three formations are defined geochemically: the Twaney Formation (Fm), The Windy Castle Fm and the Tinagh Fm. The Tinagh Fm is calc-alkaline lavas and tuff with non-arc eMORB. Twaney Fm is eMORB to Ocean Island Basalts (OIB). In mafic volcanic rocks, LREE depletion usually indicates a tectonic setting of an intra-oceanic arc, such as a negative Nb concentration against MORB LREE levels (Draut 2002, Hollis 2013, Hutton 1985). The lavas of the lower TVG are depleted in LREE, low in silica (SiO_2), low Zr/Y, and although high in magnesium oxide (MgO) they are interpreted as primitive arc basalts. The Windy Castle Fm and the Tinagh Fm, enriched in LREE, are calc-alkaline andesites and tuffs and occur stratigraphically above the primitive basalts. The intermediate volcanics are interpreted as evolved lavas. Therefore, volcanics and tuffs evolve as one passes up the stratigraphy and reflects an increase in continental crust supply - rich in LREE content (K and Ba) - consistent to the model of Phanerozoic slab subduction and arc development prior to accretion (Draut 2002 & 2009).

2.3 Metallogeny

Hydrothermal fluids, associated with extension and rifting, can manifest at surface as ironstones or exhalative horizons, formed at the surface and in the subsurface layers. The TVG has numerous occurrences of ironstones such as Brougberg, and Slieve Gallion (Hollis et al 2013). Exhalative horizons of the TVG are blood red in colour, aphanitic, silica rich with veining quartz, and have a quartz-hematite-magnetite mineral association. Trace element geochemistry studies of exhalative horizons (high Eu, Cu-Pb-Zn, Au, Fe/Ti, Fe/Mn, Fe+Mn/Al, and low REE) indicate vent proximal signatures (Hollis et al 2015). Often proximal to zoned sulphide mineralisation (Hollis et al 2016), the trace element geochemistry of ironstone exhalative horizons can be used to vector to massive sulphides.

Arc and orogeny related type sulphide deposits of the Caledonian trend are volcanogenic massive sulphide (VMS), orogenic gold, and porphyry intrusion. Arc terranes are well known hosts to VMS deposits (Herrington et al 2005, Hollis et al 2013) and arc-orogen belts host dual deposit types of VMS and orogenic gold, such as the Abitibi belt and NFL. Exceptional VMS deposits in Atlantic Canada form in sedimentary basins and relate to prolonged extension. Deposits such as New Bruswick's Bathurst number 12 mine totalled 229 Mt with a polymetallic lode of 7.7% zinc, 3% lead, 0.5% copper, 91 grams per tonne (g/t) of silver, and 0.46 g/t gold. The Bathurst deposits are south of the Iapetus suture in Gondwana terrane, but many deposits occur at or north of the suture, or Red Indian Line, e.g., Huntington Qubec 11.8 Mt with 0.9% copper, and the Buchans deposits in Newfoundland where the total number of VMS deposits is over 40. The Buchans-Roberts Arm arc is a type example of Kuroko VMS sub-types, host to 16.2 Mt of high-grade Zn-Pb-Cu-Ag-Au, and may be a correlative of the TIC (Hollis 2016). Rift related eMORB type basalts within felsic volcanic sequences are prospective for VMS type mineralisation (Hollis et al 2012).

With a confirmed history of arc development and rifting, the MVT is a possible setting for VMS type mineralisation. Indeed, mineralisation on the TIC occurs as gold and base metal showings of the volcanic group members (Hollis et al 2013). Geochemical and geological inferences led Hollis to interpret these showings as VMS related. Silicified boulder mineralisation and recent drilling of the TVG identify sub-economic gold and copper concentrations (Hollis, pers. comms. June 2019). In Ireland, the Charlestown VMS deposit occurs in the accreted arc terrane of the Irish MVT, increasing the terrane's potential for further VMS style deposits.

Other deposit styles may occur. Intrusion related, epigenetic base metal occurrences, such as those in in Scotland (Doon Loch and Carinsmore of Fleet), may be the source of metals for the 18th and 19th Century mining districts of the SULDT of Ireland and Scotland e.g., the mining district of South Armagh. A history of base metals Pb-Zn-Sb mines in SULDT correlates to the Dunnage zone of NFL and Atlantic Canada where intrusion related epigenetic base metal deposits occur. On the SULDT gold occurs as very fine and refractory, sub-economic grades. Remobilisation of the SULDT gold may occur, and hydrothermal Pb-Zn-Cu-Ag epigenetic vein emplacement using transverse structures during extension. Economic orogenic gold deposits are hosted within the Grampian terrane with two in production and one in development. The Curraghinalt deposit of Northern Ireland has a mineral resource of 6 million ounces gold (https://dalradian.com/) and sulphide dating at 456 Ma (Rice 2016). Further potential for VMS exists in the SULDT, while metals concentrated in carbon rich shale lenses of the SULDT may act as a trap for primary ore deposition, or as a source for further remobilisation.

SSZ Ophiolites occur throughout the Caledonian-Taconic trend and are associated with significant mineralisation. From the Leka ophiolite of Central Norway to Shetland's chromite pits, Vildin's sulphide deposit, and the Baie Verte ophiolites of Newfoundland, magmatic sulphide deposit types occur with significant copper-cobalt mineralisation. The latest rifting episode at 65 Ma is seen in the Antrim flood basalts, part of the North Atlantic Igneous Province (Mitchel 2014). At rifting, the global position of the basalts is interpreted to be in the low latitudes due to extensive tropical weathering. The tropical weathering profile is 3-8 metres (m) deep and enriches the weathered zone in iron and aluminium. This iron-aluminium enrichment gives laterites and bauxites.

Collectively, these ore deposit types make a metallogenic belt in the Caledonian terranes of Ireland and Scotland, with important extensions along strike in Scandinavia and Atlantic Canada.

3. Methodology and Results

3.1 TIC field work

3.1.1 Magnetic Susceptibility

The magnetic properties of minerals and rocks is a useful tool for identifying mafic rock types in the field and in the interpretation of magnetic survey reduction images (Dentith 2015). The magmatic gabbro in the Orritor and Carrickmore quarries contain a remnant magnetism of their bulk minerals, which is resistant to regional metamorphism (Dentith 2015). In addition, sulphide ore deposits and alteration, such as serpentinization, have a strong effect - increasing magnetism with serpentinization and decreasing olivine and orthopyroxene (Dentith 2015). Therefore, interpretation of the airborne Tellus magnetic regional survey, such as Figure 4, relies on *a priori* knowledge of the rock type's magnetic properties and structural data.

Magnetic susceptibility (SI) readings, taken of the dominant lithologies at Carrickmore and Orritor quarries using a portable magnetic susceptibility meter, or MagSus. When rock types recognised in the field are targeted with the MagSus, the charts of the measurements have clear groupings, Figures 5 and 6. Basic statistical descriptions are shown in Tables 1 and 2. At Orritor the total count was 201 measurements across six rock types and provided median (avg.) susceptibility for ultramafic rocks at 281 x10^{-3} SI, gabbro at 119 x10^{-3} SI, altered gabbro at 1.91 x10^{-3} SI, sheared gabbro at 1.38 x10^{-3} SI, dolerite at 2.44 x10^{-3} SI, and pegmatite at 0.24x10^{-3} SI. At Carrickmore 102 measurements across three rock types defined in the field provided avg. susceptibility for gabbro of 10.6x10^{-3} SI, altered gabbro 0.27x10^{-3} SI, and gossan 0.37x10^{-3} SI.

These MagSus measurements demonstrate the ultramafic very high magnetism (median value of 281 x10-3 SI) and the gabbro's high remnant magnetism. Where lithologies are altered a reduction in MagSus represents magnetite destruction, inset of Figures 5 and 6. Therefore, the ultramafic rock can be classified as highly magnetic, followed by gabbro, and altered gabbro. Dolerite, sheared gabbro and pegmatites can be classified as non-magnetic. The specific type of alteration resulting in magnetite destruction in unknown, but shear associated with the brittle-ductile shear zone of the quarry certainly decreases magnetism by destruction or removal of magnetite. An increase in silica from late hydrothermal alteration associated with stockwork veins may explain some of the altered gabbro de-magnetism. Under normal conditions serpentinization involves magnetite formation, along with silicification, and growth of green minerals such as epidote and chlorite. Findings from these results can be applied to the Tellus magnetic images of the TIC and aid further interpretation of the ophiolite.

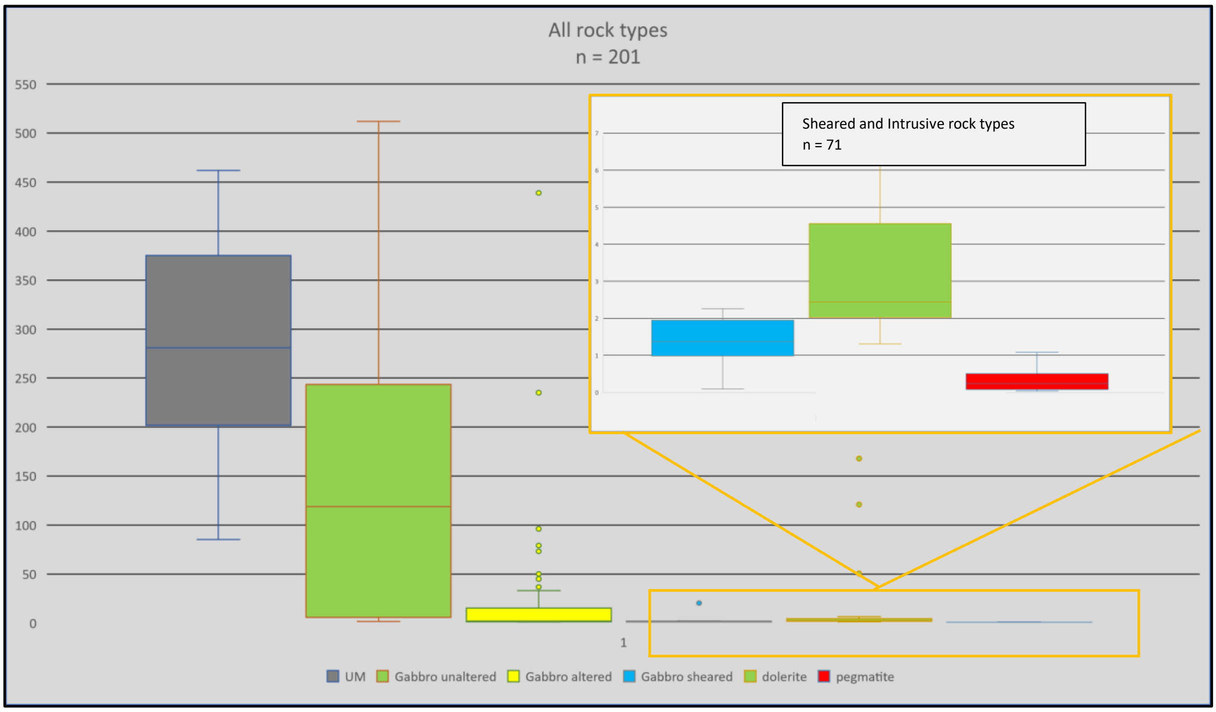

Figure 5 Susceptibility (SI x10^{-3}), Orritor Quarry, inset shows very low magnetic properties for sheared gabbro, dolerite and pegmatite.

Table 1 Descriptive statistical summary, MagSus readings, Orritor quarry.

	UM (SI x10^{-3})	Gabbro unaltered	Gabbro altered	Gabbro sheared	dolerite	pegmatite
min	*85.4*	*1.57*	*0.467*	*0.09*	*1.31*	*0.032*
max	*462*	*512*	*439*	*20.3*	*220*	*1.08*
median	281	119	1.91	1.38	2.44	0.2395
standard dev	*91*	*117*	*33*	*3*	*29*	*0.24*
n=	*15*	*58*	*57*	*12*	*33*	*26*

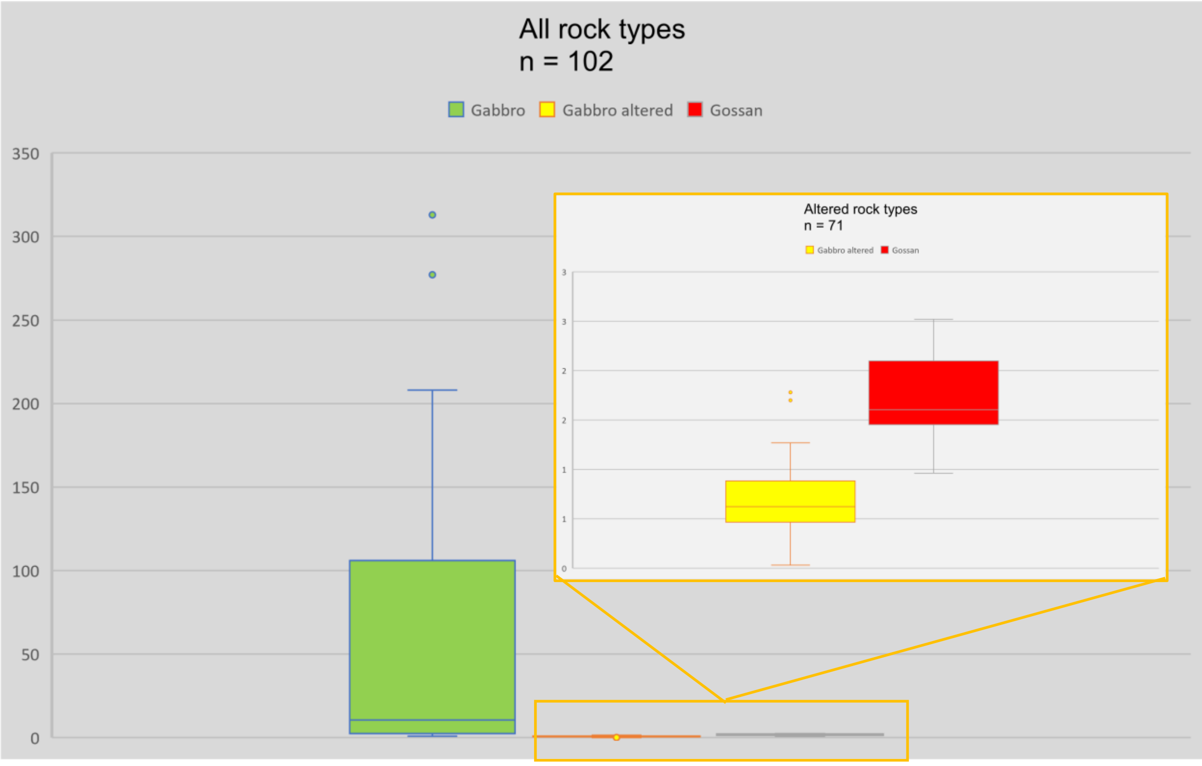

Figure 6 Susceptibility (SI x10⁻³), Carrickmore Quarry. Inset shows very low magnetic properties for altered gabbro and gossan.

Table 2 Descriptive statistical summary, MagSus readings Carrickmore quarry

	Gabbro (SI*10-3)	Gabbro altered	Gossan
min	*0.828*	*0.032*	*0.963*
max	*313*	*1.78*	*2.52*
median	*10.6*	*0.6*	*1.6*
standard dev	*71*	*0.27*	*0.37*
n=	*31*	*49*	*22*

3.1.2 pXRF

An Olympus Delta^{TM} DP 6000 pXRF unit with prolene film was used for field-based sample screening, and identification of sulphides. The correct radiation safety training was given prior to use by Onephoton Ltd, Broughshane, Northern Ireland (NI) - funded by Shackleton Resources Ltd. Based on the findings of an in-house orientation study which assessed both accuracy and precision, operation of the pXRF used rock/ geochem mode and 30 second beam time. With a manufacture date of Sep-2012, the unit does achieve analysis of light elements – elements with a Z value <18. One element of interest is magnesium (Mg), Z = 12, and while the element is missed in some serpentinite samples, the non-vacuum (normal) void between the sample and detector is estimated to be the reason for the discrepancy in not registering Mg in serpentinites with every analysis (Adams 2020). Routine QAQC was performed on each start up with the standard material of the Olympus calibration disc. When analysing a sample, a flat surface was chosen. The primary target of the field work was to identify sulphide mineralisation, host to cobalt, for later lab analysis. Subsidiary pXRF targets, or general usefulness in the field, was to supplement the MagSus measurements, the identification of minerals, mapping of large structures, vein textures, and alteration. During quarter 1 of 2020 five locations were visited, Figure 7. Using the pXRF, 14 samples were selected for thin section. In addition, key lithologies of the TCI and TPG were collected for reference material, and samples of key veining and breccia textures. The pXRF unit proved highly useful in the field to discriminate between sulphides and to select samples for thin section based on their sulphide and trace elements of interest: cobalt (Co), copper (Cu), nickel (Ni), chromium (Cr), iron (Fe), magnesium (Mg), bismuth (Bi), lead (Pb), and silver (Ag).

3.1.3 pXRF Results

Table 3 displays peak concentration data collected from the pXRF targeting sulphides. Peak concentrations for Orritor disseminated sulphide mineralisation are 2,012 parts per million (ppm) Co, 2,239 ppm Ni, 2,200 ppm Cr, 12% Fe and 18% Mg. Peak concentrations for Corvanaghan Quarry are 1,999 ppm Co, 1,669 ppm Ni, 3,199 ppm Cr, 16% Mg, and 6.2% Fe.

Table 3 Summary table showing peak pXRF trace element concentrations at different sample sites.

Location	Peak ppm							Peak %	
	Co	**Cu**	**Ni**	**Cr**	**Bi**	**Pb**	**Ag**	**Fe**	**Mg**
Orritor	2,012	117	2,239	2,200	-	-	-	12	18
Corvanaghan quarry qtz-py, T1	1,999	658	-	-	26	438	-	33	-
Corvanaghan quarry qtz-tourmaline-py, T2	658	170	84	-	2	190	-	29	2.4
Corvanaghan quarry serp	547	-	1,669	3,199	-	-	-	16	6.2
Golden Hollow	810	23,388	-	-	31	49	38	21.6	-
C. Patrick	500	-	3,000	1,000	-	-	-	-	-
Carrickmore	<400	900	<400	<400	-	-	-	-	-
Ballantrae, Falcon cove	-	-	2,200	3,100	-	-	-	-	-
Ballantrae, Swaneys cove	1,300	7,200	3,200	1,800	-	-	-	30	-

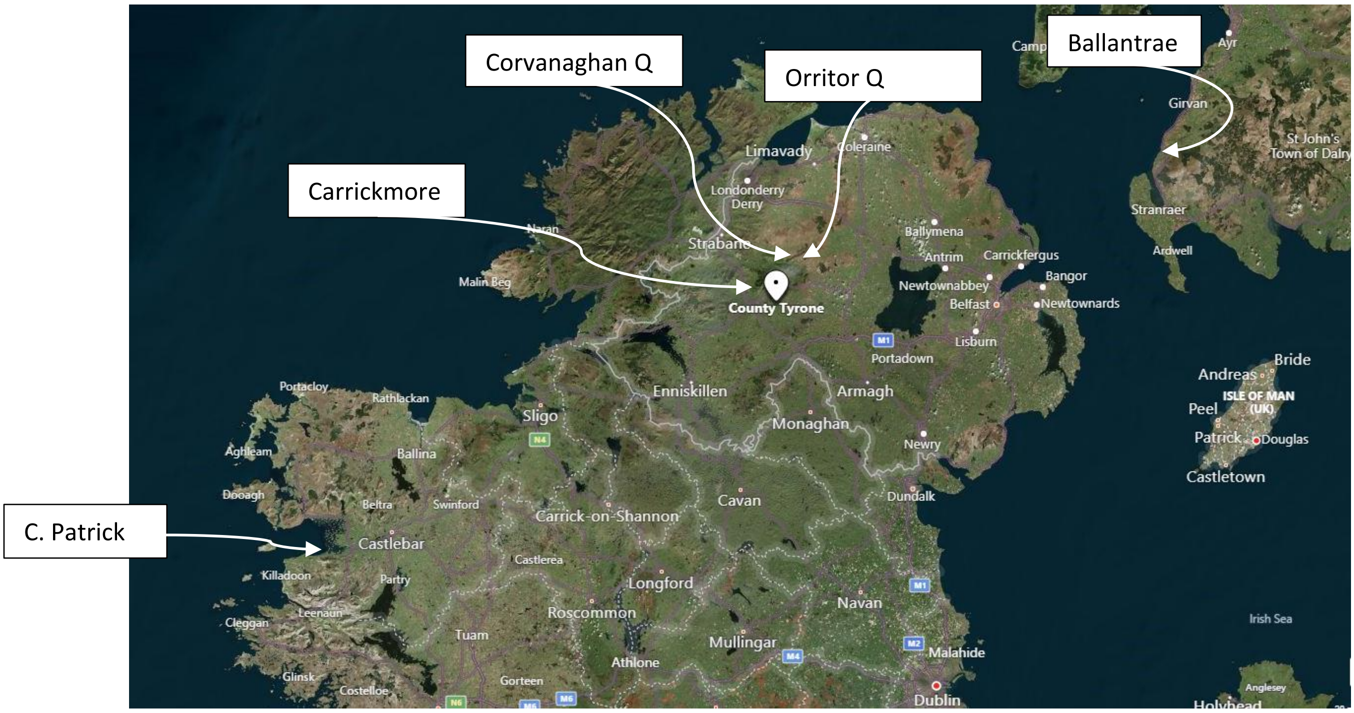

Figure 7 Field sites and pXRF sample locations. Source: Bing maps.

3.1.4 Whole rock geochemistry

Whole rock geochemistry data were made available for this project by Shackleton Resources. During a prospecting campaign, Shackleton Resources collected rock grab samples from quarries and streams which were analysed by ALS, Loughrea for gold and trace elements under the ALS laboratory codes Au-ICP21 and ME-MS61. The ALS laboratory maintains an internal lab quality assurance quality control (QAQC) for these codes and the results received detail the standards used in the analysis of these Shackleton Resources samples. Sample selection targeted sulphides found in veins and rocks. Compared to pXRF results, the whole rock dataset represents accurate concentrations of major and trace element on a meso-scale associated with the study areas.

The Shackleton Resources dataset includes a total of 24 whole rock geochemistry samples from the Corvanaghan Quarry, Orritor Quarry, Golden Hollow, and Carrickmore Quarry. These samples gave peak analysis values of 1,200 ppm Co, 2.7% Cu, 5,960 ppm Bi, 61.5 ppm Ag, 0.332 ppm Au, and 24% Fe. A summary statistical table is shown, Table 4.

Table 4 summary table for elements of interest.

	Co ppm	*Cu ppm*	*Bi ppm*	*Ag ppm*	*Au ppm*	*Fe%*
min	3.9	6.7	0.02	0.02	0.001	1.65
max	1,200	27,000	5,960	61.5	0.332	24.1
mean	262.4	1,558.6	1,013.6	7.3	0.039	10.2
standard deviation	357.6	5391.7	1505.4	13.4	0.1	5.9
count	24	24	24	24	24	24

Comparison between whole rock and pXRF datasets can be made for the elements of interest. Some caution is used when interpreting pXRF results e.g., concentrations of light elements are not accurate using in the XRF detector. In addition, the field use of the pXRF targets heterogenous minerals in an unprepared sample. Without preparation, which homogenises a sample, results of the pXRF are treated with extra caution as errors may be large.

Samples with both whole rock geochemistry and pXRF analysis data are plotted in Figures 8 and 9. The correlation shows the pXRF over-reports for most elements of interest Ag, Bi, Co, Cu, and Fe (e.g., Figure 8, cobalt). Ag in high-grade whole rock samples (61.5 ppm) correlates well with the XRF (38.6 ppm) when the high-grade samples are targeted. Overall, the pXRF analytical capabilities are deemed to be accurate for screening purposes, i.e., Figure 9 - the accuracy of pXRF high-grade copper grouping is confirmed with laboratory analysis, with a relatively high precision.

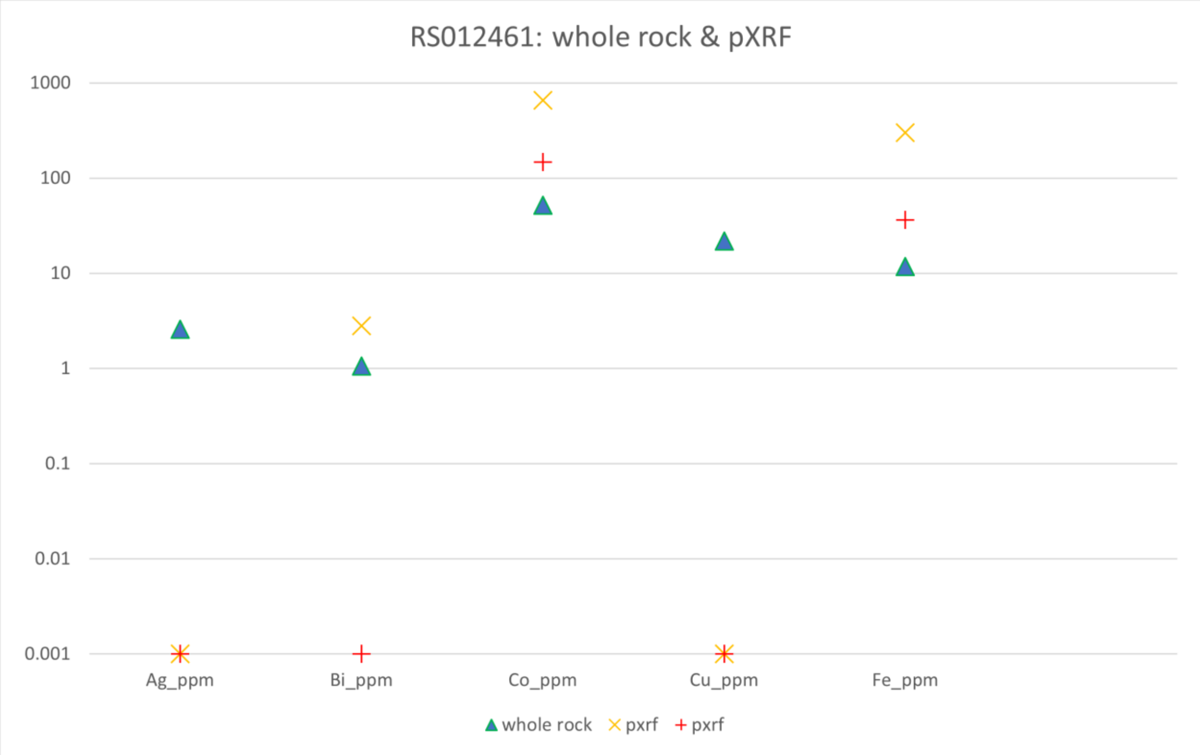

Figure 8 Sample RS012461, log scale correlation between lab and pXRF data. Corvanaghan Quarry en-echalon vein, T2. Two pXRF readings were made for each sample, seen as a yellow cross, and a red plus.

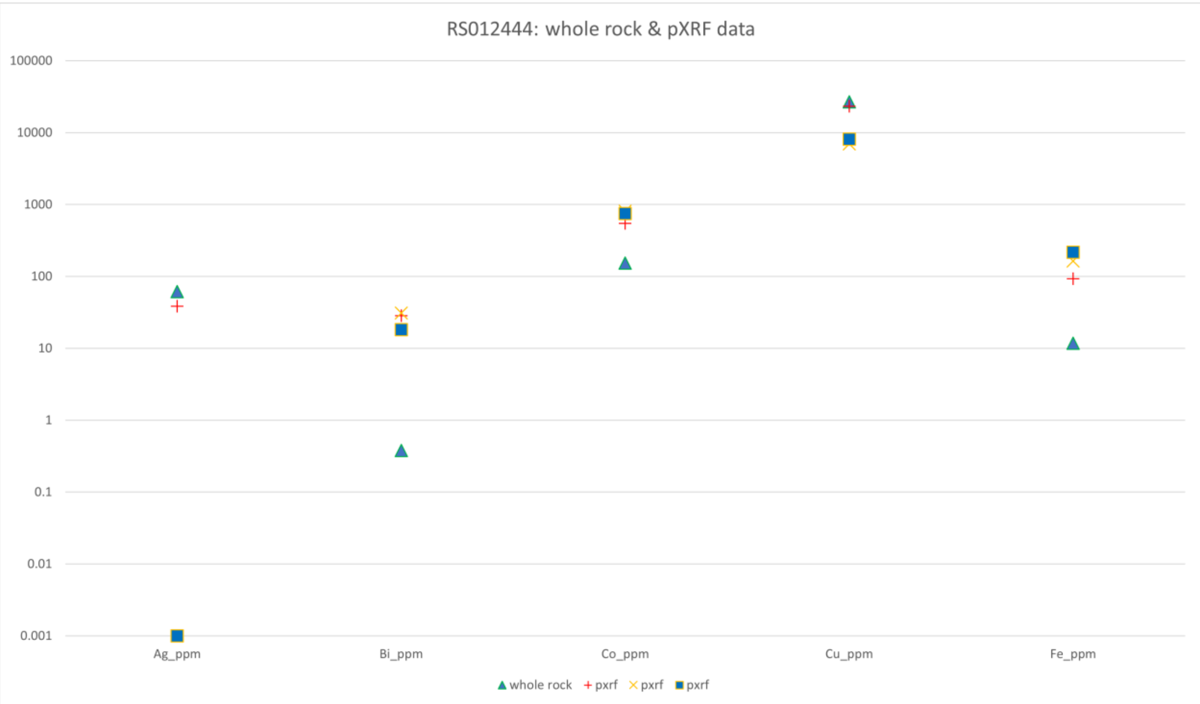

Figure 9 RS012444, log scale correlation between lab and pXRF data. Golden Hollow MS type. Three separate pXRF results are shown by a red plus, a yellow cross, and a green square.

3.1.5 Field Observations

At Carrickmore Quarry outcrop is well exposed. Vertical sheeted dolerite dykes and medium grained gabbro are seen in excellent and dramatic exposure. Sulphides are present as fracture hosted pyrite, chalcopyrite, and bornite. Widespread and pervasive alteration of purple and pale colour is seen in a western section of the quarry, Figure 22. Altered basalt-dolerite sections are pale purple to green, possibly bleached, and host to disseminated sulphides, Figure 25, which are too small for use as thin section material. Alteration is interpreted as argillic alteration of the mafic ophiolite to produce clay rich rocks containing chlorite, and possible smectite. In addition, a horizontal silica rich horizon of 30cm is immediately above the alteration and in stratigraphic contact. The silica rich layer contains has iron hydroxide staining on weathered surfaces and is interpreted as a cap gossan, Figure 23. Therefore, Carrickmore represents the alteration halo of a possible buried VMS deposit based on the field relations of host rocks, sulphides, alteration, and gossan.

At Orritor Quarry isotropic course gabbro and micro-gabbro are unaltered, and host black, amphibolite-sulphide rich material. Ultramafic float material, interpreted as quarry derived, are possibly a pyroxenite. The black ultramafic rocks contain cobalt in disseminated sulphide minerals where the black colour may be black chlorite, amphiboles, olivine, pyroxene, or assemblages of these minerals. Based on the pXRF results at Orritor, black ultramafic cobbles were selected for this section sampling as TS03 and TS04.

The serpentinization alteration reaction produces a talc-magnetite-quartz mineral. This classic serpentinite occurs at Orritor quarry location and the Tellus TMI image, Figure 4, shows possible magnetite banding (Hollis, pers. comm, June 2020). Alteration of gabbro in the quarry is silicified, with thin anastomosing (stockwork texture) veining of quartz-epidote-sulphide (+hematite) assemblage. Magnesite is identified on joint surfaces, Figure 16. Serpentinites are in immediate proximity to a vertical, east-west orientated, brittle-ductile shear zone, Figure 13. The shear zone is large-scale, with a zone of influence over 4-10m, and a gouge clay core of 1m. In addition, the shear zone is host to thin felsic sheets, 20 to 30cm wide. With coarse crystals pink feldspar and quartz, these felsic dykes are interpreted at pegmatite veins, Figure 15. The pegmatite's texture shows them to be syn-deformation to the shear. Talc present on the pegmatite contacts indicating continued shear post-crystallisation. These pegmatic sheets may be the only syn-orogenic intrusions outside of Connemara's syn-orogenic magmatism (Cliff et al 1996).

Corvanaghan quarry is the largest and most extensive quarry on the TCI. At Corvanaghan quarry, persistent, planar, north-south fractures are host to banded quartz-tourmaline veins. Sulphides occur as pyrite filled tension gashes in en-echelon arrangement within the quartz-tourmaline banded veins, and are seen in large boulders, Figure 28. In addition, thick quartz-sulphide veins are seen which contain significant concentrations of cobalt, bismuth, and silver in pyrite and lindstrome, a silver-bismuth sulfosalt (Stratford 2019, Figure 26). Importantly, northwest-southeast (NW-SE) orientated fractures host the quartz-sulphide veins which pinch and swell in thickness. The quartz-sulphide veins are exposed high in the quarry's north face and contain anomalous trace elements Co-Pb-Bi-Ag. The TCI structural features are complex involving brittle-ductile structural features and multiple hydrothermal veins.

3.1.6 Vein types

Within Corvanaghan quarry two mineral assemblages are exposed as veins: quartz-sulphide veins, Type 1 (T1), and quartz-tourmaline-pyrite vein, Type 2 (T2). As mentioned, T1 veins have a pinch and swell geometry and brecciate the paragneiss wall rock. A study on the microstructures, by Trinity College Dublin (TCD) for Shackleton Resources, show pyrite brecciated textures (Stratford 2019). T2 type veins are hosted in persistent, planar, north-south orientated fractures, steeply dipping to the east, and display distinctive internal texture of en-echelon sulphides. Field sampling with a pXRF confirms T1 high cobalt concentrations, Table 3. Sulphides are sampled, T1 is sampled as TS01 and T2 vein sampled as TS02. In the quarry, field relationships of T1 and T2 are not visible, and relative ages cannot be determined. However, Figures 10 and 11 select the elements of interest Au, Ag, Co, Cu, and Bi with these data normalised to 100%. Figure 10 demonstrates in T1 veins high-grade cobalt correlates well to high concentrations of bismuth. Figure 11 displays T2 veins where lower grades or concentrations across all elements of interest are seen, and a correspondingly weaker correlation between bismuth verses cobalt values.

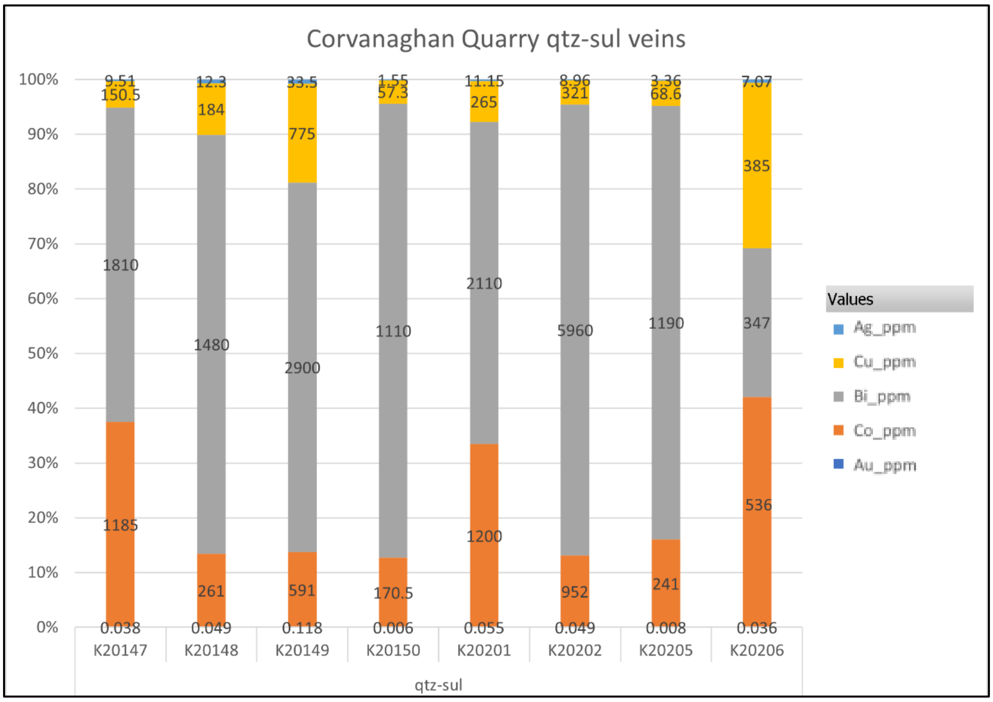

Figure 10 Corvanaghan Quarry quartz-sulphide veins T1. High-grade cobalt with associated elements of interest.

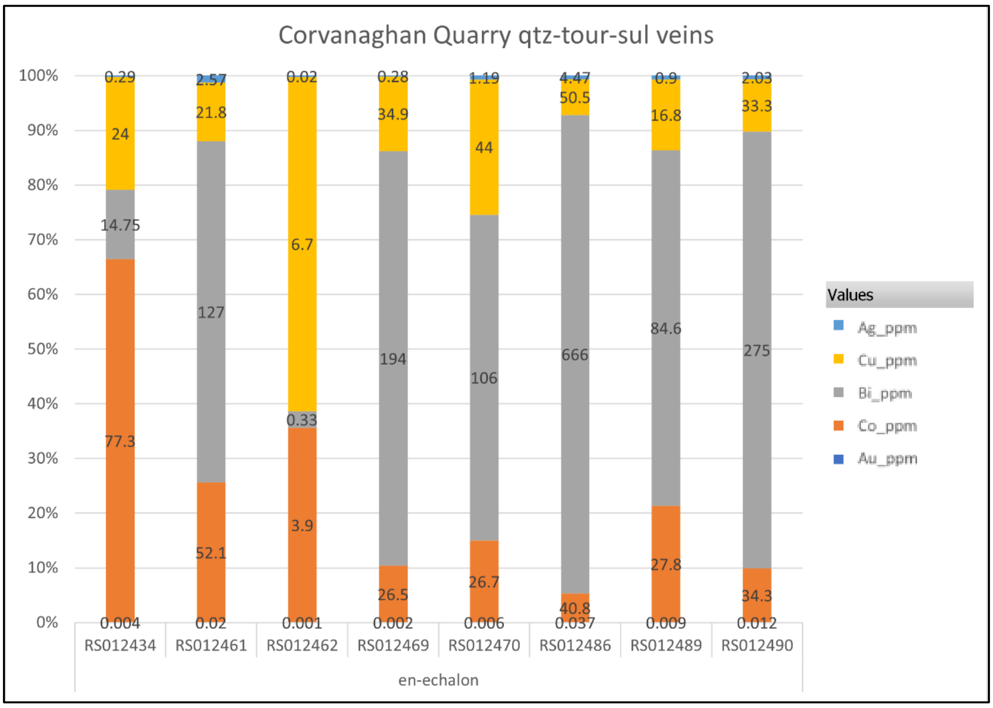

Figure 11 Corvanaghan Quarry quartz-tourmaline-sulphide veins. Low-grade cobalt with associated elements of interest.

On the Tyrone ophiolite (TPG), different sulphide mineralisation types are seen. In addition to vein hosted sulphides (Figure 26), sulphides are present as disseminations (Figure 12, Orritor quarry), and fracture hosted (Figure 24, Carrickmore Quarry). However, sulphide mineralisation in a boulder at Golden Hollow, Figure 27, between Orritor and Corvanaghan quarries, shows silica and sulphides flooding an altered mafic rock. Shackleton Resources whole rock geochemistry (RS012444) gives peak values of 27% Cu, 4,520 ppm Bi, 9% S, 61 ppm Ag, and 0.332 ppm Au. A sample of the boulder's sulphides is made for this study as TS05, Table 5. The Golden Hollow boulder mineralisation type may be classed as sulphide flooding, or massive sulphide.

Lastly, at Orritor quarry, the stockwork veins are hosted in serpentinites. Shackleton Resources whole rock geochemistry (sample K20232) contains 0.096 ppm Au, 2.5 ppm Ag, 6 ppm Bi, 199 ppm Co, and 664 ppm Cu (and pXRF peak results yield 3,000 ppm Cu and 1,000 ppm Co). pXRF analysis of the gabbro host rock minerals give 8% Mg and 13% Si. High gabbro Mg and Si percentages denote serpentinisation to produce magnetite, magnesite ($MgCO_3$), and Mg silicates.

3.2 Regional field work

At Croagh Patrick in County Mayo, the pilgrim route follows for its lower part good exposure along the stream. The stream section was mapped (Appendix, section 6.6), where ophiolite mafic rocks, shearing, and serpentinite rocks are seen. Away from the stream the Deerpark ophiolite was traversed. During the traverse, three samples were taken, of which one shows significant sulphide mineralisation, Figure 21. LA ICP-MS samples were selected on field observations of intense alteration, sulphide concentration, and screening using the pXRF. High background values of nickel, chromium, and copper are seen in the pXRF analysis on the Deerpark ophiolite. Peak pXRF results are 300 ppm Co, 2,700 ppm Cr, and 3,300 ppm Ni. Samples of the Deerpark ophiolite selected for thin section and LA ICP-MS are TS10, TS11, and TS12.

At Ballantrae, on the south-west coast of Scotland, excellent coastal sections of mafic basalts pillows, dolerite, and agglomerates of the Ordovician ophiolite give significant sulphide showings. Agglomerate float material containing sulphides is present on the northern beaches at Pinbain Burn. To the south at Swaney's Cove, a quartz-carbonate-sulphide vein brecciating pillow lavas and dolerite is seen at low tide, Figure 20. Continuing south, at Snib's Cave, outcrop cut from the current wave platform shows vertically dipping pillow lavas with inter-pillow ironstones and, significantly, sulphides, Figures 18 and 19. At Snib's Cave, inter-pillow sulphides were sampled (TS14). The styles of mineralisation seen and sampled at Ballantrae are interpreted to be hydrothermal vein type (sample TS13), and mafic VMS type setting (sample TS14). A summary of samples selected for thin section and LA ICP-MS analysis is shown in Table 5.

Table 5 Sample description for thin section, and LA-ICPMS analysis. Highlighted in green are the samples with traceable results.

Sample	Location	Setting	Type	sulphides	Hand Sample Description
TS01	Corvanaghan	quarry	SC	Py vein hosted, semi massive	grey + white qtz-py vein material
TS02	Corvanaghan	quarry	SC	py/ cpy veins, en-echalon	qtz-tourmaline-py/cpy vein. Py + bournite assoc n-s structure
TS03	Orritor	quarry	SC	Py disseminated	Black, med grained, mineral alignment/ foli, amphibole/ pyroxenes. SiO_2 <45%. Serpentine ultramafic
TS04	Orritor	quarry	SC	py/ phyrr 5%	UM, high mag intensity w/ MagSus, black fine grained
TS05	Golden Hollow	stream	float	py/ cpy 30%, sulphide flooded	Boulder. Fresh surface black, fine grained silica + sulphides
TS06	Carrickmore	quarry	OC	fresh sulphides and malachite	banded qtz rich lens, grey qtz, w/n med grained altered and bleached k-fld & qtz. Extensive alteration
TS07	Carrickmore	quarry	OC	py/ cpy stringers	black grey, fine to med grained, qtz + biotite, Dolerite host
TS08	Carrickmore	quarry	OC	tiny sulphide grains. Py	pink and white on fresh surfaces = k-fld (70%)
TS09	Carrickmore	quarry	OC	tiny blebs of fresh sulphides and bright blue azurite/ malachite	Iron oxides on all weathered surfaces. Fissile. Highly siliceous, banded in places. dolerite?
TS10	Croagh Patrick	track	OC	-	black, mafic, fine grained rock w/ moderate foliation. green serpentinite
TS11	Croagh Patrick	stream	OC	-	black, sheared mafic, mod foli, white qtz
TS12	Croagh Patrick	boulder	float	mag	orange surface jarosite, fine grained, dense, black, mafic/ UM, magnetite
TS13	Ballantrae	beach	OC	py + cpy	qtz-carb vein with sulphides py+cpy <5%. irregular, branching, & Bx texture. Host: light green, fine grained, mafic, some silicification = serpentinite
TS14	Ballantrae	beach	OC	py	MS fine grained py in 10-15cm thick pods, <30% sulphides. Intense weathered purple, jarosite on joints. Ironstone along strike

Figure 12 Disseminated pyrite/ pyrrhotite of the ultramafic rocks with high magnetic susceptibility, Orritor Quarry. Figure 13 Orritor Quarry gabbro host a steeply dipping shear zone to right of picture. Figure 14 Magma mixing of gabbros and dolerite. Figure 15 Red pegmatites with internal ductile weak deformation. Figure 16 Altered gabbro, increase in silica content and green minerals, magnesite on the surface. Figure 17 Shear fracture with slickensides indicating horizontal movement – strike slip

Figure 18 Ironstones at Snib's Cave, Ballantrae. Figure 19 Interpillow sulphides at Snib's Cave, Ballantrae. Figure 20 Brecciation of mafics with quartz-carbonate-sulphide veins at Swaney's Cove, Ballantrae. Figure 21 Orange coloured alteration, probably jarosite, of mineralised boulder at Croagh Patrick. Figure 22 Carrickmore Quarry, bleached alteration, and silica cap to left of picture. Figure 23 Top of the silica cap, limonite on surfaces

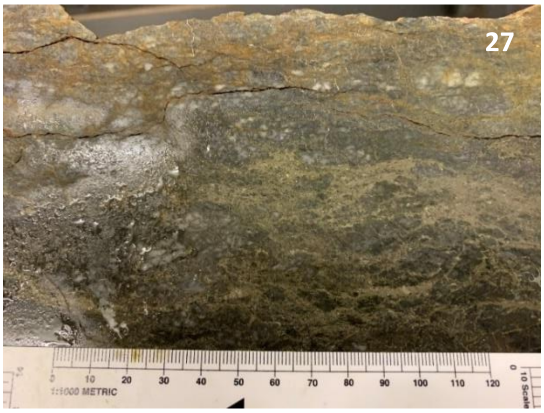

Figure 24 Carrickmore Quarry, fracture hosted sulphides. Figure 25 Carrickmore Quarry, malachite in the altered units. Figure 26 Corvanaghan Quarry T1 type veins, quartz pyrite. Figure 27 Silica and sulphide flooding of an originally mafic rock type at Golden Hollow, RS012444. Figure 28 Corvanaghan Quarry, T2 type vein of quartz-tourmaline with en-echelon sulphide phase.

3.3 LA ICP-MS Results

Fourteen samples were submitted to TCD for polished thin section sample preparation. Sulphide samples were polished by TCD laboratory and analysed in the ore laboratory at TCD. Due to the high levels of travel restrictions in force during this phase of the study, no time in the laboratory was allowed. Therefore, all the laboratory analyses were performed by TCD technicians. Elements analysed by the LA ICP-MS were manganese (Mn), Co, Ni, Cu, zinc (Zn), gallium (Ga), arsenic (As), selenium (Se), molybdenum (Mo), Ag, indium (In), tin (Sn), antimony (Sb), tellurium (Te), gold (Au), mercury (Hg), Pb and Bi. Internal QAQC for all elements was made using reference material codes: UQAC-FeSB, MASS1, and MUL-ZnS. Results for nine thin sections were received from the LA ICP-MS laboratory at TCD. The processing of results used outlier rejection of two standard deviation (2SD), baseline reverse trim of 17 seconds, baseline duration of 16 seconds, and a match cut-off of 0.4.

Of nine results, locations of only three thin sections can be identified due to poor sample chain of custody. Identification codes for 11 of the 14 samples do not match the codes of samples submitted for analysis. These location identifiable samples are called traceable samples. Traceable results are received for Golden Hollow (TS05), Carrickmore Quarry fracture hosted stringers (TS07), and Ballantrea interpillow basalts (TS14).

Tables 6 and 7 show the summary statistics for ablation sites for pyrite and chalcopyrite respectively. For pyrite, cobalt has an avg. mean ppm of 1,420, and maximum (max.) of 14,779 mean ppm. Other peak elements of interest are 2,517 ppm Ni, of 1,073 ppm Cu, 1,917 ppm As, 7.5 ppm Ag, 0.8 ppm Au, 214 ppm Pb, and 355 ppm Bi.

Table 6 Summary statistics for traceable return results (TS05, TS07, & TS14), pyrite ablation.

Pyrite, mean ppm	Co ppm	Ni ppm	Cu ppm	As ppm	Ag ppm	Au ppm	Pb ppm	Bi ppm
min	0.001	0.001	0.001	0.001	0.001	0.001	0.001	0.001
max	14,779	2,517	1,073	1,917	7.5	0.8	214.6	355
Avg.	1,420	309	84	93.8	1.1	0.1	18.1	24.5
standard deviation	3,143	511	179	298.8	1.9	0.2	44.5	68.8
variance	9,878,552	261,274	32,162	89,294	3.7	0.0	1,979	4,728
count	54	54	54	54	54	54	54	54

For chalcopyrite cobalt has an avg. mean ppm of 0.1, and maximum (max.) of 1.0 mean ppm. Other peak elements of interest are 35.8 ppm, Ni, 346,415 ppm Cu, 7.8 ppm As, 125 ppm Ag, 0.7 ppm Au, 7.8 ppm Pb, and 353 ppm Bi. These chalcopyrite ablation data are summarised in Table 7.

Table 7 Summary statistics for traceable return results (TS05), chalcopyrite ablation.

Chalcopyrite	Co ppm	Ni ppm	Cu ppm	As ppm	Ag ppm	Au ppm	Pb ppm	Bi ppm
min	0.001	0.001	346,415	0.001	0.001	0.001	0.001	4.12
max	1.0	35.8	391,318	7.8	125	0.7	7.8	353
Avg.	0.1	1.9	369,194	0.7	10.9	0.1	2.3	61.1
standard deviation	0.2	8.0	12,101	2.0	27.2	0.2	1.9	89.3
variance	0.0	63.9	146,429,157	4.0	740	0.0	3.5	7979
count	19	19	19	19	19	19	19	19

Figure 29 shows the ablation locations for thin section sample TS05 chalcopyrite - Golden Hollow. LA ICP-MS site mapping gives three of five site locations, with results displayed as histograms, Figure 30. Later figures show the ablation results for the three remaining, traceable thin sections: TS05 pyrite, TS07, and TS14.

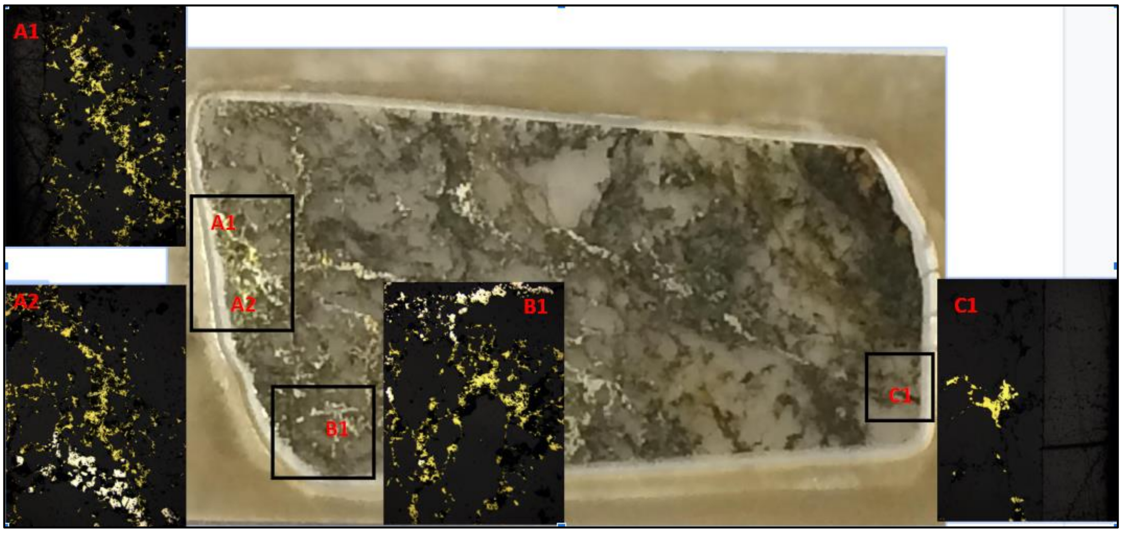

Figure 29 TS05 ablation site locations for chalcopyrite ablation.

Composite histograms of the ablation sites of TS05, chalcopyrite are presented in Figure 30. For TS05, very high values for copper are consistent. In addition to copper mineralisation, a bismuth-silver-lead association is seen with the probable mineral the silver-bismuth-sulphide sulfosalt.

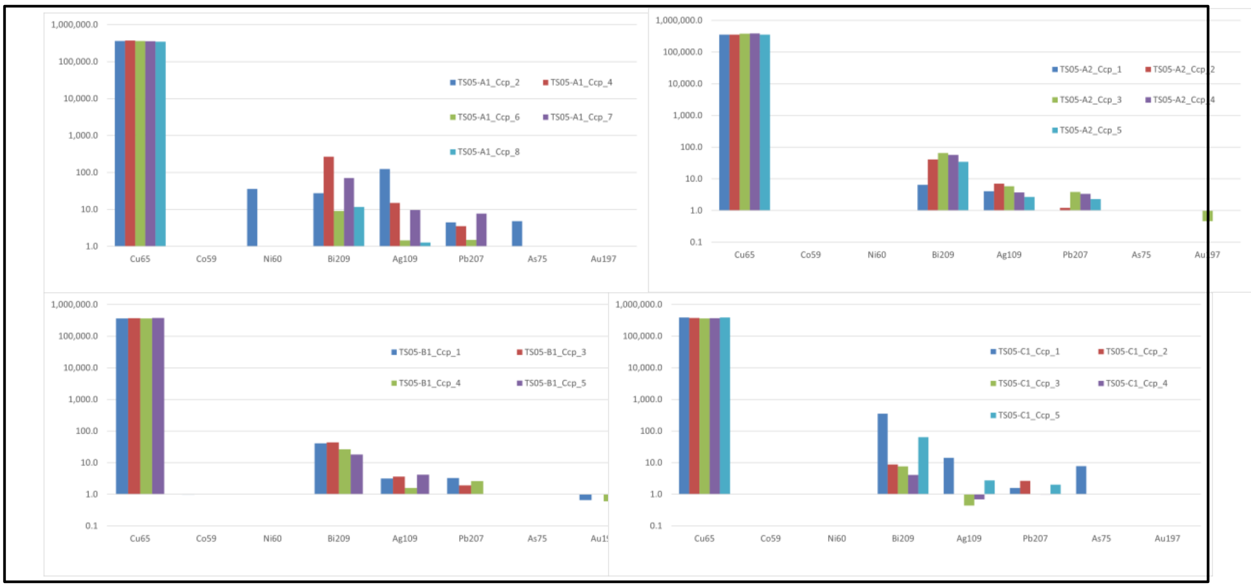

Figure 30 Results displayed as histograms for TS05 sites A1, A2, B and C. Log scale.

Ablation data for TS07 and TS14 are displayed as histograms, Figure 31. Charts are selected to show the highest concentrations and strongest associations of elements of interest from all traceable ablation samples and sites. TS07, Carrickmore Quarry, shows consistent high peak values of cobalt of 14,779 ppm Co site B, 13,078 ppm Co site F, and 6,503 ppm Co site D. TS14, Ballantrae, ablation data for sites C, D, and G shows strong positive associations of copper-cobalt-nickel-arsenic-lead-silver.

Figure 31 Pyrite ablation sites for TS05 E, TS07 B. TS07 C, TS07 D, TS07 F, TS14 C, TS14 D, & TS14 G.

4 Discussion

4.1 Cobalt

Though incomplete, the LA ICP-MS results are encouraging. The analysis has identified significant anomalous cobalt (14,779 ppm Carrickmore TS07), copper (391,318 ppm Golden Hollow TS05), and nickel (2,517 ppm Carrickmore TS07) in traceable polished samples. In addition, a strong association of Bi-Ag-Pb-(Au) is seen in ablation of chalcopyrite (Golden Hollow sample TS05). Previous work done by Stratford and Shackleton Resource on T1 veins at Corvanaghan Quarry identified lindstrome, a silver-bismuth sulfosalt. At Ballantrae, Co-Cu-Ni-As association is clear in ablation of pyrite samples, TS14. Chromium was not analysed at the TCD laboratory, and no chromium results were received Results received for thin sections SL02 and SL03 polished thin sections may or may not be the T1 or T2 type veins from Corvanaghan Quarry.

Previous research on Curraghinalt (Stratford 2019) demonstrates cobalt is present in sulphides in a mineralisation event, Figure 32. The image shows cobalt concentrations for pyrite present in the Curraghinalt gold-copper ore deposit, formed by a late-stage mineralisation, orogenic event. From this pyrite mapping and the high cobalt values of the TCI, a question is raised regards the source of cobalt in Curraghinalt, Orritor, and Corvanaghan.

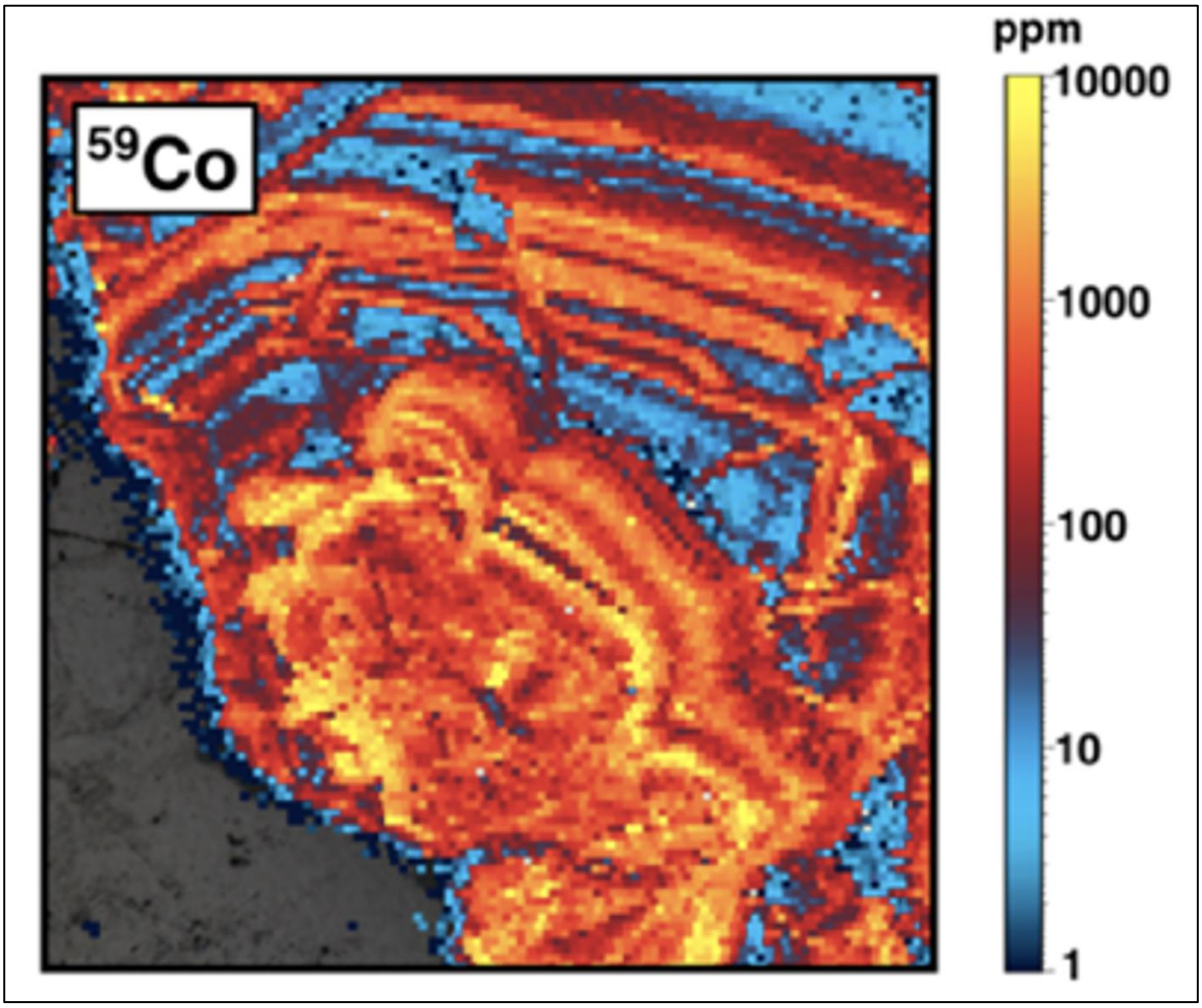

Figure 32 Cobalt raster map of pyrite, Curraghinalt deposit (Stratford 2019)

Previous research on the Golden Hollow boulder used analysis of the white bismuth minerals spectra and identified a strong element association of Cu-Bi-S (Hollis unpublished 2019).

Corvanaghan Quarry T1 veins, due to their high cobalt concentration, micro to macro vein textures, and bismuth values can be interpreted as remobilised sulphides from a primary source area. The identification of silver-bismuth sulfosalt lindstrome (Stratford unpublished 2019) has important implications for soil survey interpretation, such as the regional Tellus soil survey, or dense mineral exploration surveys. Corvanaghan Quarry T2 veins may or may not be from the same sulphide phase as T1 veins, although the whole rock geochemistry and pXRF values suggest, while T2 veins contain anomalous values for cobalt, bismuth, and silver, they are not as high-grade as T1 veins. However, T2 internal vein textures of en-echelon sulphides within a banded quartz-tourmaline host vein means the host fracture – a persistent planar fracture – has opened in brittle extension for the tourmaline and quartz minerals to become banded fracture fill. These minerals seal the fracture. After the initial fracture seal, en-echelon sulphide filled tension gashes are kinematic indicators to show the sense of shear within a later, brittle deformation event (Cosgrove & Hudson 2016).

4.2 Dating

Tectonic models of obduction for the TIC rely on absolute dates with relatively large margin of error ranges. A large margin of error in the model overlaps tectonic events and creates ambiguity in the tectonic reconstruction. The TPG is in structural contact with the interpreted microcontinent of the TCI and Ordovician volcanic units, but some uncertainty exists. Relative age relationships were made by Hartley 1930 and Hutton 1985. Absolute ages date obduction to a range from 493 Ma (Draut et al 2009) to 479 Ma (Cooper et al 2011). Absolute ages of the TIC are circa 467 Ma (Chew et al 2008). The Ballantrae ophiolite formation is dated to 483 Ma and obduction at 478 Ma (Bluck 1980). Therefore, the tectonic model of Hollis is favoured, of rifting, possibly back-arc, within an evolving arc, and arc-continent collision. Correlations of the TPG to the Annieopsquotch accretionary tract and the Ballantrae ophiolite are generally agreed (Hollis et al 2013). However, some problems with the model remain: several options are feasible using current literature dates.

Previous research by Hollis and Chew use the TCI as an anchor to which the now obducted ophiolite and the TVG are pinned with accretion and peak metamorphism at 470 Ma. However, its present position could be due to thrusting. A tectonic model of Tyrone arc which incorporates data from the syn-deformation pegmatites will refine the main deformation event and the obduction model: ophiolite over-rides arc, or ophiolite faulted against arc.

The British Geological Survey (BGS) technique of chemical abrasion isotope dilution-thermal ionization mass spectrometry (CA ID-TIMS) has the potential to resolve the timing of TPG obduction and the mode of SSZ ophiolite emplacement. Sub-Ma error ranges, a feature of the CA ID-TIMS technique, eliminates overlap and resolves tectonic events. When using the CA ID-TIMS analysis, zircon cores and rims are targeted. Zircon cores relate to magmatic origins, inherited from deeper rocks, where a match to existing zircon datasets could be possible. Zircon outer rims surround zoned zircon cores and denote intense metamorphic events. Applied to the shear hosted deformed pegmatites of Orritor quarry, CA ID-TIMS analysis may give sub-Ma error range of a zircon's metamorphosed outer rim. By dating both rims and cores of zircons and matching the results to dates already calculated, different models of ophiolite obduction may be discarded or strengthened.

4.3 Structures

Major structural features on the TPG are rarely seen. At Orritor a large, vertical, east-west brittle-ductile shear zone, hosts deformed, pegmatitic intrusions, Figure 15. Altered gabbro, or serpentinites, are adjacent to the shear zone. Use of the pXRF analysing gabbro and serpentinites bulk composition minerals found high values for economic metals chromium, nickel, and copper which confirm the area's anomalous values for these elements in stream surveys and soil surveys. Therefore, high background values exist for economic minerals copper-nickel-cobalt on the TPG.

Serpentinites are host to small sub-cm quartz-carbonate-sulphide veins in a stockwork texture, which contain 0.096 ppm Au, 2.5 ppm Ag, and 664 ppm Cu (Shackleton Resources whole rock sample number, K20232), and pXRF analysis of these sulphides gave peak values of 2,012 ppm Co, 117 ppm Cu, 1,655 ppm Cr, and 2,239 ppm Ni. These stockwork type veins may be sulphide rich at depth. Late, near horizontal, brittle fractures seen throughout the quarry are interpreted as unloading fractures (Cosgrove & Hudson 2016) as the vertical confining pressures from the overburden are removed during weathering.

Serpentinite emplacement related to the Orritor Quarry may be due to the shear zone in extension, exposing serpentinite, or allowing serpentinised gabbro to protrude up through mantle. Inversion tectonics may play a role in serpentinite extrusion. Previous research has described serpentinites associated with early Proterozoic Iapetus extensional faults (Chew 2001), decollement along terrane boundaries in south dipping major detachment faults (Clift et al 2004), and serpentinites are recorded along the FHCBL-HBF (Hollis unpublished). Vertical fracture faces show horizontal slickensides in outcrop, Figure 17, associated with an increase in vertical stresses as the deformation changes from thrust to strike-slip regime (Cosgrove & Hudson 2016).

4.4 Basement structures

The discussion on pegmatites and serpentinites is closely related to deep basement faults, or trans-lithospheric structures. Serpentinites and serpentinite alteration occurs at the three study locations of TPG, Clew Bay, and Ballantrae. SSZ ophiolites are more likely to be obducted and preserved in the rock record (Draut 2007) rather than underplated. For example, ophiolite detritus appears in the fore-arc basin of the South Mayo Trough at c.480 Ma (Chew, Dewey & Manage 1999). The presence of ophiolite material in fore-arc sediments suggests exhumation and weathering of the Deerpark ophiolite took place by 480 Ma. Oslistoliths of serpentinised peridotite at Achill Beg, County Mayo are interpreted as being formed by significant extension which allows water to penetrate the upper mantle and allowed serpentinised mantle protrusion, e.g., the Iberian margin, eastern Atlantic, and the Rockall Basin, Ireland (Chew 2001). In Scotland, the Highland Boundary fault zone (HBFZ) contains an association of ophilitic melange and serpentinised mantle (Chew et al 2010). Furthermore, ophiolites and ophiolite derived material are found in a continuous ribbon on the Laurentian continental side, off-set from the Iapetus subduction zone. Therefore, Orritor's shear zone may be a major structural feature, or extensional faults, which allow travel of fluids, serpentinization, and serpentinite protrusion (Chew 2001).

In the geological terranes of Ireland and Great Britain, all surface exposed units are structurally riven with basin architecture most recently active during Carboniferous inversion tectonics (Parnell 2000). The terranes and terrane boundaries have a distinct and obvious NW-SE orientation. However, the alignment of volcanic centres, geomorphology, geophysical features, mineralisation patterns, and faults give more subtle, underlying pattern of NE-SW orientation. The NE-SW orientation underlies the NE-SW overprint from the Iapetus closure. Due to its basement nature, the NW-SE orientation is generally not exposed, but some evidence is at surface. Fold sequences of County Mayo have syncline-anticline axis-oriented NW-SE, adjacent to contemporary supra-subduction zone (SSZ) blue schist pelites of the Dalradian and related to the D_2 deformation event (Chew 2003). TMI images (Tellus aeromagnetic survey) of the TCI and TPG can delineate geological surface mapping of lithology contacts. Mafic dykes align NW-SE, intruded during Tertiary extension and penetrate almost all rock types.

Further interpretation of Tellus TMI images gives insight into the Midland Valley basement architecture of Northern Ireland. TPG units are meso-crustal, crystalline rocks of high metamorphic grade and appear unaffected by Tertiary rifting of the North Atlantic Igneous Province. Within the already deeply eroded Caledonian orogen, the TPG is an inlier of crystalline basement at a same erosional level as supracrustal sequences, i.e., the TVG. The TPG may be a horst structure, too stiff for Tertiary extensional fractures to penetrate. Therefore, an interpretation is the TPG is without internal major NW orientated structures and bounded by controlling NW orientated faults. Furthermore, during orogenic cycles intense peak metamorphism is followed by extension with orogenic collapse (Alsop 1993). Caledonian orogenic collapse at 467-464 Ma (Dewey 2005) or 457-458 Ma (Chew et al 2008) reactivated structures in the basement, resulting in basement block rotation e.g., the Antrim Inlier, and sedimentary basin formation. Rotation or deviation of the orientation is estimated, trends WNW-ESE to NNW-SSE are anticipated. Transverse NW structures may reactivate on peak metamorphism and invert.

Basement structures allow multiple tectonic and magma movements over many epochs. In Ireland and Britain, northwest orientated faults control the location of sedimentary basins, volcanic centres, and igneous intrusions, e.g., Ordovician Newry Granite, Tertiary basalt dykes, and Tertiary Mourne granites. Dyke swarms orientated NW-SE cluster on Tertiary and early Devonian intrusions, Figure 33, have uranium rich geochemistry (Gunn 2008).

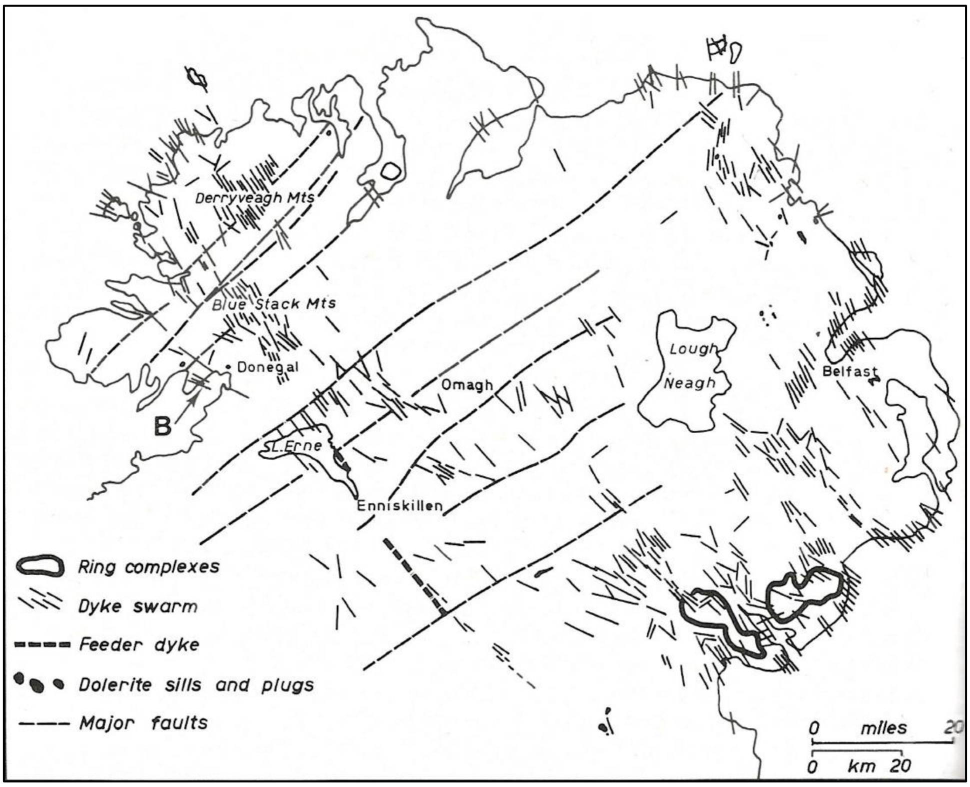

Figure 33 Diagrammatic map of the dyke swarms in the north of Ireland. Pitcher and Berger 1972

Words such as ‘enigmatic’ and ‘elusive’ are used to describe the evidence of lineaments in Dalradian sequences. Lineaments have been used to explain the Silurian mafic intrusions (Cooper et al 2013) demonstrate the effects on deep dyke plumbing systems and lineament locations, Figure 34.

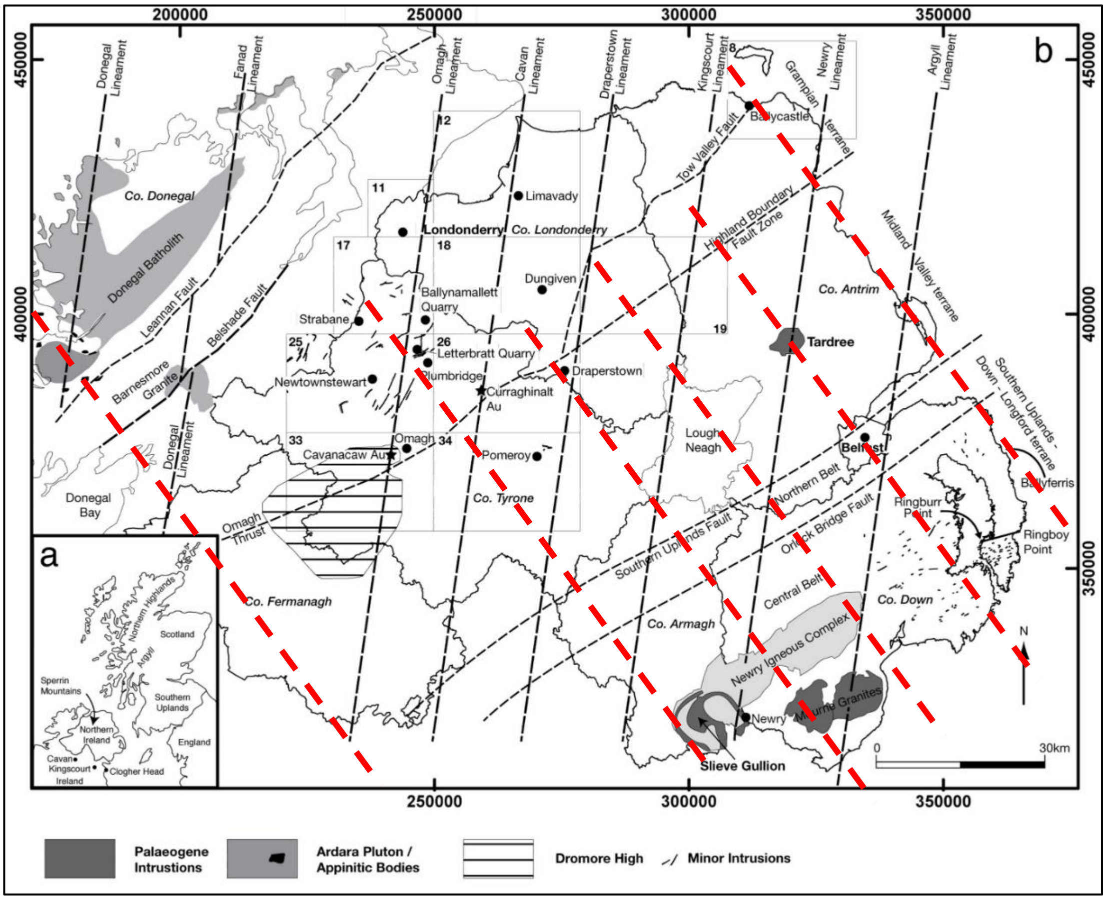

Figure 34 The northern part of the island of Ireland and lineaments, Cooper et al 2013. Basement structure orientations redefined as red dashed lines

Previous research by Hutton and Alsop interprets the dominant Dalradian strike swing, from an east-west orientation in Connemara to NE-SW in Northern Ireland and Scotland, to the interaction with a Greenland promontory during the Ordovician. Soper 1994 interprets WNW orientated lineaments within the Caledonian strike swing. Dewey and Strachen 2003 interpret NW-SE structures to Riedel shears at 90 degrees to the dominant NE structures of the orogen and granite emplacement. Recent structural data on the northwest alignment is provided in a fracture study of the Lewisian basement rocks (McCaffery 2020). McCaffery correctly asserts large regional features are replicated in outcrop and core scale fractures. In addition, offshore oil exploration of Mesozoic sedimentary basins follows the NW basement trend. Sedimentary basin boundaries are often NW-NE orientated faults initiated from Meso-Proterozoic amalgamation of Archean terranes, with shear zones and dyke swarms (McCaffery 2020, Vernon 2014). Basement shear zones are active at 1.55 giga annum (Ga) (Holdsworth 2020) while basement quartz-sulphide mineralisation is dated to 2.249 Ga (Vernon 2014). NW basement faults propagate upwards and interact with supra-crustal rocks of the Caledonian trend.

Long lived basement structures control the Mesozoic sedimentary basins in offshore environments of Britain and Ireland, Figure 35. The sedimentary basin of Minch is interpreted to be a half-graben controlled by a syn-sedimentary NW orientated structure. Other offshore controlling faults along a NW orientation are Permian-Triassic basins of the North Sea, Irish Sea, Antrim eastern coastline, and Lough Neagh. Indeed, the interaction between basement faults and Caledonian trend cover faults permits Lough Neagh to be interpreted as a pull apart basin. In summary, volcanic centres, sedimentary basin boundary faults, fracture analysis of basement blocks, and glacial scouring all reveal a NW-SE axis developed here as the 'NW concept'.

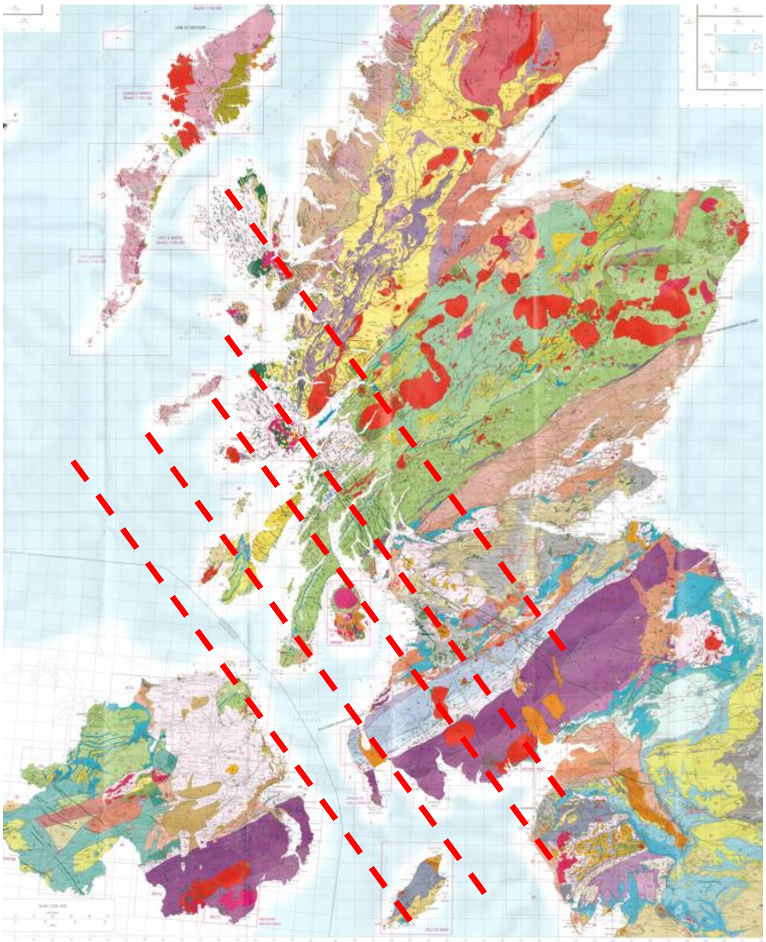

Figure 35 Bedrock UK North geological map, BGS, 1:625,000 scale. Interpreted basement structures as red dashed lines

Quaternary glaciation exploits wide zones of weakness, described by Arthur Holmes as shatter zones in the example of the Great Glen fault zone (Holmes 1969). Visible geomorphological surface features orientate with volcanic centres such as the loughs of Ireland e.g., Lough Erne and Loch Etive. Furthermore, in the northern part of the Fennoscandian Shield, basement structures of similar orientation are evident. Across a wide area of Norrbotten, Sweden and northern Finland, quaternary glaciation pits the landscape with NW oriented surface lakes. Caledonian nappes north-eastern front covers the Archean basement in a strong Caledonian trend, to be deeply eroded and revealing the basement structures.

4.5 Mineral system assessment

Based on field observations and previous research, the model of vein emplacement selected is of orogenic, structurally hosted veins such as the quartz-tourmaline-sulphide veins of Corvanaghan quarry, the gold bearing, quartz-sulphide veins of Curraghinalt, and gold mineralisation in NW-SE orientated lodes in Foreburn, Scotland (Charley 1989) - identified by mineral exploration companies. Dates of mineralisation vary. Re-Os dating of micro shear hosted molybdenite from Dalradian units yields a 455.8 ±3 Ma age (Rice 2016) indicates a minimum age for mineralisation. While a late Ordovician constraint for the timing of gold mineralisation of 410 Ma (Rice 2016) is given for the three phases of Curraghinalt gold precipitation (Parnell 2000). From potassium-argon (40K-40Ar) fault gouge dating (Parnell 2000) the Curraghinalt gold vein yields a minimum age of 325 and 315 Ma. Parnell's dates define Caledonian structural remobilisation and may have important ramifications for this study when considering cobalt sulphide and bismuthide remobilisation. Regional evidence suggests structural reactivation occurred during Carboniferous, Permian, and Palaeogene eras during extensional stress regimes and within existing fault bounded basins (Rice 2015). On extension, mineralised hydrothermal fluids travel upward (Rice 2016) enabled by orogen rapid uplift and subsequent orogenic collapse, and post-peak metamorphism (Clift et al 2004). Thus, in Ireland and Scotland, hydrothermal cells use space created by extensional tectonics on collapse of the orogen.

Orogenic mineralising systems are closely related to volcanogenic massive sulphide (VMS) type deposits, such as eastern Canada's Abitibi greenstone belt (Monecke et al 2017). The Ballantrae ophiolite has several mineralisation showings visited in this study. Field work at Snib's Cave, Bennane Head shore front, observed red ironstone or exhalative horizons in immediate association with massive sulphides. Lenses of iron rich, red exhalative form to a maximum thickness of 20 cm, pinching out into thin sulphide horizons. Steeply dipping pillow formations are seen immediately along strike in the same outcrop where fine grained, granular sulphides accumulate in the inter-pillow areas. Armstrong (1999) may of sampled the exhalative deposits, and made an interpretation to their being red cherts using rare earth element (REE) plots. A comparison of Ballantrae REE plots with Hollis TVG exhalative horizons would be beneficial. In addition, further north at Pinbain Burn beach, agglomerate float material contains disseminated sulphides. The significance of pillow lavas, ironstones, and sulphides in the Ballantrae ophiolite demonstrates hydrothermal venting at the seafloor interface and sulphide deposition.

Arcs are conceived from detritus found in the SULDT. The Iapetus suture and Red Indian Line are first order structures. Between the Laurentian margin and the Red Indian line are the arc terranes of Newfoundland - Baie Verte group and the Annieopsquotch accretionary tract (Van Staal et al 1998). The zone between Laurentia and the Red Indian Line may contain arcs covered by a thrust wedge (thrust of greywackes and turbidites). County Mayo's Clew Bay Complex and Scotland's Highland Boarder Complex are contemporaneous (Chew and Stillman 2009) and both seen by Van Staal, Dewey, and Mange, as extensions of the Baie Verte Oceanic Tract (Van Staal et al 1998, Dewey & Mange 1993). Therefore, the possibility of covered arcs within the MVT (Armstrong & Owen 2001, Van Staal et al 1998) exists from the correlation to NFL and from sedimentation studies and detrital provenance. It has been suggested an early Palaeozoic arc lies covered by later Palaeozoic sedimentary units of the SULT (Armstrong & Owen 2001). These 'lost arcs' may be under the extensive cover of Phaerozoic basins, such as NFL's Popelogan Arc of the Exploits subzone (Van Staal et al 1998). In addition, evidence for covered arcs could be in the source of metals for the metal mining districts of County Armagh and southern Scotland.

5 Conclusions

To aid future exploration, this study has described primary and secondary sulphide mineralisation using, i) macro-scale vein textures and whole rock geochemistry have extensional multiphase hydrothermal fluids with a late, brittle sulphide phase, ii) association meso-scale mineral system exploitation of NW-SE fractures, and iii) micro-scale laser ablation mineral geochemistry of pyrite and chalcopyrite show anomalous cobalt and Bi-Ag-S. From this study, the following conclusions may be made:

- Systematic pXRF sampling of Orritor quarry's gabbro identifies significant disseminated sulphide hosted cobalt.
- Extension in the stiff paragneiss host rocks of Corvanaghan Quarry give a history of repeated mineral fluid flows in persistent extensional fractures, with sulphides belonging to at least one extensional phase. Cobalt is significant at peak concentrations of 1,200 ppm Co (whole rock) and 2,012 ppm Co (pXRF).
- Bismuthide lindstrome is confirmed in T1 veins and Golden Hollow, important for future exploration studies.
- Sulphide mineralisation is a regional event as demonstrated with 1) seafloor sulphides deposited at interpillow locations at Ballantrae, 2) supra-crustal fracture hosted sulphides (with LA ICP-MS values of 14,779 ppm cobalt) in dolerites at Carrickmore Quarry, and 3) meso-crustal sulphides seen at the Deerpark ophiolite, Golden Hollow, and Orritor Quarry.
- Metal associations of gold-silver-copper-cobalt-bismuth are present in most cases of mineralisation.
- Regional sulphide mineralisation may be remobilised as quartz-sulphide veins during the post-peak metamorphism phase of the Caledonian orogeny.

It is unfortunate the impact of COVID affected the TCD laboratory sample chain of custody, sample preparation, and analysis. Due to the significant COVID impact, a main goal to identify the mineral host to cobalt remains incomplete, other than identifying a pyrite as a host to the cobalt rich sulphide. Subsidiary goals of dating the mineralisation and establishing, or not, a connection between the quarries of Orritor and Corvanaghan have not been met. However, in these quarries there remains an interesting dating study and the dating of deformed pegmatites at Orritor Quarry.

Acknowledgements

Many people have supported me through this period in conducting the study. Special thanks go to Sean McClenaghan of TCD, the ore analysis laboratory staff at Trinity College Dublin, James Stratford (TCD), Steve Hollis (University of Edinburgh), Mark Patton (GSNI), Richard Belcher, Andrew Cunningham, Garth Earls, John Arthurs, the residents, and the farmers of Slieve Gallion district.

6 References

Adams C, Brand C, Dentith M, Fiorentini M, Caruso S, and Mehta M, 2020, *The use of pXRF for light element geochemical analysis: a review of hardware design limitations and an empirical investigation of air, vacuum, helium flush and detector window technologies.* Geochemistry: Exploration, Environment, Analysis, pp.geochem2019-076.

Alsop G, and Hutton D, 1993 *Major southeast-directed Caledonian thrusting and folding in the Dalradian rocks of mid-Ulster: implications for Caledonian tectonics and mid-crustal shear zones.* Geological Magazine, 130(2), pp.233-244.

Alsop G and Hutton D, 1993, Caledonian extension in the north Irish Dalradian: implications for the timing and activation of gravity collapse. Journal of the Geological Society, 150(1), pp.33-36.

Arthurs J, Knowles P, Strachan S, and Calvert-Harrison E, 1975 *The Geology And Metalliferous Mineral Potential Of The Sperrin Mountains Area.*

Armstrong H, and Owen A, 2001*, Terrane Evolution of the Paratectonic Caledonides of Northern Britain.* Journal of the Geological Society, 158(3), pp.475-486.

Cawood P, McCausland P, Dunning G, 2001, *Opening Iapetus: Constraints from the Laurentian margin in Newfoundland.* GSA Bulletin; v. 113; no. 4; p. 443–453

Barrow G, 1893, *On an Intrusion of Muscovite-biotite Gneiss in the South-eastern Highlands of Scotland, and its accompanying Metamorphism*. Quarterly Journal of the Geological Society 1893 v.49; p330-358

Bird A, Thirlwall M, Strachan R, & Manning C, 2013, *Lu–Hf and Sm–Nd dating of metamorphic garnet: evidence for multiple accretion events during the Caledonian orogeny in Scotland*. Journal of the Geological Society, London, Vol. 170, 2013, pp. 301 –317

Chew D, 2001, *Basement protrusion origin of serpentinite in the Dalradian. Irish Journal of Earth Sciences.* Jan 1:23-35.

Chew D, Daly J, Magna T, Page L, Kirkland C, Whitehouse M, and Lam R, 2010, *Timing of ophiolite obduction in the Grampian orogen.* Geological Society of America Bulletin, 122(11-12), pp.1787-1799.

Chew D, Flowerdew M, Page L, Crowley Q, Daly J, Cooper M, & Whitehouse M, 2008, *The tectonothermal evolution and provenance of the Tyrone Central Inlier, Ireland: Grampian imbrication of an outboard Laurentian microcontinent?* Journal of the Geological Society, 165(3), pp.675-685.

Chew D, Stillman CJ, 2009, *Late Caledonian Orogeny and Magmatism.* The Geology of Ireland (pp. 143-173). Edition 2nd. Dunedin Academic Press

Cliff R, Yardley B, & Bussy F, 1996, *U-Pb and Rb-Sr geochronology of magmatism and metamorphism in the Dalradian of Connemara, western Ireland*. Journal of the Geological Society, London, Vol. 153,1996, pp. 109-120

Clift P, Dewey J, Draut A, Chew D, Mange M, Ryan P, 2004, *Rapid tectonic exhumation, detachment faulting and orogenic collapse in the Caledonides of western Ireland*. Tectonophysics 384 (2004) 91– 113

Cooper M, Crowley Q, Hollis S, Noble S, Roberts S, Chew D, Earls G, Herrington R, & Merriman R, 2011, *Age constraints and geochemistry of the Ordovician Tyrone Igneous Complex, Northern Ireland: implications for the Grampian orogeny*. Journal of the Geological Society, 168(4), pp.837-850

Cooper M, Crowley Q, Hollis S, Noble S, & Henney P, 2013, *A U–Pb age for the Late Caledonian Sperrin Mountains minor intrusions suite in the north of Ireland: timing of slab break-off in the Grampian terrane and the significance of deep-seated, crustal lineaments*. Journal of the Geological Society, 170(4), pp.603-614.

Cooper M, Crowley Q, & Rushton A, 2008*, New age constraints for the Ordovician Tyrone Volcanic Group, Northern Ireland*. Journal of the Geological Society, 165(1), pp.333-339.

Cosgrove JW, & Hudson JA, 2016, *Structural Geology and Rock Engineering.* World Scientific Publishing Company.

Daly J & Flowerdew M, 2005, *Grampian and late Grenville events recorded by mineral geochronology near a basement–cover contact in north Mayo, Ireland*. Journal of the Geological Society; v. 162; p. 163-174

Herrington R, Hollis S, Cooper M, Stobbs I, Tapster S, Rushton A, McConnell B, Jeffries T, 2018, *Age and Geochemistry of the Charlestown Group, Ireland: Implications for the Grampian orogeny, its Mineral Potential and the Ordovician Timescale.* Lithos 302–303 (2018) 1–19

Hollis S, Roberts S, Cooper M, Earls G, Herrington R, Condon D, Cooper M, Archibald S, & Piercey S, 2012, *Episodic arc-ophiolite emplacement and the growth of continental margins: Late accretion in the Northern Irish sector of the Grampian-Taconic orogeny*. Geological Society of America Bulletin, 124(11-12), pp.1702-1723.

Hollis S, Cooper M, Herrington R, Roberts S, Earls G, Verbeeten A, Piercey S, Archibald S, 2015, *Distribution, mineralogy and geochemistry of silica-iron exhalites and related rocks from the Tyrone Igneous Complex: Implications for VMS mineralization in Northern Ireland*. Journal of Geochemical Exploration 159 (2015) 148–168

Hollis S, Cooper M, Earls G, Roberts S, Herrington R, & Piercey S, 2016, *Using Tellus data to enhance targeting of volcanogenic massive sulphide mineralisation in the Tyrone Igneous Complex*. Unearthed: impacts of the Tellus surveys of the north of Ireland. Dublin. Royal Irish Academy.

Hutton D, & Alsop G, 1996, *The Caledonian strike-swing and associated lineaments in NW Ireland and adjacent areas: sedimentation, deformation and igneous intrusion patterns*. Journal of the Geological Society, 153(3), pp.345-360

Flowerdew M, Daly J, Guise P, Rex D, 2000, *Isotopic dating of overthrusting, collapse and related granitoid intrusion in the Grampian orogenic belt, northwestern Ireland*. *Geol. Mag.* 137 (*4*)*, 2000, pp. 419–435*

McAteer C, Daly S, Flowerdew M, Connelly J, Housh T, Whitehouse M, 2010, *Detrital Zircon, Detrital Titanite and Igneous Clast U–Pb Geochronology and Basement–cover Relationships of the Colonsay Group, SW Scotland: Laurentian Provenance and Correlation with the Neoproterozoic Dalradian Supergroup* Precambrian Research 181 (2010) 21–42

McConnell B, Rogers R, Crowley Q, 2016, *Sediment provenance and tectonics on the Laurentian margin: implications of detrital zircons ages from the Central Belt of the Southern Uplands–Down–Longford Terrane in*
Co. Monaghan, Ireland. Scottish Journal of Geology

Mitchell W, 2004, *The geology of Northern Ireland: our natural foundation.* Geological Survey of Northern Ireland, Belfast.

Monecke T, Mercier-Langevin P, Dubé B*, 2017, Archean Base and Precious Metal Deposits, Southern Abitibi Greenstone Belt, Canada.* SEG vol 19

Pitcher WS, & Berger AR, 1972. *The Geology of Donegal: A Study of Granite Emplacement and Unroofing*. p374

Rice S, Cuthbert S, & Hursthouse A, 2018, *Tectono-magmatic controls of post-subduction gold mineralisation during late Caledonian soft continental collision in the Southern Uplands-Down-Longford Terrane, Britain and Ireland: A review.* Ore Geology Reviews, 101, pp.74-104.

Rice C, Mark D, Selby D, Neilson J, & Davidheiser-Kroll B, 2016, *Age and Geologic Setting of Quartz Vein-Hosted Gold Mineralization at Curraghinalt, Northern Ireland: Implications for Genesis and Classification*. Economic Geology, 111(1), pp.127-150.

Rooney A, Chew D, & and Selby D, 2011*, Re–Os geochronology of the Neoproterozoic–Cambrian Dalradian Supergroup of Scotland and Ireland: Implications for Neoproterozoic stratigraphy, glaciations and Re–Os systematics.* Precambrian Research, 185(3-4), pp.202-214

Soper N, Ryan P, & Dewey J, 1999, *Age of the Grampian orogeny in Scotland and Ireland*. Journal of the Geological Society, 156(6), pp.1231-1236.

Stratford JP, McClenaghan SH, 2019, *Geochemical paragenesis of pyrite associated with orogenic gold at Curraghinalt, Northern Ireland.* Trinity College Dublin. Irish Centre for Research in Applied Geosciences. SGA Glasgow 2019

Steltenpohl M, Kassos G, Andresen A, Rehnström E, & Hames W, 2011, *Eclogitization and exhumation of Caledonian continental basement in Lofoten, North Norway Geosphere*. v. 7; no. 1; p. 202–218.

Waldron J, Van Staal C, 2001, *Taconian orogeny and the accretion of the Dashwoods block: A peri-Laurentian microcontinent in the Iapetus Ocean*. Geological Society of America. *Geology;* September 2001; v. 29; no. 9; p. 811–814

Van Staal C, Whalen J, McNicoll V, Pehrsson S, Lissenberg C, Zagorevski A, Breemen O, Jenner G, 2007, *The Notre Dame arc and the Taconic orogeny in Newfoundland*. The Geological Society of America Memoir 200

Van Staal C, Dewey J, Niocaill C, & McKerrow W, 1998, *The Cambrian-Silurian tectonic evolution of the northern Appalachians and British Caledonides: history of a complex, west and southwest Pacific-type segment of Iapetus.* Geological Society, London, Special Publications, 143(1), pp.197-242.

7 Appendix

7.1 Abbreviations

Abbreviation	Full description
%	percent
Ag	silver
Al	aluminium
Au	gold
Avg.	median
Ba	barium
BABB	back arc basin basalts
Bi	bismuth
Bx	breccia
C.	Croagh
CA ID-TIMS	chemical abrasion isotope dilution-thermal ionization mass spectrometry
carb	carbonate
cm	centimetre
Co	cobalt
Co.	County
Cpy	chalcopyrite
Cr	chromium
Cs	caesium
Cu	copper
D_1	Deformation, first event
D_2	Deformation, second event
D_3	Deformation, third event
eMORB	enriched mid-ocean ridge basalts
Eu	europium
Fe	iron
FHCBL	Fair Head-Clew Bay Line
fld	feldspar
Fm	Formation
g/t	grams per tonne
H_1	hypothesis
HBO	Highland Boundary Ophiolite
Hf	hafnium
HFSE	high field strength elements
H_o	null hypothesis
IAB	island arc basalts
ID-TIMS	Isotope Dilution Thermal Ionization Mass Spectrometry
K-Ar	potassium – argon
kbar	kilobars
km^2	kilometres squared
LA ICP-MS	laser-ablation inductively-coupled-plasma mass-spectrometry
LILE	large ion lithophile element
LREE	light rare earth element

m	metres
Ma	mega annum
MgO	magnesium oxide
Mn	manganese
MORB	mid-ocean ridge basalt
Mt	Million tonnes
MVT	Midland Valley Terrane
Nb	niobium
NE	north east
NFL	Newfoundland
Ni	nickel
OIB	ocean island basalts
pXRF	portable x-ray diffraction
py	pyrite
Q	quarry
QAQC	quality assurance quality control
qtz	quartz
Rb	rubidium
REE	rare earth element
Re-Os	rhenium-osmium
RTZ	Rio Tinto Zinc
S	sulphur
S_0	bedding, original
S_2	Structures of the deformation second event
S_3	Structures of the deformation third event
Sb	antimony
SI	magnetic susceptibility
SiO_2	Silica
Sm-Nd	samarium-neodymium
SSZ	supra-subduction zone
SUF	Southern Upland Fault
SULDT	Southern Uplands Longford-Down Terrane
SW	south west
T1	Type 1 vein
T2	Type 2 vein
Ta	tantalum
TCD	Trinity College Dublin
TCI	Tyrone Central Inlier
Th	thorium
Ti	titanium
TIC	Tyrone Igneous Complex
TMI	Total Magnetic Intensity
TMO	Thetford Mines Ophiolite
TPG	Tyrone Plutonic Group
TVG	Tyrone Volcanic Group
U-Pb	uranium lead

VMS	Volcanogenic massive sulphide
WHO	World Health Organisation
Y	yttrium
Z	atomic number
Zr	zirconium

7.2 Susceptibility measurements

Carrickmore Q		
Gabbro	Gabbro altered	Gossan
8.56	0.065	1.48
3.26	1.7	1.48
2.75	1.27	1.78
1.98	0.455	2.01
2.68	0.452	2.09
3.19	0.557	2.24
2.49	0.636	2.3
98.2	1.23	2.23
208	0.541	1.63
313	0.547	1.23
130	0.716	1.58
84.3	0.704	1.49
156	0.361	1.7
183	0.588	1.98
182	0.562	1
277	1.78	0.963
7.82	0.915	1.52
10.6	0.452	1.04
56.3	0.704	2.52
21.1	0.529	2.13
1.22	0.608	1.54
42.3	0.46	1.37
23.8	0.398	
106	0.475	
77.5	0.089	
2.51	0.563	
1.74	0.89	
0.828	0.888	
1.62	0.032	
4.15	1.01	
2.47	1.19	
	1.05	
	1.17	
	0.96	
	0.865	
	0.067	
	0.881	
	0.443	
	0.836	
	0.604	
	0.798	
	0.659	
	0.571	
	0.675	
	0.624	
	0.578	
	0.834	
	0.623	
	0.058	

Orritor Q					
Gabbro unaltered	Gabbro altered	Gabbro sheared	dolerite	pegmatite	UM
4.7	36.8	1.48	2.97	0.079	462
1.62	1.65	1.32	3.1	0.413	366
3.59	46.6	2.26	5.73	0.591	302
269	6.6	0.98	220	0.425	274
4.79	44.9	1.4	1.31	0.486	375
33.2	23	1.83	1.52	0.083	202
270	1.67	20.3	50.7	0.041	432
131	12	0.09	5.14	0.032	152
269	1.56	0.983	6.6	0.376	425
370	2.88	0.828	168	0.081	235
240	1.73	1.99	2.25	0.559	281
157	50.1	1.36	3.39	0.072	85.4
2.13	2.92		121	0.506	151
102	18.7		3.98	0.088	275
271	2.63		1.88	0.051	372
6.94	1.48		2.27	0.051	
223	0.467		1.9	0.507	
78.4	0.967		2.24	0.584	
194	1.21		5.26	0.087	
82.5	1.09		1.91	0.749	
122	2		2.03	1.08	
102	1.86		2.66	0.42	
91	1.91		2	0.425	
4.5	1.06		2.44	0.103	
5.25	1.46		2.31	0.102	
242	1.09		2.31	0.056	
70.8	1.25		2.48		
178	1.41		2.58		
59.4	1.37		2.02		
116	1.52		1.55		
5.45	1.36		2.21		
166	1.34		2.06		
10.4	1.05		2.7		
248	5.2				
4.21	1.46				
5.97	2.56				
4.5	1.3				
275	1.73				
468	1.68				
270	2.05				
265	2.13				
2.12	1.43				
54.4	73.6				
218	79.1				
29.9	33				
150	37.8				
144	5.86				
209	0.977				
2.27	96.1				
4.73	1.85				
242	439				
364	73.2				
181	1.87				
1.57	2.72				
499	5.07				
512	2.11				
457	235				
20.6					

7.3 Sample details

Samples submitted for polished thin section preparation and laser ablation analysis = 14

Sample number	Easting (IGR)	Northing (IRG)	Setting	Type	Location	Hand Sample Description	Initial interpretation	Mineralised	Preperation	Analysis
TCD-TS-01	271848	381505	quarry	SC	Corvanaghan	grey + white qtz-py vein material <8cm wide. Py massive @40-50%. pXRF shows Co-Cu-As-Bi-Zn-Mo. Original sample K20201 wkt db.		massive py, pyrrho,	thin section	LA, Re-Os date
TCD-TS-02	271900	381234	quarry	SC	Corvanaghan	qtz-amph-py/cpy vein. Py + bournite? filled tension gashes. No wall rock. Py @ 20-30%. assoc n-s structure. Original sample RS012486. Koza db		en-echalon veining py/ cpy	thin section,	LA, Re-Os date
TCD-TS-03	277451	379745	quarry	SC	Orritor	Grey, black, med grained. Mineral alignment/ foli, diss py t/o. black amphiobole/ pyroxenes. Green chl alt weak, talc surfaces. SiO2 <45%. Serpentine ultramafic?		py	thin section,	LA, Re-Os date
TCD-TS-04	277451	379745	quarry	SC	Orritor	UM, high mag intensity w/ MagSus, black fine grained host, amphioboles?, weak shear/ foli, yellow metallic sulphides ass w/ light green SiO2 on irregular shear and fresh surfaces ~5% sul. Talc on surface (shear)		py/ phyrr	thin section	LA, Re-Os date
TCD-TS-05	273841	381743	stream	float	Golden Hollow	Boulder. Deep red weathered surface of iron oxides. Fresh surface black, fine grained silica + sulphides, banded w/ bx of silica. Impressive		py/ cpy 30%, sulphide flooded		Re-Os date, SEM
TCD-TS-06	260762	372236	quarry	OC	Carrickmore	banded qtz rich lens, grey qtz, w/n medgrained altered and bleached k-fld & qtz. Extensive alteration	quartz lens in clay alteration	fresh sulphides and malachite	thin section	LA, Re-Os date
TCD-TS-07	260862	372384	quarry	OC	Carrickmore	black grey, fine to med grained, qtz + biotite, SiO2<50% assoc w/ weak green colour = chl?, red haematite on some surface . Dolerite	Dolerite with stringers	py/ cpy stringers	thin section	LA, Re-Os date
TCD-TS-08	260796	372246	quarry	OC	Carrickmore	pink and white on fresh surfaces = k-fld (70%) and qtz as porphyroblasts and vlts. Some qtz porhyroblasts assoc w/ weak green colour - epidote? & dark small mineral? Chl vein seen. K-fld from alteration? Protolith uncertain. Weathered surface looks bleached. large area alteration in quarry (50x500m). Unaltered dolerites close.	Clay altered mafics - pink	tiny sulphide grains. Py?	thin section	LA, Re-Os date
TCD-TS-09	260791	372251	quarry	OC	Carrickmore	exposure 3x25m w/n altered rock of RS014211. Iron oxides on all weathered surfaces. Fissile. Highly siliceous, banded in places. Granular siliceos texture in places = protolith? Fine to med grained = dolerite?	Gossan	tiny blebs of fresh sulphides blue azurite/ malachite	thin section	LA, Re-Os date
TCD-TS-10	092399	281602	track	OC	Croagh Patrick	black, mafic, fine grained rock w/ moderate foliation. 70/030/w. green serpentinite/ epidote staining on qtz t/o. O/C size 10x8m		-	thin section	-
TCD-TS-11	092592	281848	stream	OC	Croagh Patrick	black, sheared mafic, mod foli, white qtz		-	thin section	-
TCD-TS-12	091612	281820	boulder	float	Croagh Patrick	orange surface due to jarosite, fine grained, dense, black, mafic/ UM, magnetite		mag	thin section	LA, Re-Os date
TCD-TS-13	(BNG) 09927	(BNG) 87596	beach	OC	Ballantrae	qtz-carb vein with sulphides py+cpy <5%. Vein very irregular, branching, & Bx texture. Host: light green, fine grained, mafic, some silicification = serpentinite		py + cpy	thin section	Re-Os, SEM
TCD-TS-14	(BNG) 09141	(BNG) 86113	beach	OC	Ballantrae	MS fine grained py in 10-15cm thick pods, 30-40cm long. <30% slphides. Intense weathered purple, jarosite on joints. Ironstone along strike		py	thin section	Re-Os, SEM

7.4 pXRF Geochemistry

Summary table of metal trace element data

Location	description	Cr_ppm	Co_ppm	Ni_ppm	Cu_ppm	Ag_ppm	Pb_ppm	Bi_ppm	Mg_ppm	Fe_ppm
Corvanaghan quarry	Qtz-py vein material, 30% py, 'dirty' py, surface limonite, mas	0	409.9	0	62	0	54.1	2.7	-	45,647
Corvanaghan quarry	Qtz-py vein material, 30% py, 'dirty' py, surface limonite, mas	0	1146.3	0	333	0	427.7	26.7	-	193,449
Corvanaghan quarry	Qtz-py vein material, 30% py, 'dirty' py, surface limonite, mas	0	1417.2	0	211	0	236.8	20.6	-	238,646
Corvanaghan quarry	Boulder of metabasite Bx w/ Qtz-py veining py @ 20%, massiv	0	1999.2	0	658	0	438.1	17.7	-	333,005
Corvanaghan quarry	Boulder host Bx margin py-qtz infil, Py@ 10% as large veining	0	1440	0	159	0	87.5	7.4	-	172,811
Corvanaghan quarry	med grained Ps, pale-deep green colour, intesly alt chl w/ rust	3199.3	547.6	1669.9	-	0	0	0	62,749	163,047
Corvanaghan quarry	Thin qtz vein (5cm) qtz vlts, w/ chl/ epidote alt of host rock. V	0	0	87.4	-	0	0	0	42,960	128,194
Corvanaghan quarry	qtz-amphibole?-py/ cpy vein + alt chl wall rock. Py/ cpy @ 10-	0	0	26.6	18	0	0	0	-	6,620
Corvanaghan quarry	thin vein (5cm) of black CHL (?)-py-qtz a0 Ps wallrock, w/n fau	0	348.3	84.5	171	0	0	0	24,640	72,269
Corvanaghan quarry	Qtz-chl-py vein. Py as gashes @15% w/n vein. Ps host Chl.	0	658.1	0	-	0	190.3	2.8	-	298,638
Corvanaghan quarry	Qtz-amph-py vein, high graded. Assoc w/ n-s structures. Py/ c	0	0	39.3	-	0	0	0	-	37,093
Corvanaghan quarry	Qtz-chl-py vein. Py as gashes	0	147.3	0	-	0	13.6	0	-	36,212
Golden Hollow	Calc-alk basalt heavily altered w/ silica + py flooding	0	550	0	23,388	38.6	0	28.4	-	93,346
Golden Hollow	Calc-alk basalt heavily altered w/ silica + py flooding	0	810.3	0	7,010	0	49.7	31	-	164,391
Golden Hollow	Calc-alk basalt heavily altered w/ silica + py flooding	0	749.7	0	8,125	0	27	18.2	-	216,422

7.5 Whole Rock Geochemistry

Shackleton Resource whole rock dataset for quarry areas. ALS lab analysis Au-ICP 21 & ME-MS61

SAMPLE ID	K20147	K20148	K20149	K20150	K20201	K20202	K20203	K20204	K20205	K20206	K20230	K20231	K20232	K20234	K26616	RS012434	RS012444	RS012461	RS012462	RS012469	RS012470	RS012486	RS012489	RS012490
Au_ppm	0.038	0.049	0.118	0.006	0.055	0.049	<0.001	0.045	0.008	0.036	0.001	0.001	0.096	0.013	0.008	0.004	0.332	0.02	-0.001	0.002	0.006	0.037	0.009	0.012
Ag_ppm	9.51	12.3	33.5	1.55	11.15	8.96	0.22	9.77	3.36	7.07	0.03	0.06	2.57	0.44	0.64	0.29	61.5	2.57	0.02	0.28	1.19	4.47	0.9	2.03
Al_%	1.03	1.53	3.35	3.52	1.18	0.78	4.37	4.77	3.11	2.18	7.97	7.59	1.9	6.79	4.4	6.57	1.4	3.06	1.9	5.4	4.19	0.42	2.58	4.42
As_ppm	36.8	20.5	55.4	8	44.5	27.5	2.3	8.9	11.9	44	3.7	4	9.8	10.5	51.5	2.4	27.8	3.9	1.3	1.6	2.8	1.8	1.7	2.2
B_ppm	0	0	0	0	0	0	0	0	0	0	0	0	0	0	0									
Ba_ppm	80	210	200	570	80	70	690	370	280	100	10	120	50	20	330	320	30	120	10	400	200	10	140	80
Be_ppm	0.18	0.71	1.22	0.69	0.28	0.2	1.09	1.3	0.76	0.51	0.47	0.44	0.16	0.25	1.88	2.03	0.38	1.06	0.68	1.64	1.28	0.17	1	1.33
Bi_ppm	1810	1480	2900	1110	2110	5960	250	1160	1190	347	0.08	0.02	6.17	3.96	12.65	14.75	4520	127	0.33	194	106	666	84.6	275
Ca_%	0.03	0.04	0.05	0.16	0.02	0.01	0.22	0.21	0.04	0.03	10.55	5.53	2.56	7.14	0.12	0.75	0.02	1.37	0.18	0.97	0.8	0.19	0.6	0.81
Cd_ppm	0.24	0.08	0.04	0.04	0.98	0.11	<0.02	0.12	0.15	0.03	0.04	0.11	0.06	0.04	0.09	0.02	0.21	0.07	0.02	0.03	0.03	0.07	0.05	0.03
Ce_ppm	7.51	21.5	37.7	26.6	9.42	3.43	18.3	52.4	26.1	11.65	9.25	4.37	8.38	7.33	31.1	82.7	10.65	44.3	1.4	86.9	64.7	3.67	31.9	72.9
Co_ppm	1185	261	591	170.5	1200	952	27.7	133.5	241	536	11	23.1	199.5	283	40	77.3	153	52.1	3.9	26.5	26.7	40.8	27.8	34.3
Cr_ppm	31	39	31	67	35	28	58	45	46	38	114	9	26	42	38	99	29	41	28	75	52	22	34	65
Cs_ppm	0.69	0.85	1.99	1.71	0.66	0.5	2.16	3.1	1.87	0.88	0.26	0.41	0.26	0.42	2.47	1.34	0.24	1.14	0.19	2.34	1.67	0.08	0.92	2.31
Cu_ppm	150.5	184	775	57.3	265	321	18.6	4540	68.6	385	45.3	94.5	664	2180	425	24	27000	21.8	6.7	34.9	44	50.5	16.8	33.3
Dy_ppm	0	0	0	0	0	0	0	0	0	0	0	0	0	0	0									
Er_ppm	0	0	0	0	0	0	0	0	0	0	0	0	0	0	0									

Eu_ppm	0	0	0	0	0	0	0	0	0	0	0	0	0	0	0									
Fe_%	21.8	5.73	10.15	5.68	24.1	18.35	3.73	6.44	6.85	13.45	6.56	7.4	12.25	12.6	4.13	6.13	11.8	11.8	1.65	5.7	7.1	21	8.72	11.8
Ga_ppm	3.75	5.02	10.8	8.51	3.98	2.64	11.05	14	8.42	3.85	23.9	21.5	5.73	21.5	12.2	21.1	3	9.61	6.13	17.55	13.05	1.44	8.5	14.5
Gd_ppm	0	0	0	0	0	0	0	0	0	0	0	0	0	0	0									
Ge_ppm	1.91	1.88	1.59	0.1	1.55	1.33	<0.05	0.09	0.06	<0.05	0.1	0.11	0.25	0.2	<0.05	0.21	0.17	0.07	0.19	0.09	0.09	0.1	0.08	0.13
Hf_ppm	0.2	0.5	0.9	0.9	0.2	0.1	1.1	0.8	0.7	0.3	0.6	0.4	0.4	1.2	1.2	0.9	0.4	0.5	<0.1	0.9	0.7	<0.1	0.3	0.8
Hg_ppm	0	0	0	0	0	0	0	0	0	0	0	0	0	0	0									
Ho_ppm	0	0	0	0	0	0	0	0	0	0	0	0	0	0	0									
In_ppm	1.07	0.098	0.182	0.163	1.295	0.175	0.168	1.27	0.243	0.088	0.053	0.043	0.025	0.418	0.216	0.077	11.15	0.037	0.011	0.079	0.054	0.005	0.027	0.056
K_%	0.45	0.75	1.68	2.33	0.49	0.36	2.69	2.37	1.79	0.74	0.12	0.59	0.33	0.61	1.91	1.48	0.29	0.91	0.08	1.58	1.12	0.04	0.72	1.61
La_ppm	3.7	10.4	17.6	12	4.6	1.7	8	25.3	11.5	5.6	4.2	1.5	3.7	2.7	14.5	40.2	5.3	21.6	0.9	44.5	32.6	1.9	15.8	36.4
Li_ppm	5.4	6.6	13.5	14.6	6	4	19.8	19.3	14.2	6.6	17	7.8	14.1	61.1	13.1	19.5	3.2	5.2	2.8	24.4	9.9	1.2	4.5	8.4
Lu_ppm	0	0	0	0	0	0	0	0	0	0	1.41	2.1	0.97	4.12	0									
Mg_%	0.08	0.14	0.29	0.45	0.1	0.06	0.65	0.57	0.37	0.18	726	1030	585	1380	0.41	1.08	0.1	0.74	0.41	0.89	0.69	0.11	0.5	0.7
Mn_ppm	62	87	89	300	68	80	410	364	178	97	0.32	0.19	2.51	0.12	175	556	90	761	247	1060	880	156	436	1050
Mo_ppm	2.46	15.9	33.1	0.71	2.97	5.15	0.88	3.93	0.63	9.1	0	0	0	0	4.06	2.1	4.44	0.26	0.43	0.31	0.34	0.3	0.32	0.35
Na_%	0.11	0.05	0.04	0.08	0.15	0.08	0.11	0.05	0.06	0.49	0.04	2.85	0.09	1.41	0.1	0.49	0.04	0.32	0.16	0.73	0.57	0.05	0.21	0.52
Nb_ppm	1.1	1.4	2.9	5.1	1.1	0.5	6.8	9	4.2	1.4	0.7	0.6	2.6	0.4	5.3	9	2.1	3.5	0.2	10.5	7.2	0.2	2.3	8.4
Nd_ppm	0	0	0	0	0	0	0	0	0	0	0	0	0	0	0									
Ni_ppm	249	57.9	87.4	46.3	180.5	172	21.7	44.9	57.3	143	38.2	3.3	13.6	67	31.4	95.3	43.1	61.7	11.6	48.5	45.5	61.1	40.7	55.3
P_ppm	60	120	250	240	50	20	410	480	130	70	290	320	330	300	390	1280	140	140	10	340	310	<10	130	320
Pb_ppm	323	415	570	137	463	932	24.3	393	128	92.7	9.9	5.4	105.5	5.7	20	8.2	43.7	41.4	2.3	49.9	32.2	154.5	15.9	74.3

Pr_ppm	0	0	0	0	0	0	0	0	0	0	0	0	0	0	0									
Rb_ppm	27.9	45.7	103	99.9	28.3	21.2	124	148.5	95.3	44.9	3.8	3.3	14.9	16.5	107.5	88.5	17.7	53.6	5.6	65.5	47.6	1.8	43.8	71.1
Re_ppm	<0.002	0.005	0.004	<0.002	0.003	<0.002	<0.002	<0.002	<0.002	<0.002	0.002	<0.002	0.004	0.004	0.002	<0.002	<0.002	<0.002	<0.002	<0.002	<0.002	<0.002	<0.002	<0.002
S_%	>10.0	5.03	8.79	4.06	>10.0	>10.0	0.88	4.19	5.66	>10.0	0.03	0.15	>10.0	5.33	2.19	3.69	9.53	>10.0	0.07	1.95	4.79	>10.0	8.08	9.56
Sb_ppm	2.17	1.71	2.27	0.48	2.17	4.72	0.3	0.27	0.72	0.37	1.38	0.11	0.44	0.94	0.62	0.4	3.27	1.31	0.16	2.35	1.51	1.17	0.79	1.85
Sc_ppm	1.3	2	5.3	4.8	1.3	0.7	5.8	7.4	4.1	1.9	29	30.9	11.8	27.2	4.6	14.9	2	6.5	2.6	12	9	0.7	5	9.6
Se_ppm	7	6	5	1	7	6	<1	1	1	2	<1	<1	32	5	2	2	9	4	<1	1	2	9	3	4
Si_ppm	0	0	0	0	0	0	0	0	0	0	0	0	0	0	0									
Sm_ppm	0	0	0	0	0	0	0	0	0	0	0	0	0	0	0									
Sn_ppm	1.4	1.6	2.2	0.9	1.4	1.2	1.4	1.9	1	0.3	0.6	0.4	0.4	1.4	1.2	1.9	3.1	1.2	0.9	2.2	1.8	<0.2	0.7	1.7
Sr_ppm	9	5.2	5.9	29.2	9	5.6	37.9	15.1	13.7	27.1	484	287	17.3	242	18	95.3	6.8	76.4	36.9	120	97.4	12.6	45.4	81.1
Ta_ppm	0.05	0.07	0.17	0.32	0.09	<0.05	0.42	0.6	0.22	0.08	0.05	<0.05	0.16	<0.05	0.32	0.59	0.13	0.21	<0.05	0.55	0.39	<0.05	0.13	0.46
Te_ppm	14.3	4.67	9.54	3.67	16.05	20.4	0.67	4.33	4.26	7.97	<0.05	<0.05	3.1	0.27	0.41	3.03	39.5	31.1	0.08	5.57	15.2	52.6	18.9	20.5
Th_ppm	0.96	1.37	3.25	3.89	1.23	0.37	5.45	5.07	4.16	1.2	0.32	0.09	0.42	0.29	4.65	10.05	1.17	4.91	0.16	11.4	8.54	0.26	3.63	10
Ti_%	0.037	0.057	0.128	0.247	0.043	0.015	0.305	0.259	0.21	0.057	0.318	0.278	0.344	0.437	0.247	0.215	0.062	0.108	0.03	0.254	0.166	0.01	0.077	0.178
Tl_ppm	0.21	0.27	0.6	0.61	0.13	0.14	0.71	0.93	0.51	0.29	<0.02	0.11	0.1	0.1	0.61	0.41	0.08	0.32	<0.02	0.37	0.28	0.02	0.27	0.44
Tm_ppm	0	0	0	0	0	0	0	0	0	0	0	0	0	0	0									
U_ppm	0.3	0.4	0.9	1	0.3	0.1	1.5	1.3	0.7	0.2	0.1	<0.1	0.2	0.1	0.9	1.3	0.5	0.6	0.1	1.3	0.9	0.1	0.4	1.3
V_ppm	11	18	46	40	12	8	52	57	38	16	243	349	129	268	57	101	13	45	32	76	58	7	39	63
W_ppm	4.3	83	26.3	14.2	5.4	4.9	14.5	185.5	15.6	9.3	0.5	0.2	1	0.4	165	2.1	5.3	1.3	0.2	1.4	1.4	<0.1	0.4	1.4
Y_ppm	1.3	4.5	5.9	4.5	0.9	0.5	5.1	12.7	3.6	2	16.2	7.7	9.1	21.5	7.5	11.6	2.4	7.2	0.7	10.2	9.1	0.7	5.1	12
Yb_ppm	0	0	0	0	0	0	0	0	0	0	0	0	0	0	0									

Zn_ppm	67	29	29	45	193	19	51	69	63	27	31	67	43	155	33	64	48	43	28	72	51	5	33	57
Zr_ppm	8.6	13	31.3	31.3	9.5	2.7	41.9	29.5	27	10.2	14	7.9	13.3	32.4	47.3	36.2	15.9	16.6	1.9	35.1	25.7	1.7	10	29

7.6 Laser Ablation Analysis

7.6.1 Polished thin sections

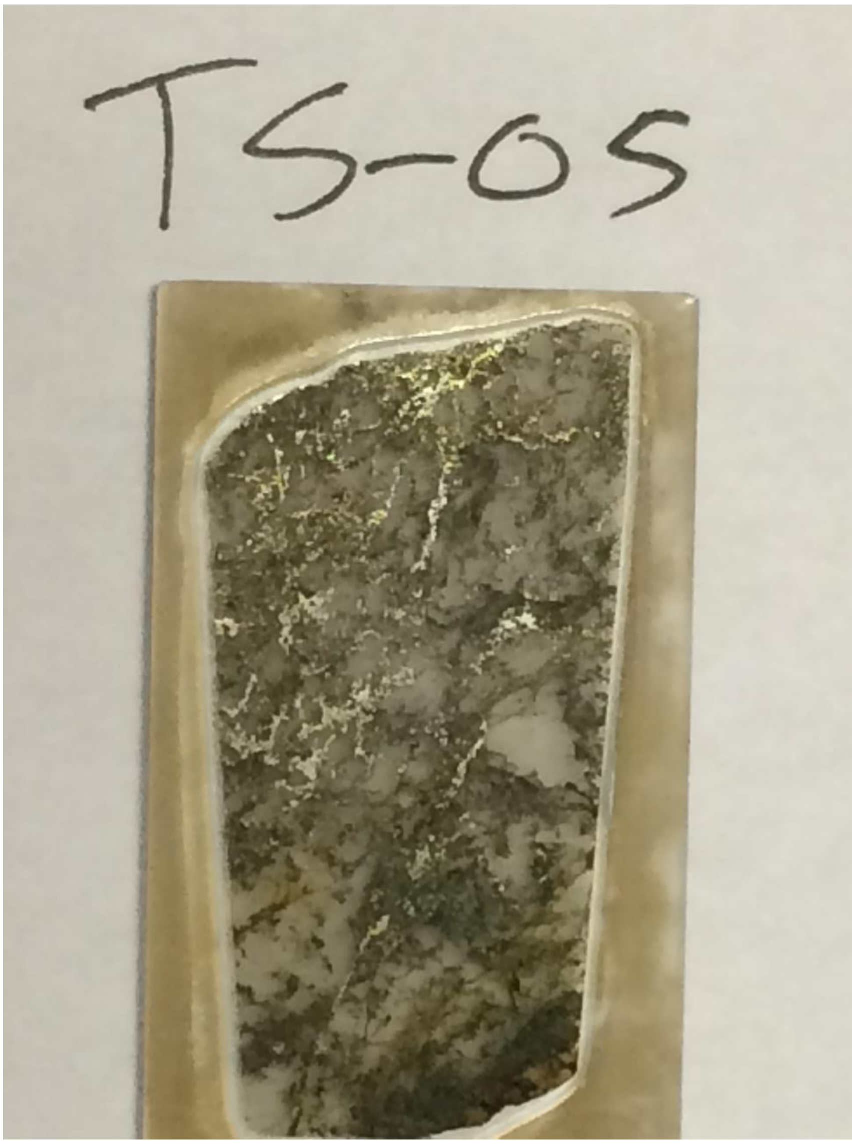

TS05 Boulder Golden Hollow. Polished thin section shows pyrite (centre) and chalcopyrite (top) sulphides.

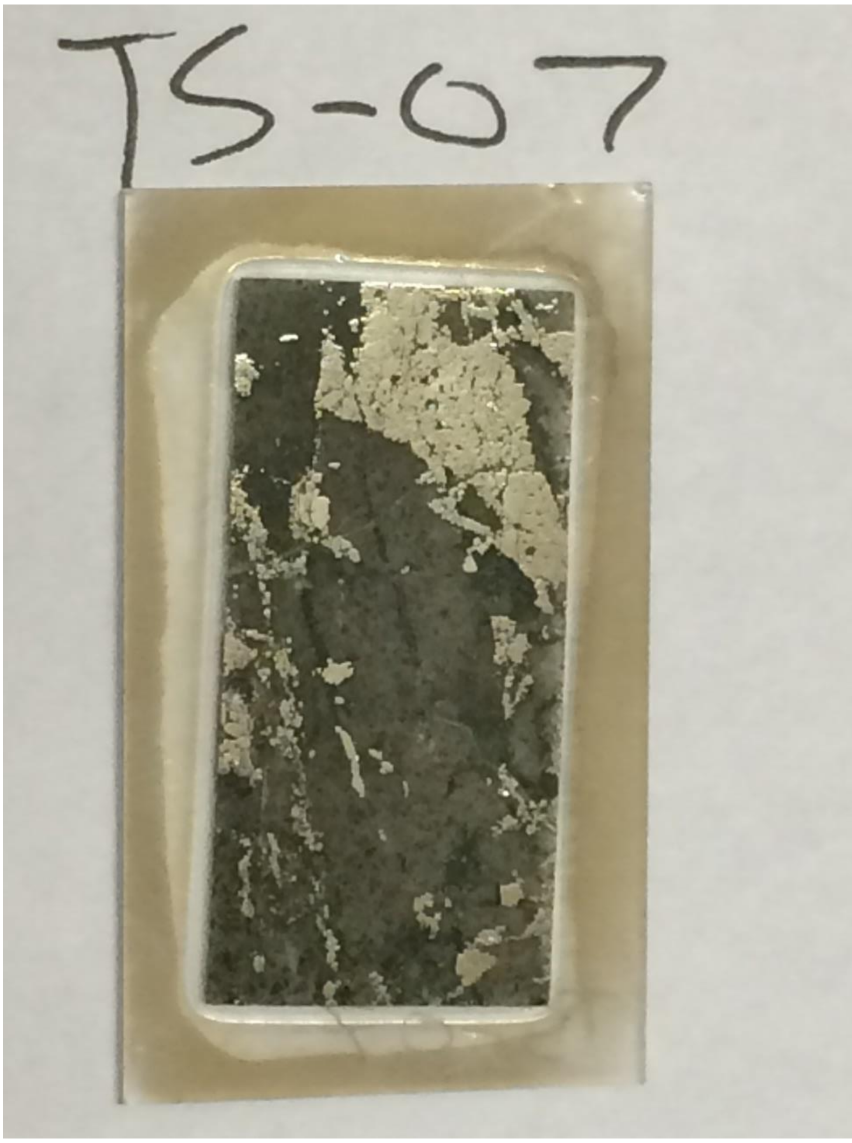

TS07 Fracture hosted pyrite from Carrickmore. Polished section shows pyrite blebs with internal detail, and thin stringers, aligned along possible fractures.

TS14 Ballantrae. Polished section shows disseminated pyrite in low concentration.

TS15 Unknown sample ID. Polished section shows pyrite bands with fine sulphide stringers. Pyrite shows euhedral form with brecciation texture.

TS16a. Unknown sample ID. Polished section is of pyrite with small disseminations. Internal pyrite texture of possible brecciation

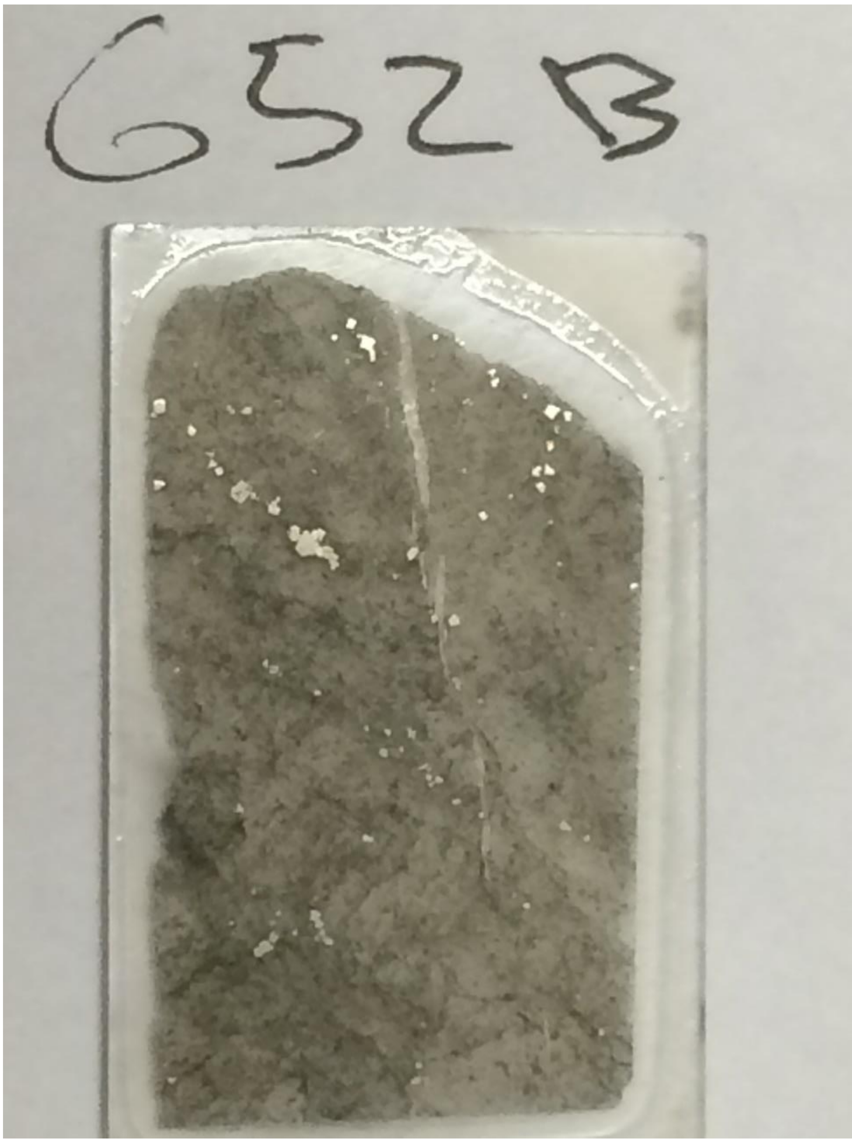

652B unknown sample ID. Polished section shows disseminated sulphides at low concentrations.

SL02 Unknown sample ID. Polished section of massive pyrite with internal brittle, brecciation texture.

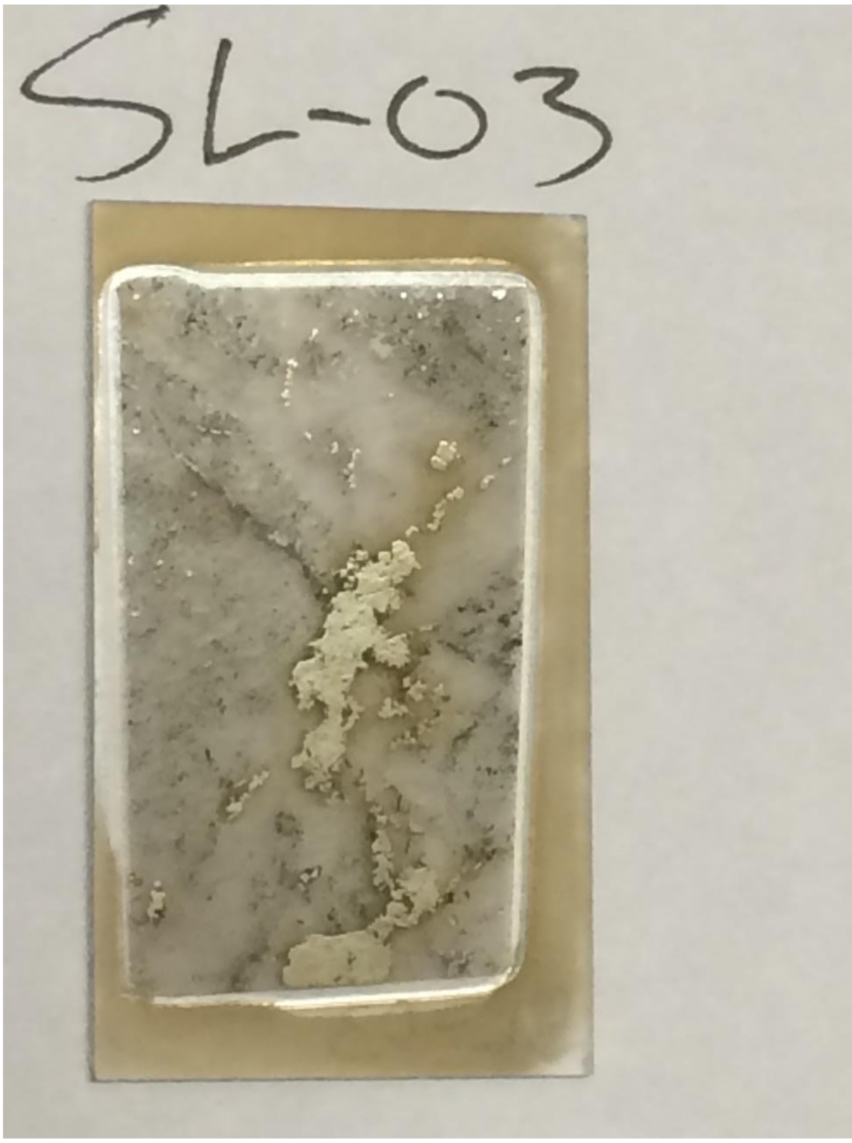

SL03 Unknown sample ID. Polished section shows pyrite blebs.

SL16 Unknown sample ID. Polished section is of pyrite with euhedral habit and brecciated texture.

7.6.2 LA ICP-MS Unit Metadata

Table supplied by TCD ore analysis laboratory.

Procedure:			
2S.D. outlier rejection for baseline selections			
2S.D. outlier rejection for normal selections			
Baseline reverse trim			17s
Baseline duration			16s
Match cutoff			0.4
Spline for baselines		AutoSmooth	
Spline for all STDs		Smooth 9	
Ext. STD	MASS1	all elements except Tl	
	MUL-ZnS	Tl	
		Int STD.	
Chalcopyrite		Fe	30.43
Pyrite		Fe	46.55
Arsenopyrite		Fe	34.3

Data Reduction Scheme Settings	
Trace Elements	
DefaultRefMat	
Full-Quant	TRUE
Howell	FALSE
IndexChannel	Fe57
Longerich	FALSE
MaskChannel	Al27
MaskCutoff	1000
MaskMethod	Laser log
MaskResults	FALSE
MaskTrim	0
Pettke	TRUE
exceptions	

7.6.3 Laser Ablation Sample Chain

The sample IDs are summarised against the received results. Samples submitted February 2020, ablation results received December 2021.

Original sample ID	**Status**	**Returned sample ID with analysis**	**Status**
TCD-TS-01	No data	TS05	Known sample
TCD-TS-02	No data	TS07	Known sample
TCD-TS-03	No data	TS14	Known sample
TCD-TS-04	No data	TS15	**unknown sample**
TCD-TS-05	Data = TS05	TS16a	**unknown sample**
TCD-TS-06	No data	SL02	**unknown sample**
TCD-TS-07	Data = TS07	SL03	**unknown sample**
TCD-TS-08	No data	SL016	**unknown sample**
TCD-TS-09	No data	652B	**unknown sample**
TCD-TS-10	No data		
TCD-TS-11	No data		
TCD-TS-12	No data		
TCD-TS-13	No data		
TCD-TS-14	Data = TS14		

7.6.4 Laser Ablation Element Data

All laser ablation element data, uncertain link to actual samples submitted. Six sample IDs in the results do not match any samples submitted.

	Mn55 ppm	Co59 ppm	Ni60 ppm	Cu65 ppm	Zn67 ppm	Ga71 ppm	Ge73 ppm	As75 ppm	Se77 ppm	Mo95 ppm	Ag109 ppm	Cd111 ppm	In115 ppm	Sn118 ppm	Sb121 ppm	Te125 ppm	Au197 ppm	Hg202 ppm	Tl205 ppm	Pb207 ppm	Bi209 ppm
Pyrite																					
TS05-A_Py_1	36.00718	52	174.0023	342.7911	0.001	0.275565	0.001	22.17963	6.030591	0.001	2.075527	0.001	1.726584	0.001	2.510919	29.90346	0.427574	4.924891	0.001	30.27707	236.189
TS05-A_Py_2	19.73976	15	431.5055	687.2575	0.001	0.341391	0.809299	174.2522	11.36787	0.117333	4.939713	0.001	2.4476	0.001	10.0357	25.60817	0.567377	2.736467	0.001	72.66932	355.3775
TS05-B_Py_3	0.001	101	149.7124	1073.489	0.001	0.001	0.777265	9.704998	7.147743	0.001	0.873983	0.001	0.560566	0.001	0.001	72.20145	0.001	3.717803	0.001	3.188086	280.2762
TS05-B_Py_5	0.001	84	153.4551	0.001	0.001	0.037638	0.001	8.001842	9.301459	0.001	0.001	0.001	0.008482	0.001	0.001	1.485557	0.001	2.823774	0.001	0.001	7.102838
TS05-C_Py_1	71.02637	18	644.016	116.9287	0.001	0.418682	0.001	5.652573	0.001	0.001	0.001	0.001	0.020409	8.019352	2.413344	1.732473	0.001	0.001	5.774094	7.060903	6.165424
TS05-C_Py_2	0.001	148	157.5608	60.84215	0.001	0.001	0.001	15.47396	6.114669	0.001	0.395059	0.001	0.001	0.001	0.001	2.211174	0.001	3.610686	0.001	0.430193	8.537026
TS05-C_Py_3	0.001	357	46.07015	15.57044	0.001	0.001	0.001	22.17423	5.060561	0.271213	2.222242	0.001	0.001	0.001	0.001	6.795911	0.465275	3.546915	0.001	3.452773	65.03135
TS05-D_Py_2	0.001	0	733.9588	11.82602	0.001	0.185027	0.001	146.8919	9.846415	0.091089	0.94097	0.001	0.007233	0.001	0.001	4.990688	0.800384	2.505563	0.06634	2.221727	24.92331
TS05-D_Py_3	0.001	1	782.6795	0.001	0.001	0.001	0.001	32.75925	7.225775	0.001	0.254234	0.001	0.002753	0.001	0.001	4.343669	0.177657	2.486111	0.001	1.099987	13.61388
TS05-D_Py_4	0.001	6	44.7369	100.2501	0.001	0.001	0.001	83.64449	8.603702	0.001	7.473342	0.001	0.320292	0.001	2.846702	6.627709	0.119076	8.321939	0.001	21.79988	99.10246
TS05-D_Py_5	0.001	0	8.88219	0.001	0.001	0.001	0.001	100.5475	11.71357	0.001	0.109802	0.001	0.010909	0.001	0.001	0.818981	0.001	4.448477	0.001	0.585263	2.68356
TS05-E_Py_1	105.9021	70	315.7148	6.756015	19.7922	0.001	0.001	2.940391	7.755076	0.062288	0.334672	0.927784	0.040457	0.001	0.001	2.827075	0.001	3.063525	0.001	0.762752	15.49274
TS05-E_Py_3	0.001	3	1941.952	7.385778	0.001	0.071052	0.865645	24.81391	22.31407	0.075814	5.085987	0.001	0.020011	0.001	0.001	17.72711	0.342816	0.001	0.001	4.309993	91.61472
TS05-E_Py_4	0.001	2	1893.564	3.279907	0.001	0.268691	1.132706	7.759782	19.37697	0.093318	0.793558	0.001	0.011416	0.001	0.001	7.467769	0.532995	0.001	0.001	5.172217	41.0617
TS05-E_Py_5	8.045736	7	2517.14	9.27178	0.001	0.052647	0.001	4.046258	13.69154	0.001	1.159864	0.001	0.0163	0.001	0.001	3.664855	0.001	0.001	0.001	3.820435	37.30537
SL-016-A_Py_1	0.001	235	1313.038	4.362525	0.001	0.001	0.811385	1.711751	5.465345	0.001	0.159757	0.001	0.001	0.001	0.001	0.431016	0.001	3.573518	0.001	0.791981	1.336113
SL-016-A_Py_3	0.001	176	1150.848	0.001	0.001	0.069056	0.001	1.19868	7.6865	0.001	0.001	0.001	0.001	0.001	0.001	2.184126	0.001	3.989991	0.001	0.001	1.82847
SL-016-B_Py_1	0.001	2658	1200.751	5.004271	0.001	0.122564	0.86326	2.469275	8.268907	0.068042	1.166638	0.001	0.00856	0.001	0.001	4.844551	0.001	6.182697	0.001	7.927209	32.2974
SL-016-B_Py_2	0.001	633	217.5591	7.945905	0.001	0.001	0.001	0.001	6.392819	0.10331	0.001	0.001	0.001	0.001	0.001	0.451766	0.001	4.69785	0.001	0.601505	2.085017
SL-016-B_Py_3	0.001	1630	365.7998	4.047637	0.001	0.001	0.001	5.842604	7.241049	0.178277	0.31129	0.001	0.001	0.001	0.001	5.640425	0.099259	6.360381	0.001	2.231231	27.89542
SL-016-C_Py_2	11.10704	3492	24.26137	3.11602	0.001	0.001	0.001	19.85259	0.001	0.001	0.001	0.001	0.001	0.001	0.001	0.001	0.001	2.749465	0.001	1.440283	1.913878

SL-016-		1051	142.540	115.074				134.041		0.06132	0.51785					6.75389		3.74412			33.9087
D_Py_3	0.001	4	4	3	0.001	0.001	0.001	6	4.47646	2	1	0.001	0.03369	0.001	0.001	8	0.001	3	0.001	2.86387	6
SL-016-			102.165	4.47351					8.91359		1.30884					11.3546		7.02617		10.9125	67.0228
E_Py_1	0.001	47	3	3	0.001	0.001	0.001	3.58483	4	0.001	9	0.001	0.001	0.001	0.001	1	0.001	7	0.001	6	7
SL-016-			154.085	4.13885				7.87041	6.34956		0.28572					5.83944				1.20220	25.7966
E_Py_2	0.001	410	6	2	0.001	0.001	0.001	9	8	0.001	7	0.001	0.001	0.001	0.001	4	0.001	5.53817	0.001	7	5
SL-016-			14.6527	4.11899				0.98253	8.30336							0.24469		5.82360		0.08203	
E_Py_3	0.001	21	7	8	0.001	0.001	0.001	1	1	0.001	0.001	0.001	0.001	0.001	0.001	9	0.001	4	0.001	3	0.001
SL-016-	10.8687		115.241				0.98054		12.8165				0.01646			1.65414					
F_Py_1	6	38	8	0.001	0.001	0.001	5	1.18126	7	0.001	0.001	0.001	6	0.001	0.001	9	0.001	7.03059	0.001	0.001	0.001
SL-016-								1.44915	12.2979							0.28059		6.00903			0.07253
F_Py_2	0.001	15	78.2349	0.001	0.001	0.001	0.001	8	1	0.001	0.001	0.001	0.001	0.001	0.001	1	0.1091	9	0.001	0.001	3
SL-016-			902.894	7.41517				15.0592	14.5278				0.01399							1.14109	9.30816
F_Py_3	0.001	1274	1	6	0.001	0.001	0.001	6	5	0.001	0.001	0.001	4	0.001	0.001	1.36804	0.001	7.06834	0.001	2	9
SL-016-			272.432					14.0976	6.97443	0.06560	0.58352		0.00734					12.1932		7.63627	26.0113
G_Py_1	0.001	2284	1	0.001	0.001	0.001	0.001	8	3	2	3	0.001	6	0.001	0.001	2.34342	0.001	4	0.001	4	9
SL-016-			755.756				1.10854		7.80470		1.41605					10.0369		10.3508		7.50960	49.9131
G_Py_2	0.001	1517	3	0.001	0.001	0.001	8	0.001	4	0.001	7	0.001	0.001	0.001	0.001	1	0.001	1	0.001	5	9
SL-016-			89.4044	4.40384				187.498			4.14599		0.00340			13.3249		14.8461		41.4329	118.381
G_Py_3	0.001	3986	2	5	0.001	0.001	0.001	6	0.001	0.001	6	0.001	9	0.001	0.001	4	0.001	2	0.001	6	3
652B-						2.37879	5.25263	17497.0	6.48675	0.06268			0.02259		4.29623		4.60163	2.60514		9.27931	0.84858
B_Py_1	0.001	0	0.001	0.001	0.001	1	7	8	4	8	0.001	0.001	9	0.001	3	0.001	9	6	0.001	2	9
652B-				8.60655		0.07521		18084.1	5.79592	0.66208	0.25169				5.23285		4.13873	4.14277		5.43213	
B_Py_2	0.001	0	0.001	3	0.001	4	0.001	3	9	7	4	0.001	0.02976	0.001	2	0.001	8	6	0.001	8	0.7309
652B-			21.9734	13.8820		3.05300		16735.8	4.44219	5.71964	0.81502			1.11318	6.15008		5.73607		0.08332	39.3155	1.23508
B_Py_3	0.001	5	2	7	0.001	4	0.001	7	6	3	7	0.001	0.03091	7	6	0.001	2	9.188	8	3	1
652B-						0.97321		16212.1		0.10214	0.40951		0.03304		6.84764		2.23782			10.5766	0.78567
C_Py_1	0.001	0	0.001	0.001	0.001	1	0.001	2	2.9014	1	8	0.001	5	0.001	6	0.001	5	6.33248	0.001	6	2
652B-	109.330			10.9124		4.12608	0.83037	14944.9		0.30280	0.77530		0.05952	6.27084	12.6358		2.75526	8.73477		20.6713	2.03044
C_Py_2	3	1	0.001	7	0.001	6	4	5	0.001	4	3	0.001	6	2	6	0.001	7	6	0.001	2	5
652B-				8.23762	31.6146		0.74770	14364.6							1.23657	0.07164	2.45483	3.95836		1.32213	0.16718
C_Py_3	0.001	0	0.001	6	7	0.001	2	4	0.001	0.001	0.001	0.001	0.01802	0.001	2	7	2	4	0.001	3	8
652B-	58.3228				19.8542	6.81934	1.35009		3.91640	0.26928	1.25991		0.16922	40.8762	8.04176		0.75327	32.1293	0.28819	86.4523	2.11680
D_Py_1	5	2	0.001	0.001	5	4	8	8761.33	9	2	1	0.001	7	5	8	0.001	9	3	8	6	3
652B-				5.89877		1.23548	0.79625	13426.7	4.32515		0.13437			0.59268	3.85487		1.27744	5.23927		5.09297	0.41348
D_Py_2	0.001	0	0.001	5	0.001	9	9	7	6	0.001	5	0.001	0.001	7	5	0.001	1	7	0.001	1	4
652B-				2.30856				8333.36		0.14067	0.26891						0.33487	7.84442		15.2097	0.19839
D_Py_3	0.001	1	0.001	9	0.001	0.15478	0.001	5	4.51302	7	7	0.001	0.001	0.001	0.89217	0.001	7	9	0.001	6	9
652B-				9.55335				194.697		0.07866	0.20422					0.53236		11.8102		11.5845	0.69147
E_Py_1	0.001	3	0.001	1	0.001	0.001	0.001	7	0.001	9	5	0.001	0.001	0.001	2.68921	3	0.001	6	0.001	9	6
652B-				4.90073		0.68851					0.26323				5.80278		0.71058	9.63191		8.80685	0.87153
E_Py_2	0.001	0	0.001	6	0.001	8	0.001	7400.32	0.001	0.001	5	0.001	0.00911	0.001	5	0.001	4	4	0.001	9	3
652B-			5.69199	3.92556		0.15978		3274.11	4.93566				0.01175		7.62301		0.53564	11.8976		18.9649	
E_Py_3	0.001	1	9	4	0.001	3	0.001	5	2	0.001	0.1787	0.001	2	0.001	7	0.001	2	9	0.001	5	1.36199
652B-						0.46364		12898.7					0.02132		2.94459		3.11933	15.6851		4.21841	
F_Py_1	0.001	0	0.001	0.001	0.001	9	1.57506	9	0.001	0.001	0.001	0.001	5	0.001	1	0.001	4	1	0.001	8	0.45412
652B-								5268.68							1.85366	0.19511	0.34658	12.8132		7.78361	0.36848
F_Py_2	0.001	1	0.001	0.001	0.001	0.001	0.001	3	0.001	0.001	0.001	0.001	0.001	0.001	5	9	3	2	0.001	1	4
652B-				9.59696		8.59189		14997.6		0.34947	0.60864				33.7984	0.22948	4.17437		0.15042	55.9669	
F_Py_3	0.001	0	0.001	7	0.001	5	0.001	6	0.001	7	1	0.001	0.001	0.001	7	5	4	18.7634	2	2	2.55691
652B-						0.82929					0.44431		0.01040		7.09250		2.10524	4.13879		19.5299	0.65386
G_Py_1	0.001	0	0.001	0.001	0.001	6	0.001	13784.8	0.001	0.001	4	0.001	3	0.001	8	0.61227	8	4	0.001	8	6

652B-G_Py_2	0.001	0	0.001	0.001	0.001	0.510888	0.001	15822.87	0.001	0.001	0.001	0.001	0.022617	0.001	0.817914	0.001	2.205778	6.191784	0.001	1.230277	0.122686
TS-15-A_Py_1	0.001	201	93.77689	6.975874	0.001	0.001	1.341506	0.001	12.55499	0.001	0.001	0.001	0.001	0.001	0.001	1.694692	0.096182	14.41292	0.001	3.277682	14.07023
TS-15-A_Py_2	0.001	104	106.6296	105.7455	0.001	0.001	0.001	3.374988	11.3731	0.001	0.001	0.001	0.001	0.001	0.001	0.981642	0.001	17.04792	0.001	0.988258	6.048998
TS-15-A_Py_3	109.939	353	107.5544	53.28572	0.001	0.440348	0.001	20.15936	5.777017	2.341284	2.723598	0.001	0.001	0.755218	0.756306	141.1191	0.277444	144.6789	0.420515	22.26203	264.0927
TS-15-B_Py_1	0.001	415	144.0302	304.4413	0.001	0.158901	0.001	10.307	14.18364	2.330298	5.670108	0.001	0.001	0.001	0.001	33.74418	0.001	94.31478	0.001	52.90077	358.5072
TS-15-B_Py_2	0.001	101	104.9394	23.90362	0.001	0.001	0.001	0.001	9.542142	0.001	0.209952	0.001	0.001	0.001	0.001	2.659484	0.001	11.34528	0.001	1.594309	11.8902
TS-15-B_Py_3	0.001	138	104.1883	16.08567	0.001	0.001	0.001	0.001	12.20692	0.143797	0.188696	0.001	0.001	0.001	0.001	3.470796	0.001	18.09656	0.001	0.226437	2.429466
TS-15-C_Py_1	0.001	174	141.9526	7.25347	0.001	0.001	0.001	3.537881	19.70648	0.001	0.001	0.001	0.001	0.001	0.001	2.561645	0.001	15.12931	0.001	0.359794	0.945093
TS-15-C_Py_2	0.001	73	84.40466	22.33438	0.001	0.124304	0.986835	0.001	10.6727	0.095909	4.909036	0.001	0.015594	0.001	0.001	15.33391	0.001	13.11545	0.001	6.261991	37.25234
TS-15-C_Py_3	0.001	141	75.08627	5.507917	21.89278	0.189452	0.001	3.6535	9.042867	0.165154	0.657381	0.001	0.039933	0.001	0.001	1.154335	0.001	13.58864	0.001	1.314224	4.837939
TS-15-D_Py_1	0.001	128	183.8832	4.788396	0.001	0.093141	1.042534	55.06668	21.61543	0.001	0.937128	0.001	0.01383	0.001	0.001	4.485548	0.001	3.951325	0.001	13.14138	29.64086
TS-15-D_Py_2	0.001	59	88.02483	0.001	0.001	0.001	1.336965	0.001	15.07872	0.001	0.001	0.001	0.001	0.001	0.001	2.098575	0.001	4.503289	0.001	0.001	0.001
TS-15-D_Py_3	0.001	79	28.2965	7.456124	0.001	0.001	0.001	2.411911	11.48834	0.178311	0.001	0.001	0.001	0.001	0.001	0.001	0.001	0.001	0.001	0.192007	0.001
TS-15-E_Py_1	0.001	77	20.51113	0.001	0.001	0.070751	0.001	0.001	11.09624	0.001	0.139804	0.001	0.001	0.001	0.001	0.524063	0.001	8.338108	0.001	0.257957	0.001
TS-15-E_Py_2	0.001	261	56.6834	5.267571	0.001	0.001	0.001	0.001	13.75642	0.262807	1.091552	0.001	0.004899	0.001	0.001	2.172151	0.126188	8.653478	0.001	1.966629	4.81285
TS-15-E_Py_3	0.001	247	91.03172	6.003017	0.001	0.001	0.001	0.001	10.73161	0.0742	0.254607	0.001	0.009958	0.001	0.001	0.944229	0.001	6.007698	0.001	1.69927	1.798378
TS-15-F_Py_1	0.001	441	345.1352	4.228483	0.001	0.001	0.813782	2.562552	19.95634	0.001	0.126992	0.001	0.00374	0.001	0.001	5.795762	0.001	8.594674	0.001	0.307121	0.001
TS-15-F_Py_2	0.001	439	194.3354	0.001	0.001	0.001	0.001	5.686153	13.64879	0.001	0.178595	0.001	0.001	0.001	0.001	3.143792	0.001	13.16651	0.001	0.125306	0.18436
TS-15-F_Py_3	0.001	338	373.1425	0.001	0.001	0.001	0.001	2.676839	36.92148	0.001	0.001	0.001	0.001	0.001	0.001	17.9055	0.001	13.32379	0.001	0.24022	0.167833
TS-15-G_Py_1	0.001	115	84.77807	4.601969	0.001	0.001	0.001	2.882268	23.72383	0.001	0.001	0.001	0.011259	0.001	0.001	5.385453	0.001	7.977226	0.001	0.283602	0.001
TS-15-G_Py_2	0.001	781	277.3047	24.59921	0.001	0.001	0.001	3.808215	15.84385	0.001	0.201834	0.001	0.022447	0.001	0.001	2.694493	0.001	9.724445	0.001	1.27906	5.542299
TS-15-G_Py_3	0.001	409	83.45725	6.808481	0.001	0.001	0.001	8.906252	10.52923	0.079899	1.601623	0.001	0.007401	0.001	0.446349	14.24865	0.001	20.71631	0.001	33.79126	69.01678
TS-16a_Py-A_1	0.001	2484	813.9007	15.59654	0.001	1.492992	1.287201	62.57152	4.606176	0.001	0.001	1.102751	0.024829	0.001	0.001	2.23885	0.001	20.3996	0.001	2.294098	16.46357
TS-16a_Py-A_2	0.001	316	1463.782	0.001	0.001	0.096947	1.166092	6.972169	8.625978	0.067271	0.228664	1.411414	0.001	0.001	0.001	0.480167	0.001	6.83336	0.001	1.244842	2.661378

TS-16a_Py-A_3	16.28637	2142	206.0445	11.53907	21.03413	0.050598	0.001	49.27279	0.001	0.001	2.588537	1.648222	0.001	0.001	0.405585	13.34841	0.001	10.5274	0.001	23.30676	107.5328
TS-16a_Py-B_1	0.001	181	279.4408	0.810102	508.8724	0.135649	0.001	2.27316	4.586082	0.001	0.001	1.093057	0.045984	0.001	0.001	0.464637	0.001	9.839495	0.001	0.621546	0.001
TS-16a_Py-B_2	0.001	635	580.8729	0.001	0.001	0.001	0.001	19.60223	5.343696	0.001	0.001	0.001	0.001	0.001	0.001	0.510885	0.001	7.716773	0.001	0.001	1.790954
TS-16a_Py-B_3	0.001	287	355.9735	5.001734	0.001	0.001	0.001	16.53378	4.645793	0.001	0.617921	0.001	0.001	0.001	0.001	7.235043	0.001	7.872398	0.001	4.770674	47.92629
TS-16a_Py-C_1	0.001	397	49.92833	4.891609	0.001	0.102949	0.001	35.71756	0.001	0.001	1.49346	0.001	0.001	0.001	0.001	2.36869	0.001	5.028892	0.001	19.54815	44.12473
TS-16a_Py-C_2	0.001	1320	476.6046	50.02035	0.001	0.001	0.582993	52.30801	0.001	0.001	1.569846	0.001	0.001	0.001	0.001	2.684662	0.001	2.325049	0.001	5.311279	28.16445
TS-16a_Py-C_3	8.757803	493	165.4676	2.320029	0.001	0.001	0.815449	67.61052	0.001	0.001	0.001	0.001	0.001	0.001	0.001	0.485759	0.001	3.183899	0.001	0.001	2.375469
TS-16a_Py-D_1	0.001	580	1029.51	3.962069	0.001	0.051708	0.001	78.21484	4.84654	0.001	0.001	0.001	0.001	0.001	0.001	1.331426	0.001	4.304125	0.001	0.492767	4.040068
TS-16a_Py-D_2	0.001	1570	504.099	0.001	0.001	0.001	0.795758	111.0537	3.185692	0.001	0.001	0.001	0.007008	0.001	0.001	1.025047	0.001	3.239153	0.001	0.309609	4.815596
TS-16a_Py-D_3	0.001	1004	314.1449	10.5035	0.001	0.001	0.001	78.40696	0.001	0.001	0.344446	0.001	0.001	0.001	0.001	5.82027	0.001	0.001	0.001	7.054486	32.64077
TS-16a_Py-E_1	0.001	183	72.92692	13.39982	0.001	0.001	0.001	10.89195	0.001	0.001	3.437966	0.001	0.001	0.001	0.001	29.31087	0.001	0.001	0.001	25.46441	160.8581
TS-16a_Py-E_2	0.001	280	96.75903	9.109907	0.001	0.001	0.001	6.913192	5.181898	0.001	1.270594	0.001	0.001	0.001	0.001	5.701632	0.001	2.355816	0.001	40.46565	292.2454
TS-16a_Py-E_3	0.001	17	20.69454	15.38973	0.001	0.001	0.001	2.175959	0.001	0.001	2.437979	0.981855	0.001	0.001	0.001	3.039124	0.001	5.095865	0.001	20.2594	39.23985
TS-16a_Py-F_1	0.001	1412	230.2898	24.1595	0.001	0.060326	0.900012	40.49232	3.3394	0.001	5.892122	1.214063	0.001	0.001	0.001	10.07197	0.001	10.15307	0.001	40.43138	213.3784
TS-16a_Py-F_2	0.001	1588	338.4335	0.379045	0.001	0.001	0.001	84.29883	3.899428	0.001	0.001	0.001	0.001	0.001	0.001	0.001	0.001	7.597266	0.001	0.001	0.231343
TS-16a_Py-F_3	0.001	3870	113.9286	4.189635	0.001	0.001	0.001	80.05871	0.001	0.001	0.981467	0.001	0.001	0.001	0.001	5.452088	0.001	7.098579	0.001	4.248546	43.95469
TS-16a_Py-G_2	0.001	474	279.2706	3.986128	0.001	0.001	0.001	48.00322	0.001	0.001	0.444643	0.001	0.022834	0.001	0.001	2.553447	0.075019	7.124913	0.001	2.426906	22.16384

TS-16a_Py-G_3	0.001	1400	607.0466	0.001	0.001	0.001	0.932995	13.2542	10.65776	0.001	0.187561	0.001	0.001	0.001	0.001	3.223418	0.001	9.487739	0.001	2.123043	15.59841
SL-03_Py-A_1	0.001	63	176.0871	4.251142	0.001	0.059842	0.001	2.781142	0.001	0.001	0.001	0.001	0.001	0.001	0.001	0.001	0.001	4.372024	0.001	0.001	0.098269
SL-03_Py-A_2	0.001	795	326.4455	15.55767	0.001	0.135901	0.001	75.01588	7.574334	0.001	2.056903	1.555222	0.001	0.001	0.439727	8.229185	0.092223	0.001	0.069225	1.2046	14.69775
SL-03_Py-A_3	0.001	240	957.1675	2.611448	0.001	0.001	0.001	9.049666	0.001	0.001	0.001	0.001	0.001	0.001	0.001	0.376103	0.001	0.001	0.001	0.001	0.001
SL-03_Py-B_1	0.001	1733	378.1816	0.001	0.001	0.106503	0.001	47.88201	0.001	0.001	0.001	0.001	0.001	0.001	0.001	2.969189	0.001	0.001	0.001	0.405157	8.081932
SL-03_Py-B_2	0.001	1534	758.7815	0.001	0.001	0.001	0.001	160.8221	0.001	0.001	0.273249	0.001	0.011409	0.001	0.001	2.952276	0.001	0.001	0.001	0.76485	18.26649
SL-03_Py-B_3	0.001	983	451.3034	0.001	0.001	0.001	0.001	237.0289	6.660849	0.001	0.001	0.001	0.001	0.001	0.001	1.633846	0.001	0.001	0.001	1.158546	5.280658
SL-03_Py-C_1	0.001	905	696.181	0.001	20.47943	0.001	0.001	111.3441	7.309886	0.001	0.001	0.001	0.004545	0.001	0.001	0.779042	0.001	0.001	0.001	0.503426	6.343869
SL-03_Py-C_2	0.001	961	197.0684	0.001	0.001	0.001	0.823679	23.47625	0.001	0.001	0.268878	0.001	0.001	0.001	0.001	4.222891	0.001	0.001	0.001	1.349797	20.21413
SL-03_Py-C_3	36.59906	3640	809.1798	0.001	0.001	0.001	0.001	156.9724	4.502074	0.001	0.483073	0.001	0.001	0.001	0.001	2.16591	0.001	0.001	0.001	4.112687	18.38253
SL-03_Py-D_1	0.001	383	631.5885	4.043322	0.001	0.001	0.001	111.8231	4.847282	0.181383	0.57452	0.001	0.001	0.001	0.001	45.34399	0.001	6.233309	0.001	3.063932	39.20613
SL-03_Py-D_2	0.001	297	528.2163	3.590947	0.001	0.080981	0.001	106.1725	3.296486	0.001	0.269298	0.001	0.008659	0.001	0.001	2.847972	0.001	5.268764	0.001	1.495104	20.3114
SL-03_Py-D_3	0.001	776	470.5641	2.530266	0.001	0.076116	0.001	139.596	0.001	0.001	0.414879	0.001	0.010094	0.001	0.001	5.256085	0.001	4.002672	0.001	2.421944	23.03712
SL-03_Py-E_1	0.001	1874	534.2153	3.674586	0.001	0.140496	1.388089	253.4671	0.001	0.001	0.713959	0.001	0.001	0.001	0.001	2.602945	0.001	0.001	0.001	4.714307	15.52791
SL-03_Py-E_2	0.001	952	1004.416	0.001	0.001	0.011872	1.115426	126.3162	0.001	0.001	0.001	0.001	0.001	0.001	0.001	0.658122	0.001	0.001	0.001	0.234211	2.19334
SL-03_Py-E_3	0.001	609	406.5575	0.001	0.001	0.039056	0.001	94.2756	0.001	0.001	0.001	0.001	0.001	0.001	0.001	0.001	0.063851	0.001	0.001	0.253586	4.282152
SL-03_Py-F_1	0.001	578	1028.002	2.085306	0.001	0.001	0.001	257.2542	6.937639	0.001	0.001	0.001	0.001	0.001	0.001	0.001	0.001	2.087338	0.001	0.001	0.001

SL-03_Py-F_2	0.001	1364	268.4006	5.275396	0.001	0.001	1.800293	200.3123	7.848958	0.001	0.001	0.001	0.001	0.001	0.001	0.001	0.067863	3.151787	0.001	0.47072	1.594704
SL-03_Py-F_3	11.37423	428	206.712	7.885316	0.001	0.001	0.001	191.0236	6.066402	0.001	0.535954	0.001	0.001	0.001	0.001	5.749935	0.001	6.107192	0.001	7.39975	54.37699
SL-03_Py-G_1	0.001	196	1701.576	0.001	0.001	0.001	0.001	8.852055	5.46679	0.001	0.30941	0.001	0.001	0.001	0.001	4.306681	0.001	3.029733	0.001	1.444858	2.543654
SL-03_Py-G_2	0.001	106	375.3351	0.001	0.001	0.001	0.001	0.001	0.001	0.172517	0.001	0.001	0.001	0.001	0.001	0.001	0.001	2.846851	0.001	0.001	0.31247
SL-03_Py-G_3	0.001	88	628.8952	4.430201	0.001	0.001	0.869815	3.022471	3.326265	0.246452	0.001	0.001	0.001	0.001	0.001	0.001	0.001	6.024521	0.001	1.262573	1.778076
TS-14_Py-A_1	214.7941	112	146.0071	85.36838	18.07397	2.721904	0.001	270.023	0.001	17.2189	0.750677	1.037111	0.023054	0.001	2.613268	0.180766	0.001	4.320668	2.48869	13.93464	0.125895
TS-14_Py-A_2	17.48616	51	56.26466	35.25885	0.001	0.365939	0.001	58.46439	0.001	23.98295	0.448666	0.001	0.014288	0.001	1.102347	0.001	0.001	6.706394	0.637041	8.299239	0.171633
TS-14_Py-A_3	54.45909	95	128.1909	123.5593	0.001	0.803063	0.001	166.9255	0.001	21.68314	0.001	8.109447	0.001	0.001	1.003936	0.001	0.001	6.278805	1.309808	52.9911	1.64335
TS-14_Py-B_1	63.55036	2	27.04903	13.365	17.09735	0.001	0.680631	0.001	0.001	0.166344	0.001	0.001	0.001	0.001	0.001	0.001	0.001	5.145109	0.26852	0.001	0.001
TS-14_Py-B_2	262.989	5	54.58621	27.30454	27.70415	0.085918	0.001	0.811324	0.001	0.213831	0.152112	0.001	0.001	0.001	0.001	0.21968	0.001	2.514592	0.001	3.062796	0.001
TS-14_Py-B_3	48.49778	198	311.6318	63.01834	0.001	0.089585	0.663364	6.192968	0.001	0.267406	0.295227	0.001	0.001	0.001	0.522373	0.212386	0.001	5.814769	0.538627	19.18659	0.001
TS-14_Py-C_1	26.33008	1547	1260.807	177.0582	0.001	0.385183	0.001	1917.049	10.77064	6.866246	5.018595	4.287286	0.015004	0.001	24.70375	1.336512	0.001	8.634486	14.86353	214.6475	0.774268
TS-14_Py-C_2	264.172	207	410.4914	142.7168	54.52418	3.7498	0.001	117.4716	0.001	0.001	1.342802	0.001	0.019096	0.001	1.073132	1.551379	0.001	9.437916	0.673495	8.069068	0.748227
TS-14_Py-C_3	28.94109	1312	1064.08	206.614	0.001	0.616797	0.765443	1179.692	7.436515	3.924168	3.951585	4.0253	0.001	0.001	20.73253	0.933852	0.001	7.635021	9.512813	213.8625	0.746046
TS-14_Py-D_1	95.01152	59	318.171	69.60166	0.001	0.206199	1.068827	39.68128	0.001	0.399958	0.321006	0.001	0.006494	0.001	0.001	0.458102	0.001	3.148898	0.001	2.398927	0.057665
TS-14_Py-D_2	68.62338	154	334.0683	110.4088	17.02806	0.420549	0.001	64.39342	0.001	0.735467	2.667381	0.001	0.001	0.001	0.001	0.351245	0.001	3.646425	0.051279	15.97815	0.221664
TS-14_Py-E_1	31.09483	82	81.16192	15.36639	0.001	0.001	0.001	6.038449	0.001	11.52791	0.001	0.001	0.040558	0.764903	1.053784	0.001	0.001	1.974976	0.112278	0.186923	0.001

TS-14_Py-E_2	33.99165	14	44.74439	7.065748	0.001	0.001	0.001	4.509475	0.001	106.7201	0.001	0.001	0.002232	0.001	0.633046	0.001	0.001	1.704202	0.001	0.001	0.001
TS-14_Py-F_1	80.88787	56	47.39039	109.0608	0.001	0.221286	1.140891	3.985242	0.001	12.75972	0.430093	0.001	0.013828	0.415132	0.322434	0.08494	0.001	5.501583	0.514096	6.441203	0.045515
TS-14_Py-F_2	146.2052	107	58.15011	53.93639	0.001	0.398218	0.001	1.720538	0.001	4.575325	0.001	0.783465	0.001	0.001	0.443333	0.001	0.001	3.83881	0.001	1.985702	0.001
TS-14_Py-F_3	157.7828	110	77.1296	128.9901	0.001	0.333813	1.033665	2.316784	0.001	4.382918	0.001	0.001	0.001	1.393361	0.472702	0.121718	0.001	6.590938	0.10571	9.268068	0.001
TS-14_Py-G_1	23.97457	87	56.91628	108.1246	0.001	0.001	0.915057	8.557143	4.458384	3.241875	0.654007	0.001	0.001	1.07853	0.874478	0.446495	0.096094	0.001	0.126507	7.246157	0.001
TS-14_Py-G_2	60.67646	488	298.6691	338.6574	0.001	0.395345	0.851136	40.87633	6.588819	7.86858	4.9103	0.001	0.058942	2.032706	4.494184	0.425381	0.001	5.838424	0.103905	75.19722	0.415758
TS-14_Py-G_3	348.8602	444	199.7162	223.5569	21.92919	0.64202	1.0117	89.62845	0.001	6.012665	6.798795	0.001	0.023676	1.081952	7.962781	0.821809	0.102935	7.102034	0.125548	119.121	3.12481
TS-07_Py-A_1	0.001	3	0.001	1.475423	0.001	0.001	0.919194	0.001	7.471043	0.001	0.001	0.001	0.001	0.001	0.001	0.001	0.001	4.956478	0.001	0.001	0.114855
TS-07_Py-A_2	0.001	64	13.86064	4.60286	0.001	0.001	1.05957	2.985388	60.48208	0.088254	0.001	0.001	0.001	0.001	0.001	0.632106	0.001	6.363732	0.001	0.294192	0.792427
TS-07_Py-A_3	0.001	39	8.573916	0.001	0.001	0.001	0.001	2.399358	61.00978	0.001	0.001	0.001	0.003114	0.001	0.001	0.813787	0.001	9.835838	0.001	0.001	0.001
TS-07_Py-B_1	0.001	14779	195.0456	3.053776	0.001	0.001	0.001	94.57714	23.88425	0.001	0.001	0.001	0.004703	0.001	0.001	0.58848	0.001	3.372882	0.001	0.001	1.504373
TS-07_Py-B_2	0.001	292	35.76236	0.001	0.001	0.001	0.001	1.367643	36.83698	0.001	0.001	0.001	0.012334	0.001	0.001	0.001	0.001	5.122189	0.001	0.001	0.001
TS-07_Py-B_3	10.77468	9796	155.874	4.126501	0.001	0.151214	0.001	31.84576	15.23515	0.001	0.001	0.001	0.001	0.001	0.001	0.230424	0.001	0.001	0.001	0.001	1.538355
TS-07_Py-C_1	0.001	1287	32.00312	0.001	0.001	0.001	0.001	6.221896	28.70164	0.001	0.001	0.001	0.006444	0.001	0.001	4.684139	0.001	10.05529	0.001	0.001	0.001
TS-07_Py-C_2	0.001	1446	17.76892	0.001	0.001	0.001	1.226637	7.040802	33.13421	0.001	0.001	0.001	0.013432	0.001	0.001	8.156673	0.001	16.62571	0.001	0.001	0.001
TS-07_Py-C_3	0.001	6243	163.1721	0.001	0.001	0.001	0.001	15.52768	46.45429	0.001	0.001	0.001	0.001	0.001	0.001	4.551617	0.001	11.19694	0.001	0.001	0.143679
TS-07_Py-D_1	0.001	6237	135.5748	0.001	0.001	0.001	1.082435	67.49414	26.96122	0.001	0.001	0.001	0.001	0.001	0.001	0.001	0.001	6.714352	0.001	0.001	0.001

TS-07_Py-D_2	0.001	566	132.9396	1.800461	0.001	0.001	0.001	17.39686	57.43727	0.001	0.001	0.001	0.001	0.001	0.001	21.30061	0.001	6.033139	0.001	0.001	0.001
TS-07_Py-D_3	0.001	6503	129.7111	2.829178	0.001	0.001	0.001	27.58716	21.79496	0.001	0.001	0.001	0.009352	0.001	0.001	0.001	0.001	5.235857	0.066123	0.001	0.001
TS-07_Py-E_2	0.001	599	11.84651	0.001	0.001	0.001	0.001	1.833783	63.56377	0.001	0.001	0.001	0.001	0.001	0.001	1.187114	0.001	9.268974	0.001	0.001	0.001
TS-07_Py-E_3	0.001	86	102.9182	2.233991	21.50027	0.001	0.001	1.604066	32.56304	0.001	0.001	0.001	0.001	0.001	0.001	0.846677	0.001	12.23615	0.001	0.177779	0.864138
TS-07_Py-F_1	26.06494	574	96.14621	51.38173	0.001	0.101681	1.893004	2.651812	34.91428	0.001	4.575399	0.001	0.001	0.001	0.001	2.759454	0.085544	10.80918	0.001	45.56551	12.06121
TS-07_Py-F_2	0.001	13078	201.973	0.001	0.001	0.001	0.001	87.22578	20.66511	0.10438	0.001	0.001	0.010578	0.001	0.001	0.881143	0.110993	8.754052	0.001	1.039781	10.76125
TS-07_Py-F_3	0.001	4445	71.41678	4.759723	0.001	0.001	1.132522	26.60185	22.83294	0.001	0.001	0.001	0.001	0.001	0.001	0.512097	0.001	12.09474	0.001	0.001	1.103893
TS-07_Py-G_1	0.001	1432	60.59449	5.262464	0.001	0.085028	0.001	11.68752	92.55208	0.001	0.001	1.996471	0.006446	0.001	0.001	17.32962	0.001	19.5268	0.077067	0.001	0.001
TS-07_Py-G_2	0.001	1520	62.55634	0.001	0.001	0.107776	0.001	10.93424	76.12484	0.001	0.001	0.001	0.006815	0.001	0.001	20.60719	0.001	9.411221	0.001	0.096218	0.19397
TS-07_Py-G_3	0.001	1697	108.3702	0.001	0.001	0.001	0.001	10.08446	75.41129	0.001	0.001	4.616797	0.001	0.001	0.001	12.70979	0.001	24.74703	0.001	0.001	0.001
SL-03-Py_A_1	0.001	4162	107.6105	31.75377	0.001	0.207908	0.001	142.0799	0.001	0.001	4.887097	0.001	0.037209	0.001	0.001	48.05155	0.001	13.22409	0.001	9.493661	147.8243
SL-03-Py_A_2	0.001	162	55.36368	0.001	58.37767	0.001	0.001	151.8279	8.29857	0.176827	0.427093	0.001	0.073907	0.001	0.001	42.06569	0.001	10.15724	0.001	2.330694	36.16524
SL-03-Py_A_3	0.001	2087	220.7969	5.031125	0.001	0.001	0.001	46.36034	0.001	0.001	0.403442	0.001	0.006202	0.001	0.001	17.3037	0.078708	10.77123	0.001	6.545664	46.42811
SL-03-Py_B_1	0.001	736	286.5751	0.001	0.001	0.001	0.001	95.05318	0.001	0.001	0.426386	0.001	0.001	0.001	0.001	0.986493	0.001	8.407345	0.001	1.463026	10.1078
SL-03-Py_B_2	0.001	186	1015.091	0.001	0.001	0.162041	0.001	143.9116	0.001	0.001	0.352103	0.001	0.001	0.001	0.001	4.865312	0.001	8.253078	0.001	4.480603	17.28413
SL-03-Py_B_3	0.001	1431	207.3886	0.001	0.001	0.001	1.59667	63.83934	0.001	0.001	0.001	0.001	0.001	0.001	0.001	0.183527	0.001	4.960539	0.001	1.083356	0.550217
SL-03-Py_C_2	0.001	3271	342.3021	9.501205	0.001	0.001	0.001	209.1362	6.445736	0.001	1.377471	0.001	0.017625	0.001	0.001	7.817732	0.001	10.28773	0.001	11.51597	61.0527
SL-03-Py_C_3	0.001	1248	330.4172	4.929414	0.001	0.037935	0.001	55.32965	4.526651	0.001	0.234955	0.001	0.001	0.001	0.001	2.723978	0.001	13.77792	0.001	0.525187	2.615814
SL-03-Py_D_1	0.001	2550	43.80195	0.001	0.001	0.001	0.001	48.53359	0.001	0.001	0.159136	0.001	0.001	0.001	0.001	0.001	0.001	8.545859	0.001	0.245661	0.452199
SL-03-Py_D_2	0.001	64	127.3176	0.001	0.001	0.001	0.001	28.5471	6.601226	0.001	0.001	0.001	0.001	0.001	0.001	0.227895	0.001	9.981513	0.001	0.1853	0.001
SL-03-Py_D_3	0.001	106	245.4361	7.60438	0.001	0.001	0.001	29.11084	0.001	0.001	0.277937	0.001	0.001	0.001	0.001	0.886397	0.001	8.056288	0.001	1.474677	12.32969

SL-03-			242.734					128.563	3.50904		1.76773	1.45700				7.08290		16.1528		3.64199	50.8548
Py_E_1	0.001	1727	2	16.6277	0.001	0.001	0.001	8	3	0.001	5	5	0.001	0.001	0.001	2	0.001	1	0.001	2	1
SL-03-			413.588					14.8276	4.93640							0.82093		10.6451			2.29401
Py_E_2	0.001	2120	9	0.001	0.001	0.001	0.001	1	2	0.001	0.001	0.001	0.001	0.001	0.001	1	0.001	4	0.001	0.001	7
SL-03-			406.932	7.49468				1.82319	6.33642							1.69638		16.8549		0.40605	5.12290
Py_E_3	0.001	1109	1	3	0.001	0.001	0.001	3	7	0.001	0.001	0.001	0.001	0.001	0.001	3	0.001	5	0.001	4	6
SL-03-			157.485			0.08700		28.9537	6.69814		0.34679		0.01223		0.22976	3.88662		17.1084		1.76333	22.7347
Py_F_2	0.001	254	4	0.001	0.001	5	0.001	7	7	0.001	7	0.001	8	0.001	1	2	0.001	8	0.001	9	4
SL-03-			550.106	3.86654				16.2105	3.49342	0.18482						0.19058		14.7841			0.44925
Py_F_3	0.001	414	5	7	0.001	0.001	0.001	7	4	4	0.001	0.001	0.001	0.001	0.001	4	0.001	2	0.001	0.001	5
SL-03-			209.839	11.6974			1.12802	164.962		0.19899	1.29471							19.6958		3.61363	30.8317
Py_G_1	0.001	3343	9	4	0.001	0.001	2	7	0.001	5	3	0.001	0.001	0.001	0.001	12.7815	0.001	4	0.08131	7	4

Laser ablation element data as histograms

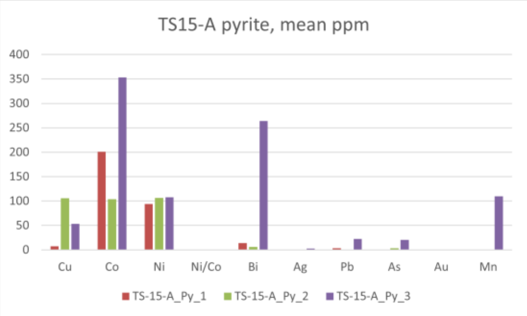

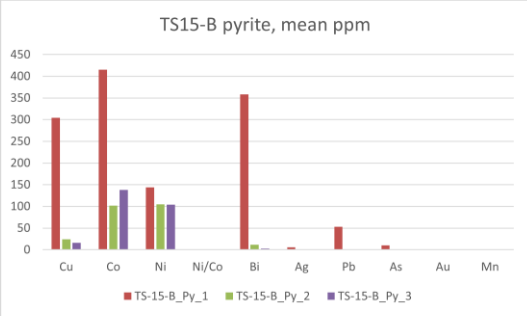

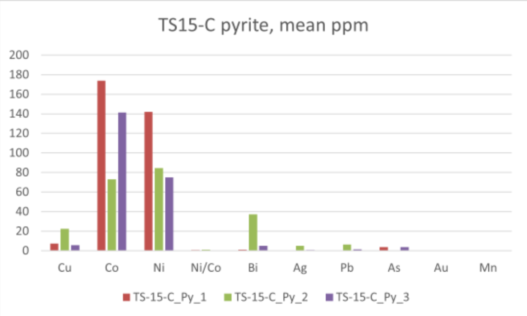

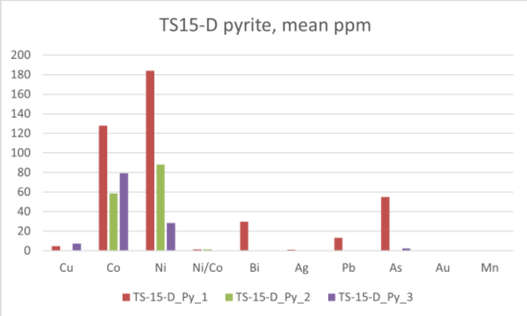

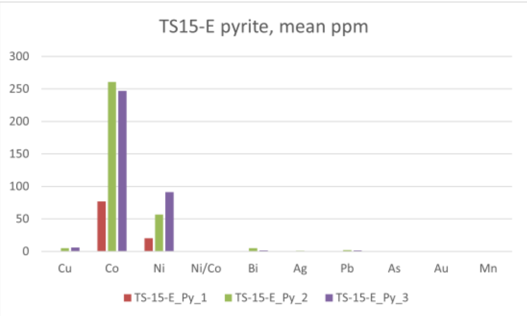

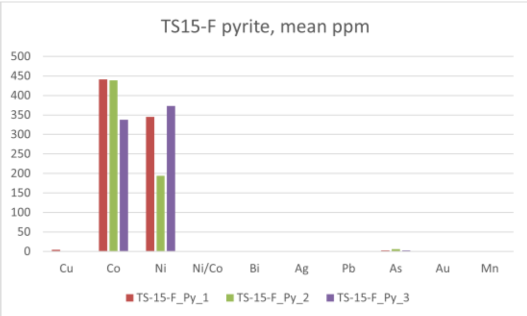

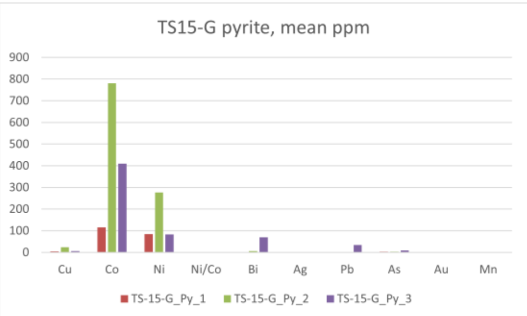

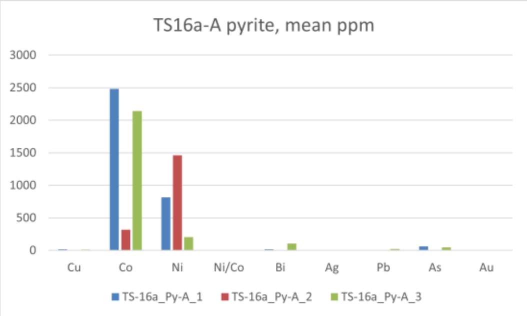
TS16a-A pyrite, mean ppm
3000
2500
2000
1500
1000
500
0
Cu Co Ni Ni/Co Bi Ag Pb As Au
TS-16a_Py-A_1 TS-16a_Py-A_2 TS-16a_Py-A_3

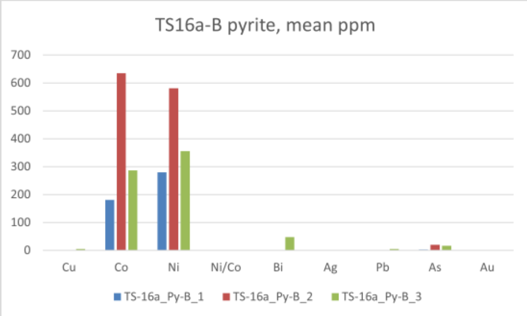
TS16a-B pyrite, mean ppm
700
600
500
400
300
200
100
0
Cu Co Ni Ni/Co Bi Ag Pb As Au
TS-16a_Py-B_1 TS-16a_Py-B_2 TS-16a_Py-B_3

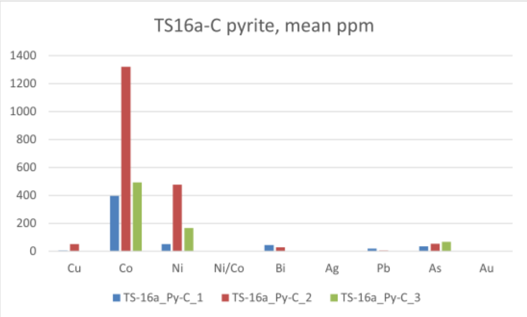
TS16a-C pyrite, mean ppm
1400
1200
1000
800
600
400
200
0
Cu Co Ni Ni/Co Bi Ag Pb As Au
TS-16a_Py-C_1 TS-16a_Py-C_2 TS-16a_Py-C_3

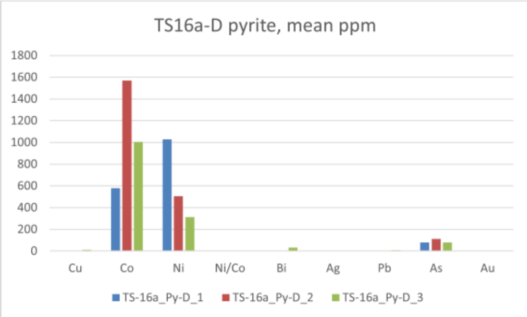
TS16a-D pyrite, mean ppm
1800
1600
1400
1200
1000
800
600
400
200
0
Cu Co Ni Ni/Co Bi Ag Pb As Au
TS-16a_Py-D_1 TS-16a_Py-D_2 TS-16a_Py-D_3

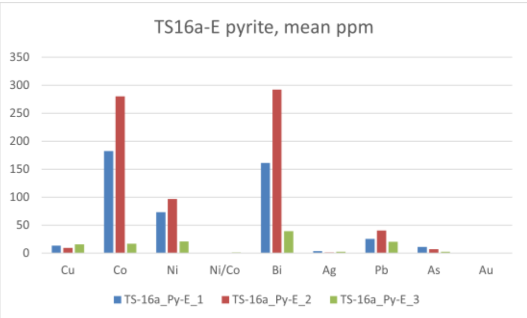
TS16a-E pyrite, mean ppm
350
300
250
200
150
100
50
0
Cu Co Ni Ni/Co Bi Ag Pb As Au
TS-16a_Py-E_1 TS-16a_Py-E_2 TS-16a_Py-E_3

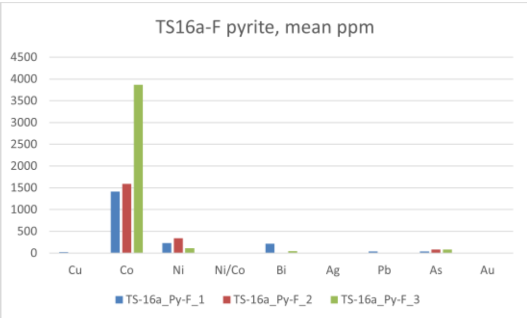
TS16a-F pyrite, mean ppm
4500
4000
3500
3000
2500
2000
1500
1000
500
0
Cu Co Ni Ni/Co Bi Ag Pb As Au
TS-16a_Py-F_1 TS-16a_Py-F_2 TS-16a_Py-F_3

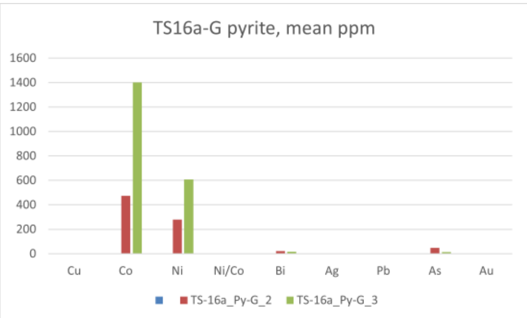
TS16a-G pyrite, mean ppm
1600
1400
1200
1000
800
600
400
200
0
Cu Co Ni Ni/Co Bi Ag Pb As Au
TS-16a_Py-G_2 TS-16a_Py-G_3

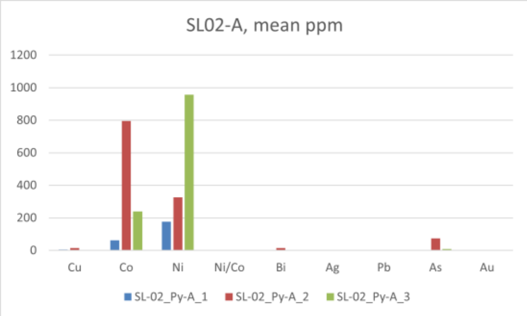
SL02-A, mean ppm
1200
1000
800
600
400
200
0
Cu
Co
Ni
Ni/Co
Bi
Ag
Pb
As
Au
SL-02_Py-A_1
SL-02_Py-A_2
SL-02_Py-A_3

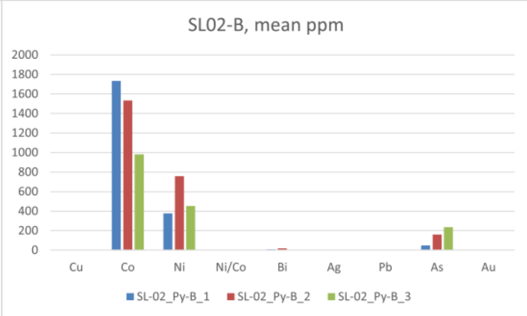
SL02-B, mean ppm
2000
1800
1600
1400
1200
1000
800
600
400
200
0
Cu
Co
Ni
Ni/Co
Bi
Ag
Pb
As
Au
SL-02_Py-B_1
SL-02_Py-B_2
SL-02_Py-B_3

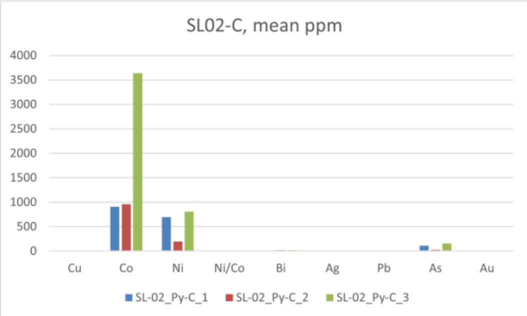
SL02-C, mean ppm
4000
3500
3000
2500
2000
1500
1000
500
0
Cu
Co
Ni
Ni/Co
Bi
Ag
Pb
As
Au
SL-02_Py-C_1
SL-02_Py-C_2
SL-02_Py-C_3

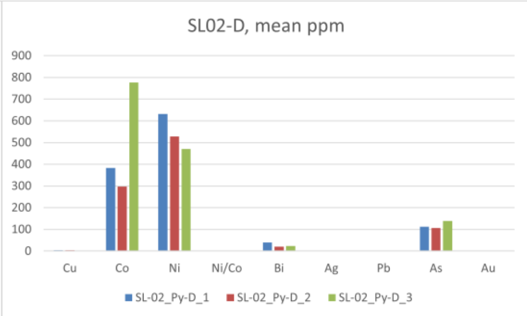
SL02-D, mean ppm
900
800
700
600
500
400
300
200
100
0
Cu
Co
Ni
Ni/Co
Bi
Ag
Pb
As
Au
SL-02_Py-D_1
SL-02_Py-D_2
SL-02_Py-D_3

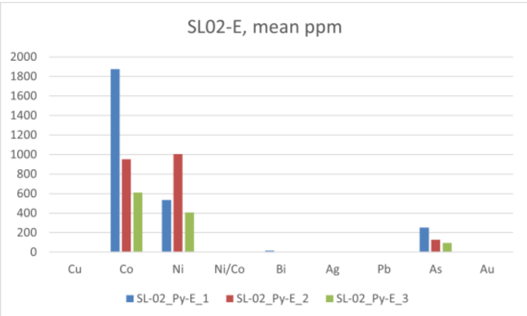
SL02-E, mean ppm
2000
1800
1600
1400
1200
1000
800
600
400
200
0
Cu
Co
Ni
Ni/Co
Bi
Ag
Pb
As
Au
SL-02_Py-E_1
SL-02_Py-E_2
SL-02_Py-E_3

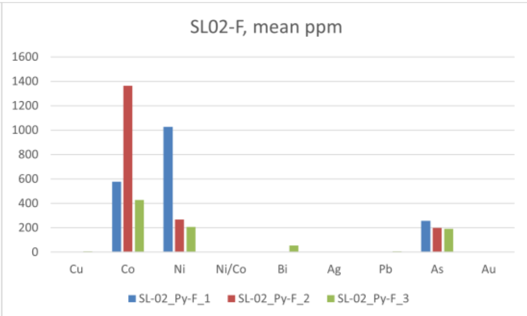
SL02-F, mean ppm
1600
1400
1200
1000
800
600
400
200
0
Cu
Co
Ni
Ni/Co
Bi
Ag
Pb
As
Au
SL-02_Py-F_1
SL-02_Py-F_2
SL-02_Py-F_3

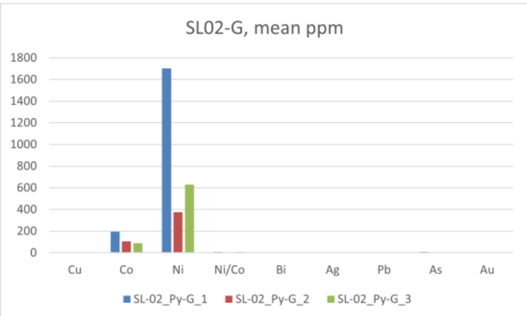
SL02-G, mean ppm
1800
1600
1400
1200
1000
800
600
400
200
0
Cu
Co
Ni
Ni/Co
Bi
Ag
Pb
As
Au
SL-02_Py-G_1
SL-02_Py-G_2
SL-02_Py-G_3

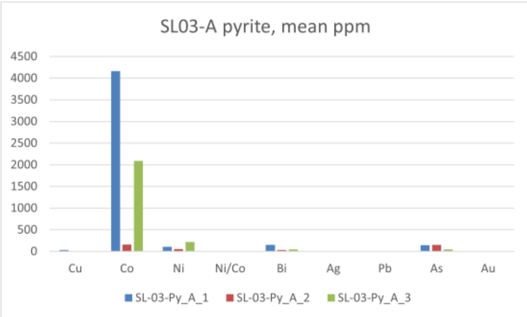
SL03-A pyrite, mean ppm
4500
4000
3500
3000
2500
2000
1500
1000
500
0
Cu
Co
Ni
Ni/Co
Bi
Ag
Pb
As
Au
SL-03-Py_A_1
SL-03-Py_A_2
SL-03-Py_A_3

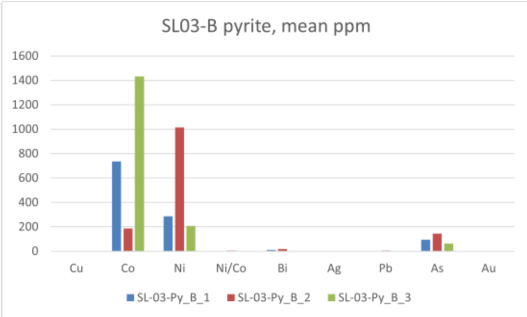
SL03-B pyrite, mean ppm
1600
1400
1200
1000
800
600
400
200
0
Cu
Co
Ni
Ni/Co
Bi
Ag
Pb
As
Au
SL-03-Py_B_1
SL-03-Py_B_2
SL-03-Py_B_3

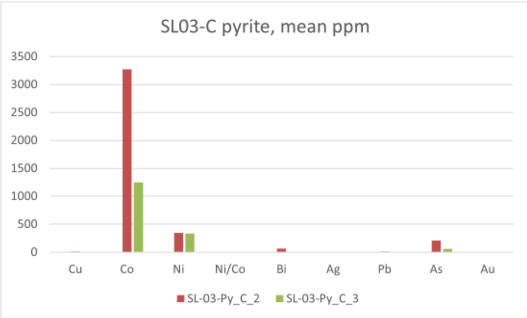
SL03-C pyrite, mean ppm
3500
3000
2500
2000
1500
1000
500
0
Cu
Co
Ni
Ni/Co
Bi
Ag
Pb
As
Au
SL-03-Py_C_2
SL-03-Py_C_3

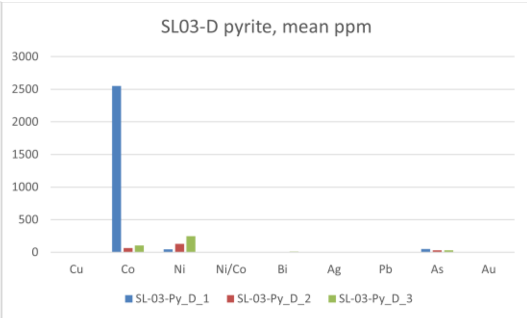
SL03-D pyrite, mean ppm
3000
2500
2000
1500
1000
500
0
Cu
Co
Ni
Ni/Co
Bi
Ag
Pb
As
Au
SL-03-Py_D_1
SL-03-Py_D_2
SL-03-Py_D_3

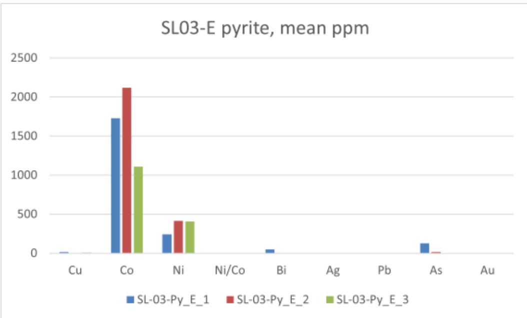
SL03-E pyrite, mean ppm
2500
2000
1500
1000
500
0
Cu
Co
Ni
Ni/Co
Bi
Ag
Pb
As
Au
SL-03-Py_E_1
SL-03-Py_E_2
SL-03-Py_E_3

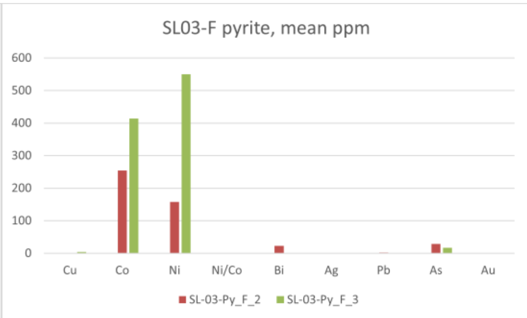
SL03-F pyrite, mean ppm
600
500
400
300
200
100
0
Cu
Co
Ni
Ni/Co
Bi
Ag
Pb
As
Au
SL-03-Py_F_2
SL-03-Py_F_3

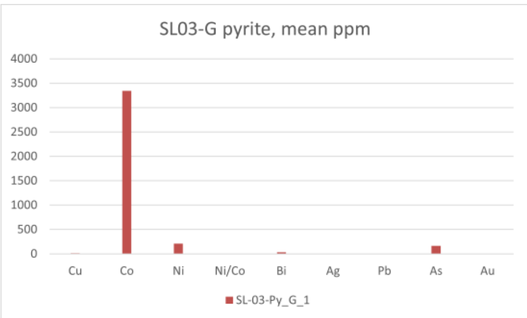
SL03-G pyrite, mean ppm
4000
3500
3000
2500
2000
1500
1000
500
0
Cu
Co
Ni
Ni/Co
Bi
Ag
Pb
As
Au
SL-03-Py_G_1

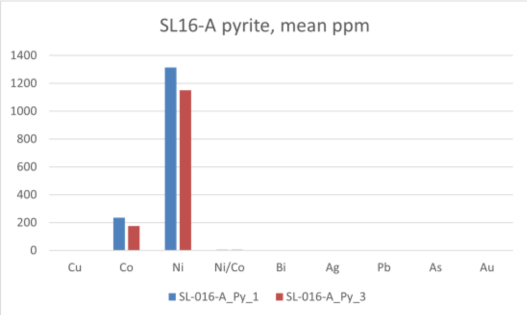
SL16-A pyrite, mean ppm
1400
1200
1000
800
600
400
200
0
Cu Co Ni Ni/Co Bi Ag Pb As Au
SL-016-A_Py_1 SL-016-A_Py_3

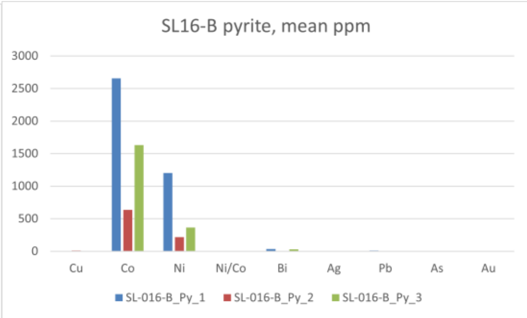
SL16-B pyrite, mean ppm
3000
2500
2000
1500
1000
500
0
Cu Co Ni Ni/Co Bi Ag Pb As Au
SL-016-B_Py_1 SL-016-B_Py_2 SL-016-B_Py_3

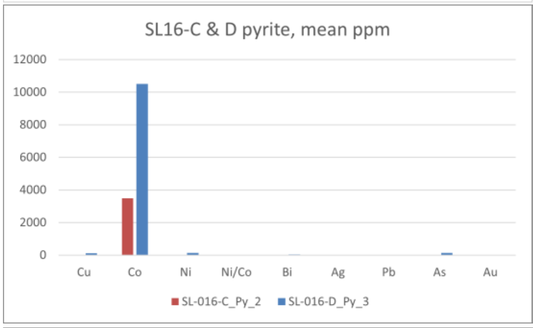
SL16-C & D pyrite, mean ppm
12000
10000
8000
6000
4000
2000
0
Cu Co Ni Ni/Co Bi Ag Pb As Au
SL-016-C_Py_2 SL-016-D_Py_3

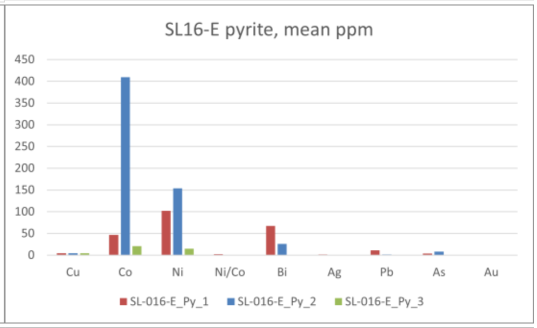
SL16-E pyrite, mean ppm
450
400
350
300
250
200
150
100
50
0
Cu Co Ni Ni/Co Bi Ag Pb As Au
SL-016-E_Py_1 SL-016-E_Py_2 SL-016-E_Py_3

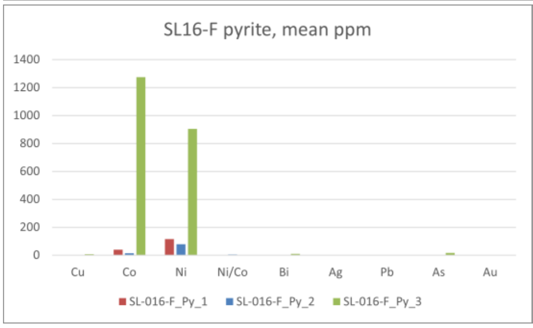
SL16-F pyrite, mean ppm
1400
1200
1000
800
600
400
200
0
Cu Co Ni Ni/Co Bi Ag Pb As Au
SL-016-F_Py_1 SL-016-F_Py_2 SL-016-F_Py_3

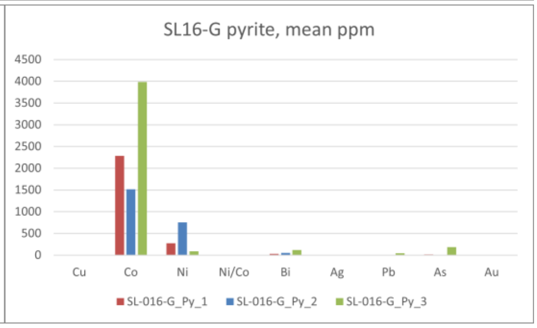
SL16-G pyrite, mean ppm
4500
4000
3500
3000
2500
2000
1500
1000
500
0
Cu Co Ni Ni/Co Bi Ag Pb As Au
SL-016-G_Py_1 SL-016-G_Py_2 SL-016-G_Py_3

7.7 Key Lithologies

Major rock types encountered in the field and important to the study. Submitted to TCD for rock saw cutting and lap polish under 'slab & polish'. No samples received back.

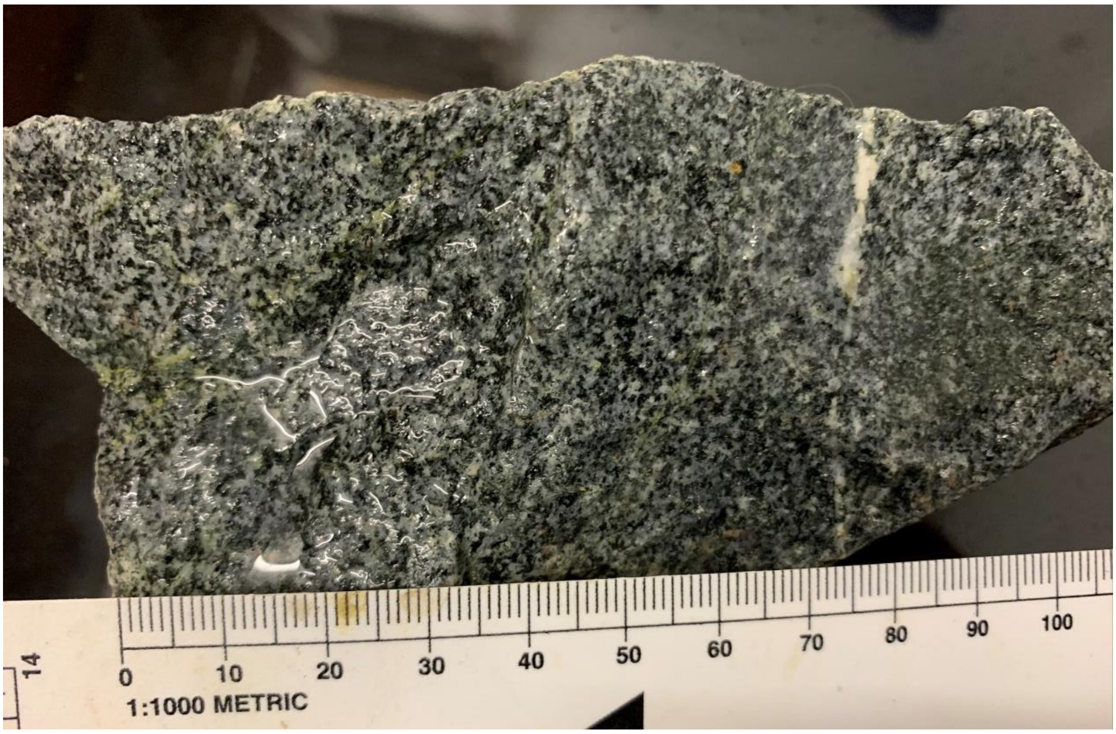

KY01 Grey, medium to coarse grained, 50-60% qtz, isotropic, biotite, minor k-feldspar. Gabbro to microgabbro. Lower opholite. Tyrone Plutonic Complex. Orritor Quarry

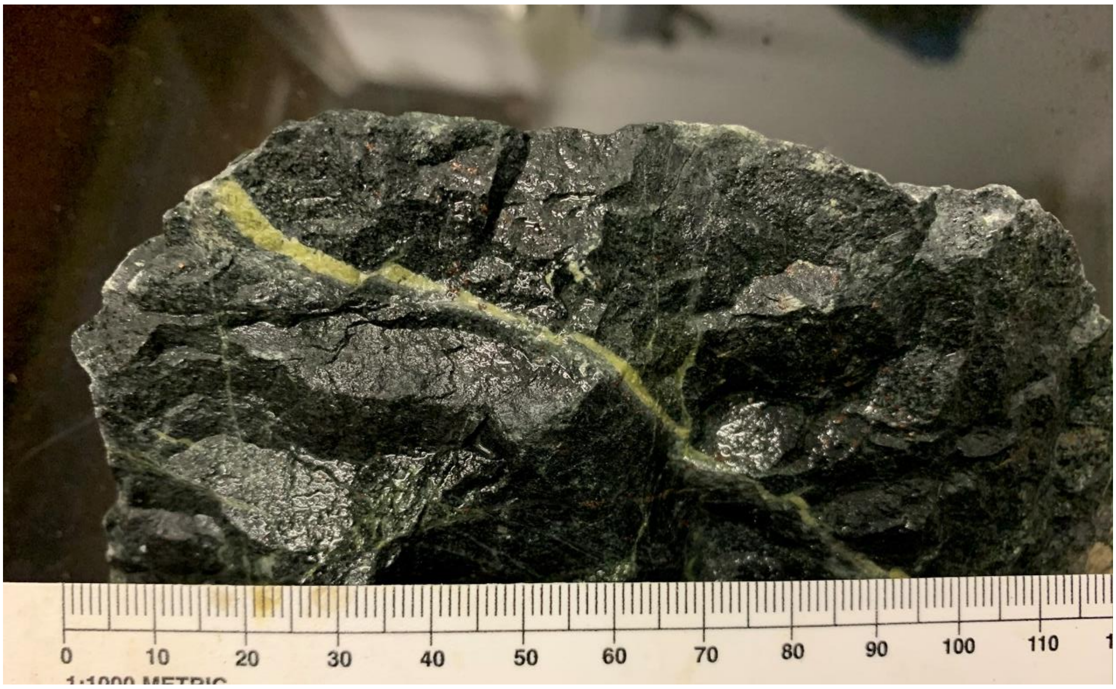

KY02 Black, fine grained, 40-50% qtz, weak chlorite throughout, late green veins - epidote. Dolerite. Upper ophiolite. TPG

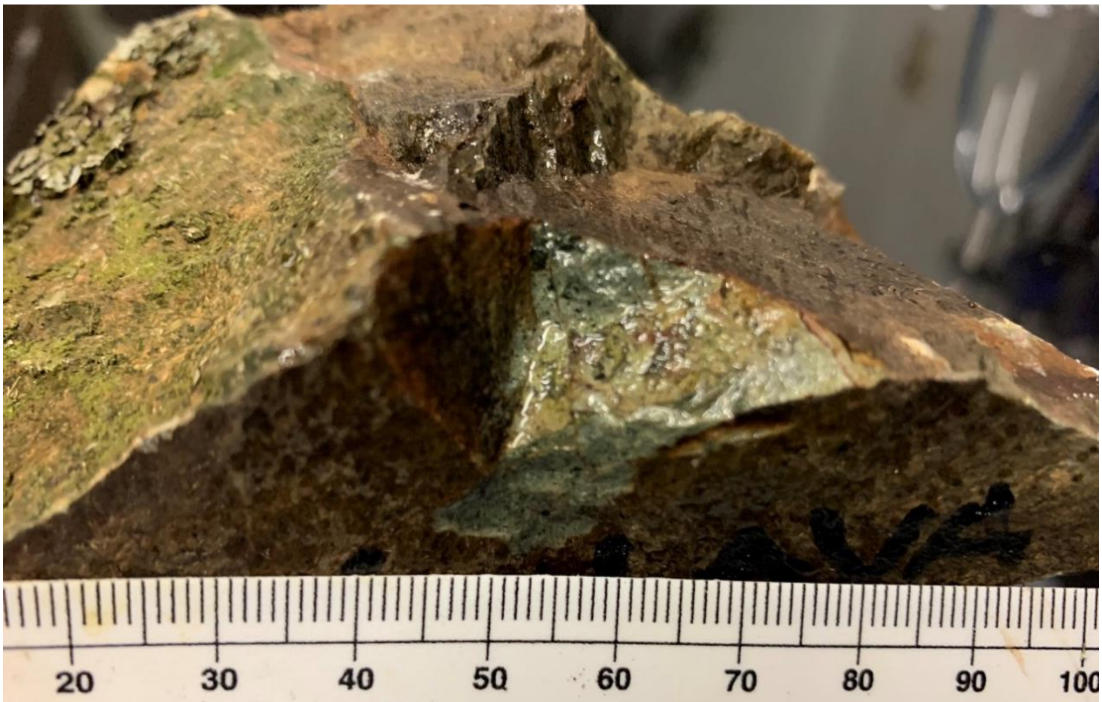

KY03 Green, fine to medium grained, heavily foliated/ deformed, 50-60% quartz, black pyroxene or amphibole. pXRF high Mg. Talc on surface. Alteration throughout, serpentinised gabbro/ serpentinite. Lower ophiolite. TPG

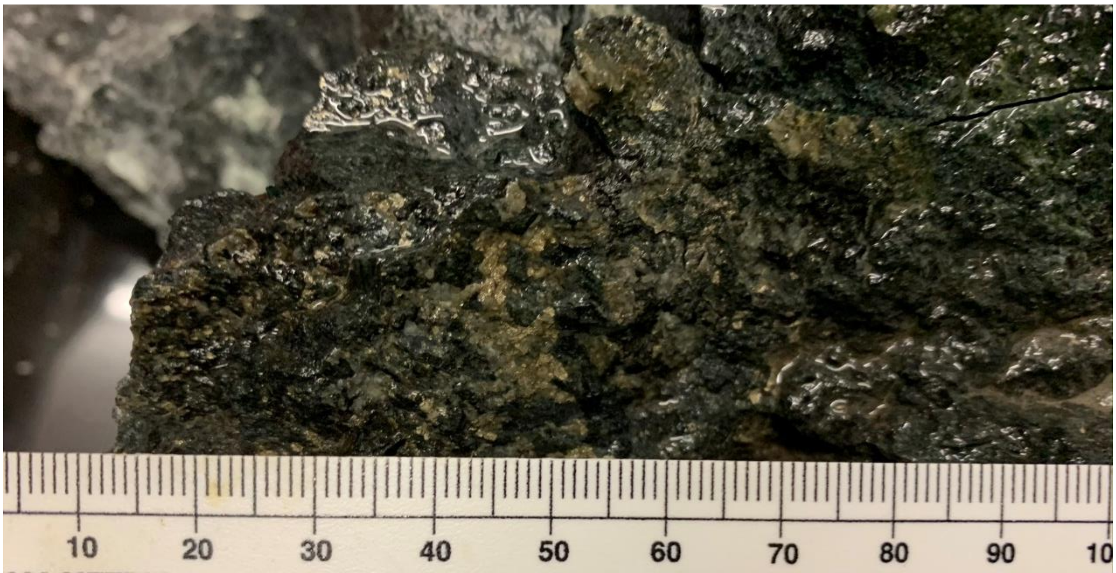

KY04 Black, fine grained, foliated host rock, pyroxene/ amphibole dominated. Occurs as small boulders on quarry floor. Pods in OC. Sulphides as pyrite/ pyrrhotite w/ quartz blebs. Ultramafic ophiolite portion

KY05 Salmon pink, coarse grained, qtz + k-feldspar, some chlorite veinlets, foliation/ deformation fabric indicates shearing. Pegmatities. Intrusives.

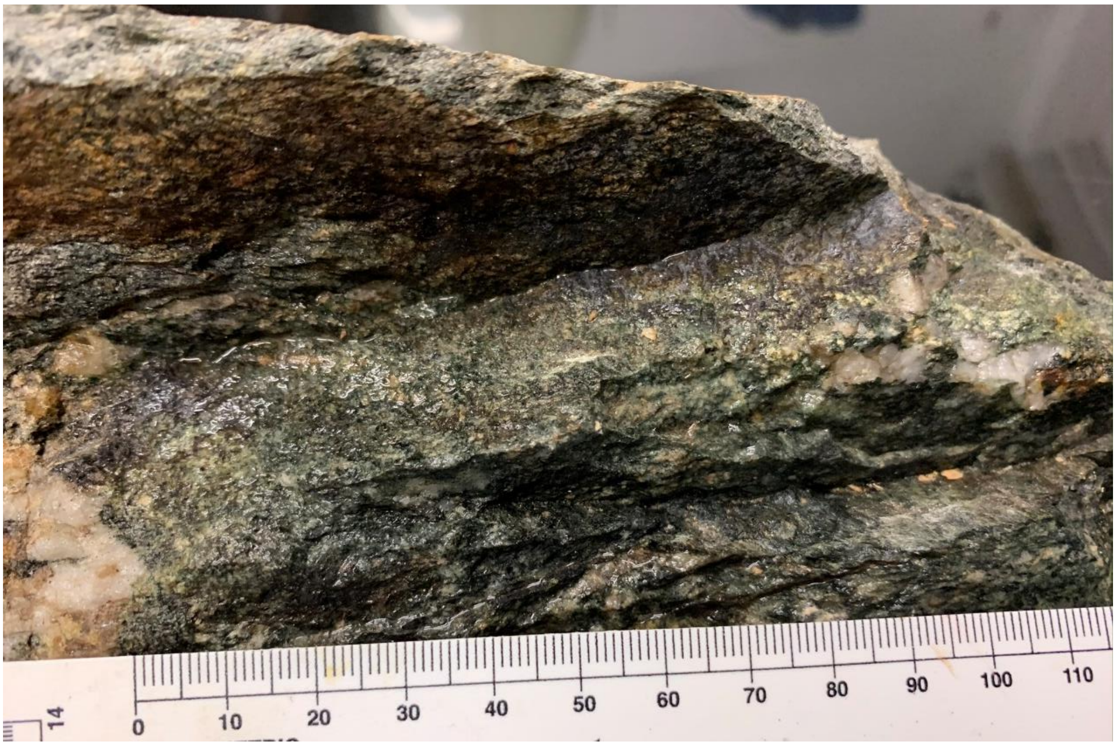

KY07 Medium grained, strong foliation, quartz porhyroblasts in grey/ green foliated quartz-mica fabric. Psammite. Some leucosome seperation. Lower amphioblite facies. Terrigenous and volcanic sediment protoliths. Island arc core.

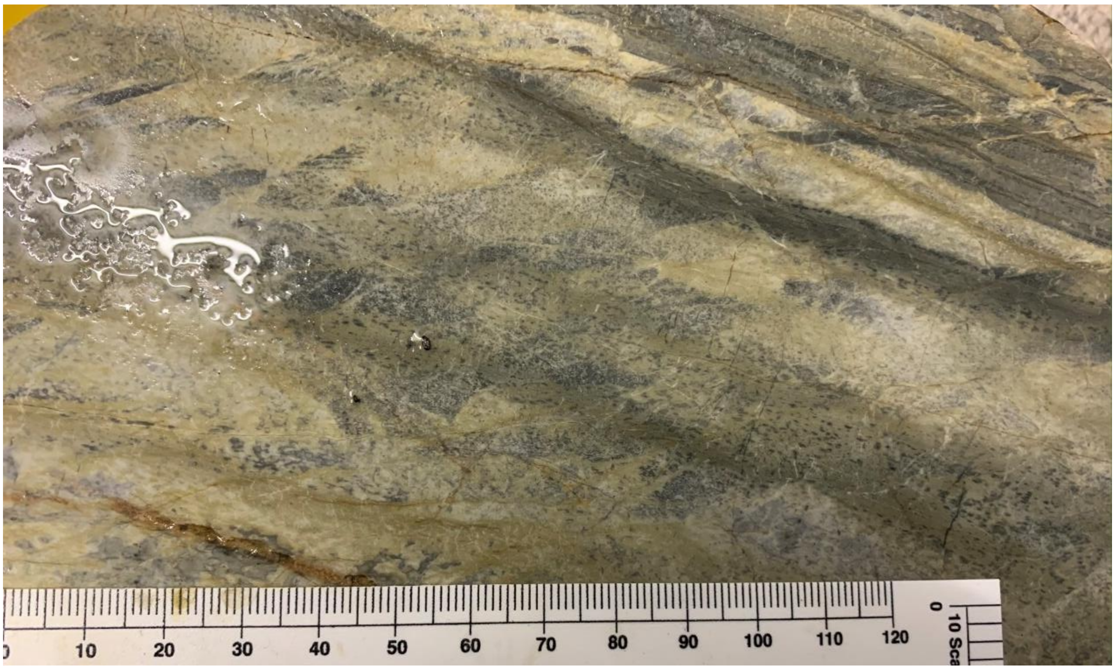

KY08 fine grained, intermediate composition, fine laminations in parts, pervasive alteration = sercitic. Layered tuff. TVG